NASA TECHNICAL TRANSLATION

NASA TT F 15,215

INVESTIGATIONS ON ELASTOHYDRODYNAMICAL LUBRICATION FILM THICKNESS FOR ELLIPTICAL HERTZ CONTACT SURFACES

P. Brüser

NASA-TT-F-15215) INVESTIGATIONS ON ELASTOHYDRODYNAMICAL LUBRICATION FILM THICKNESS FOR ELLIPTICAL HERTZ CONTACT SURFACES Ph.D. (Scientific Translation Service) 140 p HC $10.00 CSCL 11H G3/15

N74-17194

Unclas 30295

Translation of: "Untersuchungen über die elastohydrodynamische Schmierfilmdicke bei elliptischen Hertzschen Kontaktflächen." Universität Carolo-Wilhelmina zu Braunschweig zur Erlangung der Würde eines Doktor-Ingenieurs Dissertation, Braunschweig, West Germany, 1972, 144 pages.

Reproduced by
NATIONAL TECHNICAL
INFORMATION SERVICE
US Department of Commerce
Springfield, VA. 22151

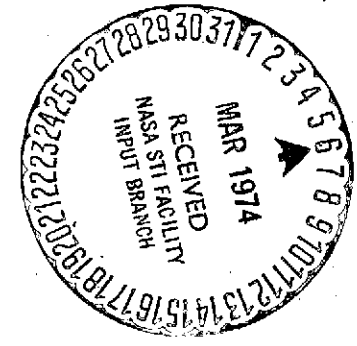

NATIONAL AERONAUTICS AND SPACE ADMINISTRATION
WASHINGTON, D. C. 20546 JANUARY 1974

N O T I C E

THIS DOCUMENT HAS BEEN REPRODUCED FROM THE BEST COPY FURNISHED US BY THE SPONSORING AGENCY. ALTHOUGH IT IS RECOGNIZED THAT CERTAIN PORTIONS ARE ILLEGIBLE, IT IS BEING RELEASED IN THE INTEREST OF MAKING AVAILABLE AS MUCH INFORMATION AS POSSIBLE.

STANDARD TITLE PAGE

1. Report No.	2. Government Accession No.	3. Recipient's Catalog No.
NASA TT F-15,215		

4. Title and Subtitle	5. Report Date
INVESTIGATIONS ON ELASTOHYDRODYNAMICAL LUBRICATION FILM THICKNESS FOR ELLIPTICAL HERTZ CONTACT SURFACES.	January, 1974
	6. Performing Organization Code

7. Author(s)	8. Performing Organization Report No.
P. Brüser	
	10. Work Unit No.

9. Performing Organization Name and Address	11. Contract or Grant No.
SCITRAN Box 5456 Santa Barbara, CA 93108	NASw-2483
	13. Type of Report and Period Covered
	Translation
12. Sponsoring Agency Name and Address National Aeronautics and Space Administration Washington, D.C. 20546	14. Sponsoring Agency Code

15. Supplementary Notes

Translation of: Untersuchungen über die elastohydrodynamische Schmierfilmdicke bei elliptischen Hertzschen Kontaktflachen. Universitat Carolo-Wilhelmina zu Braunschweig zur Erlangung der Wurde eines, Doktor-Ingenieurs Dissertation, Braunschweig, West Germany, 1972, 144 pages.

16. Abstract A numerical method has been developed for elliptical Hertz contact areas which makes it possible to calculate the phenomena in the lubrication gap. Considering the pressure dependence of the oil viscosity and oil density, the system of equations which describe the problem are solved together. Two different iteration methods provide the desired results for the inlet zone and for the Hertz region proper. A test stand and a suitable measurement method have been developed for experimentally determining the lubrication film thickness. Load levels up to the elastic deformation limit can be applied. Other possible parameters will include the circumferential velocity and the geometry of the rollers rolling along each other. Also the characteristics of the oil can be varied. The crack thickness is determined using capacity changes. The measured values are recalculated into distance values, using mathematical formulas. The theoretical and the experimental investigations therefore confirm the existance of an almost parallel lubrication film between the highly loaded roller bodies having elliptical contact surfaces. The shape of the ellipse has a secondary importance.

17. Key Words (Selected by Author(s))	18. Distribution Statement
	Unclassified - Unlimited

19. Security Classif. (of this report)	20. Security Classif. (of this page)	21. No. of Pages	22. Price
Unclassified	Unclassified	129	

TABLE OF CONTENTS

	Page
NOTATION TABLE	v
1. INTRODUCTION	1
1.1 Elastohydrodynamic lubrication	1
1.2 Influence of lubrication on the friction, wear and lifetime of rollers	2
2. STATE OF KNOWLEDGE	4
2.1 Theoretical investigation	4
2.1.1 Line contact	4
2.1.2 Point contact	7
2.2 Experimental investigations	9
2.2.1 Measurement methods	10
2.2.1.1 Measurement of the ohmic resistance	10
2.2.1.2 Measurement of voltage arcing	11
2.2.1.3 Optical measurement methods	11
2.2.1.4 Measurements with x-rays	12
2.2.1.5 Capacitive measurements	13
2.2.2 Measurement results	14
2.2.2.1 Line contact	14
2.2.2.2 Point contact	17
2.3 Collection of results	19
3. PROBLEM FORMULATION	20
4. TECHNICAL-PHYSICAL PROPERTIES OF THE INVESTIGATED ROLLER BODIES AND LUBRICANTS	22
4.1 Roller bodies	22
4.1.1 Hertz equations	22
4.1.2 Geometry and materials	28
4.1.3 Loading capacity	30
4.2 Lubricants	31
4.2.1 Density	32
4.2.2 Viscosity	34

5. BASIC EQUATIONS FOR MATHEMATICAL SOLUTION OF A PROBLEM 36
5.1 Reynolds equation of motion 38
5.2 Elastic deformation equation 41
5.3 Geometric equations 42
5.4 System of equations 44
6. NUMERICAL SOLUTION OF THE SYSTEM OF EQUATIONS 45
6.1 Solution path 45
6.2 Selection of the grid and initial pressure distribution 47
6.3 Calculation of the elastic deformation 48
6.4 Calculation of the smallest crack width h_o 50
6.5 Calculation of the crack contour from the deformation 51
6.6 Approximation of the pressure distribution in the boundary area 52
6.6.1 Calculation of the coefficients 52
6.6.2 Establishment of the system of equations 56
6.6.3 Solution of the system of equations 57
6.7 Pressure approximation in the Hertz zone 59
6.7.1 Calculation of the crack contour from the Reynolds equation 62
6.7.2 Change of the pressure 63
7. EXECUTION OF THE NUMERICAL CALCULATION AND RESULTS 64
7.1 Computer installation 64
7.2 Calculation sequence 65
7.3 Results 67
8. TEST INSTALLATION 71
8.1 Test stand 71
8.2 Measurement arrangement 72
8.2.1 Measurement of the lubricant film thickness 74
8.2.2 Measurement of the parameters 79
9. EXECUTION OF THE EXPERIMENTS 80
9.1 Calibration of the capacitive measurement installation 80
9.2 Measurement process 81
9.3 Measurement results 81

9.4 Reproducibility of the measurement results 83

10. RECALCULATION OF THE LUBRICANT CRACK CAPACITY INTO FILM THICKNESSES 85

10.1 Calculation of the capacity between two cylinders 87

10.2 Calculation of the capacity between two spheres 91

10.3 Calculation of capacity between two arbitrary bodies 93

10.4 Dielectric 96

10.5 Recalculation curves 99

11. TEST RESULTS 99

11.1 Influence on the circumferential velocity 101

11.2 Influence of the load 101

11.3 Influence of the shape of the Hertz contact area 102

11.4 Influence of oil viscosity 102

11.5 Influence of the pressure-viscosity behavior of the lubricating oil 104

11.6 Summary of the test results 105

12. SUMMARY 109

DIAGRAMS 112

REFERENCES 120

NOTATION TABLE

		Units	Units According to Law of July 2, 1969**
a	Semiaxis of the pressure ellipse in the y direction	mm	
b	Semiaxis of the pressure ellipse in the x direction	mm	
c_P	Area pressure constant for point contact	$(kp/mm^2)^{2/3}$	$(N/mm^2)^{2/3}$
c_P	Area pressure constant for line contact	$(kp/mm^2)^{1/2}$	$(N/mm^2)^{1/2}$
d_W	Roller diameter	mm	
f	Factor for changing the step in the y direction		
f	Error		
$g_1 - g_4$	Parameter for determining the lubrication film thickness		
h	Lubrication film thickness	mm	
h_o	Lubrication film thickness in the center point of the contact area	mm, µm	
h_{min}	Smallest lubrication film thickness	mm	
$\bar{h}$	Parameter for determining the lubrication film thickness		

** If the units according to the law of July 2, 1969 are used, the following conversions apply:

1 kp	= 9.80665	N ,
1 cP	= 0,001	Pa·s ,
1 kp·s/mm^2	= 9,81·10^6	Pa·s ,
1 cSt	= 10^{-6}	m^2/s .

NOTATION TABLE (CONTINUED)

		Units	Units According to Law of July 2, 1969
i	Numerical quantity in the x direction		
i*	= b/s- Number of grid points along the semiaxis b		
imin	Limitation of the field at the inlet		
imax	Limitation of the field at the outlet		
iw	Numerical quantity for deformation in the x direction		
j	Numerical quantity in the y direction		
j_{min}	Sideways limitation of the field		
j_{max}	Sideways limitation of the field		
jw	Numerical quantity for deformation in the y direction		
l	Length of the cylinders for line contact	mm	
m	Number of the equation in the matrix		
m_r	Relative error during measurements		
n	Number of unknowns in the matrix		
n	Rotation rate	l/min	
p	Area pressure	kp/mm^2	N/mm^2

NOTATION TABLE (CONTINUED)

		Units	Units According to Law of July 2, 1969
p_o	Hertz pressure	kp/mm^2	N/mm^2
p_m	Average area pressure according to Hertz	kp/mm^2	N/mm^2
q_f	Measure of the hydrodynamic pressure	kp/mm^2	N/mm^2
r	Polar coordinate		
r	Distance between pressure point and deformation point	mm	
s	Step length	mm	
t	Time unit	sec.	
u	Velocity of the flowing medium in the x direction	m/sec.	
v	Velocity of the flowing medium in the y direction	m/sec.	
w	Velocity of the flowing medium in the z direction	m/sec.	
w	Elastic deformation	mm, µm	
w'	Elastic deformation for i = iw, j = jw	mm	
w_o	Elastic deformation at the centerpoint of the contact surface	mm	
x	Coordinate in the roll direction		
y	Coordinate perpendicular to the roll direction and normal force		
z	Coordinate in direction of normal force		

NOTATION TABLE (CONTINUED)

		Units	Units According to Law of July 2, 1969
A	Pressure ellipse area	mm^2	
A_i	Exponent for determining the lubrication film thickness		
C	Capacity	pF, F	
E	Modulus of elasticity	kp/mm^2	N/mm^2
E'	$= 2 / \left[\frac{1-\nu_1^2}{E_1} + \frac{1-\nu_2^2}{E_2} \right]$		
	Reduced elasticity modulus	kp/mm^2	N/mm^2
F	Normal force	kp	N /8
F_1-F_3	Coefficient for establishing the pressure matrix	1/mm	
F_{11}-F_{33}	Dimensionless coefficient for establishing pressure matrix		
G	Material and lubrication material parameter		
H	Parameter for determining the lubrication film thickness		
H_{11}-H_{33}	Dimensionless coefficients for establishing the contour matrix		
I	Current intensity	A	
K	Hertz constant		
M	Number of grid points in the i direction		
N	Number of grid points in the j direction		
N_1-N_3	Parameter for determining the lubrication film thickness		

NOTATION TABLE (CONTINUED)

		Units	Units According to Law of July 2, 1969
P	p/p_o - dimensionless area pressure		
R	Ohm resistance	V/A	
R	Radius of the roller body	mm	
R_x	$1/(1R_1 + 1/R_2)$ replacement radius for the x direction	mm	
R_y	$1/(1/R_3 + 1/R_4)$ replacement radius for the y direction	mm	
S	Distance between the undeformed contour from the center point of contact	mm	
U	Voltage	V	
U	$0.5 \cdot (U_1 + U_2)$ Velocity of the roller in the roll direction	m/sec	
U'	Velocity of the roller in the roll direction	mm/sec.	
$\bar{U}$	Velocity parameter		
V	Velocity of the roller in the y direction	m/sec	
W	Load parameter		
X	External forces in the x direction applied to the liquid	kp/mm^3	N/mm^3
Y	External forces in the y direction applied to the liquid	kp/mm^3	N/mm^3

NOTATION TABLE (CONTINUED)

		Units	Units According to Law of July 2, 1969
z	Forces in the z direction applied to the liquid	kp/mm^3	N/mm^3
α	Pressure coefficient	mm^2/kp	mm^2/N
δ	Hertz deformation	mm	
ε	Relative Dielectric constant		
ε_o	$8.854 \cdot 10^{-12}$ Absolute dielectric constant	$A \cdot s/V \cdot m$	
η	Dynamic viscosity	cP	$Pa \cdot s$
η	Hertz coefficient		
η_o	Dynamic viscosity at atmospheric pressure	cP	$Pa \cdot s$
η'_o	Dynamic viscosity for atmospheric pressure	$kp \cdot s/mm^2$	$Pa \cdot s$
ϑ	Auxiliary angle of Hertz		
ϑ	Temperature	^oC	
ν	0.3 - Poisson ratio		
ν	Kinematic viscosity	cSt	m^2/s
ξ	Hertz coefficient		
ρ	Lubrication material density	kg/dm^3	
ρ_o	Lubrication material density at atmospheric pressure	kg/dm^3	
φ	Polar coordinate		
ψ	Ellipticity factor of Archard		
ω	Angle between the Hertz reference planes		

NOTATION TABLE (CONTINUED)

All formula symbols which occur in other dimensions or are used only once for formulas from the literature are explained in the text and have an asterisk.

INVESTIGATIONS ON ELASTOHYDRODYNAMICAL LUBRICATION FILM THICKNESS FOR ELLIPTICAL HERTZ CONTACT SURFACES *

Peter Brüser **

*** / 11

1. INTRODUCTION

1.1 Elastohydrodynamic lubrication

When two elastic roller bodies roll off of each other and when a normal force presses them together, a flattening occurs. In general, an elliptical contact area is produced which is described by the theory of Hertz. Because of the deformation and as a consequence of the difference in the radii of curvature, tangential variations of various magnitudes occur even in the case of pure rolling motion. At certain points of the contact area, this leads to microscopic slipping. In the other points of the surfaces, there is no relative motion. The contact area produced under the load can therefore always be divided into adhesion and slipping regions. The slipping portion can be considerably larger, if an external circumferential force is to be transferred or if the bodies carry out a rotational motion around the normal to the contact point, which is superimposed on the pure rolling motion. Therefore, rolling free of slip is

---

* Dissertation approved by the Mechanical Engineering and Electrical Technology Faculty of the Carolo-Wilhelmina Technical University Braunschweig.

** From Braunschweig

*** Numbers in the margin indicate pagination of original foreign text.

only a theoretical possibility and would assume that the cylindrical bodies were not loaded at all.

In order to be able to use rollers over extended time periods without damage, it is necessary to use a lubricating agent. This reduces the number of metallic contact points between the surfaces sliding with respect to each other and therefore it reduces the friction and wear. The type and amount of lubrication agent depends on the application being considered and on the surrounding conditions. At a large circumferential velocity, the lubrication agent between the rollers results in a hydrodynamic lubricating film, which partially or completely separates the surfaces. Under a high load, when investigating this lubrication film thickness, the elastic deformation of the bodies in contact and the changes in the oil viscosity and density with pressure must be considered. This type of lubrication / 12
in which there is an equilibrium state between the hydrodynamic pressure in the lubricant and the contact pressure in the elastic rollers is called elastohydrodynamic lubrication.

1.2 Influence of lubrication on the friction, wear and lifetime of rollers

The type of lubrication and in particular the thickness of the lubricating film have a considerable effect on the running behavior of the rollers. Since microscopic slipping exists, we can explain why not only the friction moment but also the wear of the surfaces is very greatly determined by the state of lubrication. For example, wear measurements after 100 hours of operation were made [1] for groove ballbearings which were operated using mineral oils having different viscosities. In spite of the fact that the load and the rotation rate was held constant, it was possible to establish a clear decrease in the wear when

the viscosity was increased.

Investigations over the last few years have shown that when the lubrication film is well developed, the lifetime of the rollers, i.e., the time elapse up to the first damage to the surface (pitting) can be extended. Thus Zaretzky, Sibley and Anderson [2] and later on the works of Zaretzky and Anderson [3] and Sibley [4] established that the fatigue lifetime also increases when viscosity, pressure coefficient α or the velocity are increased. This means that the lifetime increases with increasing elastohydrodynamic lubrication film thickness. The authors arrived at the direct relationship

$$\text{roller fatigue} \sim (h_{min})^{n^*},$$

where no certain numerical values have yet been found for the exponent n*.

Dawson [5,6,7], found a unique relationship between the film thickness and the number of roller revolutions which occur up to the first signs of pitting. Tallian, McCool and Sibley / 13
[8] proved that under otherwise equal conditions, the life time of spheres lubricated with mineral oil can be considerably increased by either increasing the circumferential velocity or by increasing the viscosity.

These results can be explained by stating that the elastohydrodynamic lubrication film reduces the friction and therefore the tangential stresses which are applied at the contact groove. This is especially important for large loads. The wear will decrease and the lifetime will increase the better the two surfaces are separated by a lubricating film. This means that an accurate description of the elastohydrodynamic lubrication processes

between two rollers is very important. In this way, it will be possible to avoid early damage. /14

2. STATE OF KNOWLEDGE

2.1 Theoretical investigation

As already mentioned, the theoretical treatment of the elastohydrodynamic lubrication problem means that the hydrodynamic laws of the liquid medium developed by Reynolds will have to be described in conjunction with the elastic properties of the rollers. In addition, there are the relationships between the density, pressure and temperature of the lubricating agent, and the relationships between the viscosity, pressure and temperature. In addition, thermal processes such as heat transfer at the surfaces and heat conductivity within the liquid have an influence. In our work, we were primarily interested in determining the smallest lubrication film thickness, because this is the most important variable for evaluating lubricated machine components.

2.1.1 Line contact

Most investigations of this relatively new area consider only the line contact between two infinitely long cylinders. Many cases found in practice can be reduced to these conditions. By ignoring the oil removal to the side, the problem becomes two-dimensional which is a considerable simplification.

The first result for hydrodynamic lubrication between rollers was presented in 1916 by Gümbel von Martin [9]. Assuming rigid bodies and an incompressible lubricating agent with constant viscosity he found the following lubrication film thickness at the center

$$\frac{h_o}{R} = 4.9 \cdot \frac{\eta_o' \cdot U'}{F/l} \quad . \qquad (2.1)$$

This formula was confirmed by other authors, such as for example by Peppler [10] in 1938. He investigated its applicability for highly loaded blowers in which there are elastic deformations. /15

Since investigations on the very substantial influence of pressure on the viscosity and density of the oil were available (see chapter 4.2), these laws were first considered together by Ertel. After his death, the work was considered by his collaborator, Grubin [11] and was published in 1949.

By using the simplifying assumptions according to which the shape of the surface outside of the Hertz contact zone is not changed by the hydrodynamic pressure of the lubricant, that the bodies are separated by a parallel film having a thickness h within the pressure zone, and that the pressure increases sharply in the inlet zone, Figure 2.1, he reached the following dimensionless result

$$\frac{h_o}{R} = 1.95 \cdot (\alpha \cdot E')^{8/11} \cdot \left[\frac{\eta_o' \cdot U'}{E' \cdot R}\right]^{8/11} \cdot \left[\frac{F}{l \cdot E' \cdot R}\right]^{-1/11} \quad . \qquad (2.2)$$

With this formula, lubrication film thicknesses are obtained which are 50 - 100 times larger than obtained with the formula of Martin. This is a characteristic feature of the large influence of the elasticity and the influence of the lubricant properties which depend on pressure.

/ 16

Crook [12] used a similar model and obtained the result

$$\frac{h_o}{R} = 2.14 \cdot (\alpha \cdot E')^{3/4} \cdot \left[\frac{\eta_o' \cdot U'}{E' \cdot R}\right]^{3/4} \cdot \left[\frac{F}{l \cdot E' \cdot R}\right]^{-1/8} \quad . \qquad (2.3)$$

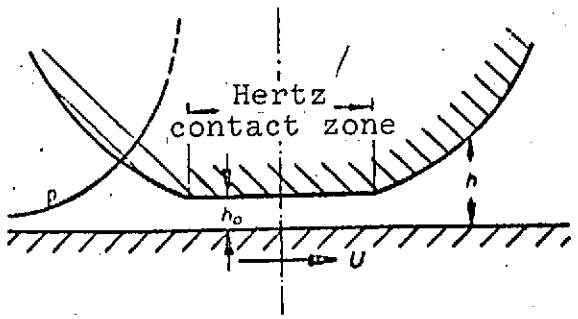

Figure 2.1. Model of Ertel-Grubin of the elastohydrodynamic lubrication problem.

The elastohydrodynamic lubrication problem was then subsequently treated by a number of authors. Most investigations were based on the results of Weber and Saalfeld [13], which found a closed form solution for liquids with constant and pressure-dependent viscosity. They used an analytical method. They assumed a pressure distribution and then solved the hydrodynamic and deformation equations. In other words, they calculated the film thickness and compared the resulting new pressure distribution with the assumed distribution. Dowson and Higginson [14, 15, 16] used this iterative method and numerical methods and arrived at the formula

$$\frac{h_{min}}{R} = 1{,}6\cdot(\alpha\cdot E')^{0.6}\cdot\left[\frac{\eta_o'\cdot U'}{E'\cdot R}\right]^{0.7}\cdot\left[\frac{F}{1\cdot E'\cdot R}\right]^{-0{,}13}. \qquad (2.4)$$

In the latter paper, the compressibility of the oil was considered in addition to the pressure dependence of the viscosity. Archard, Gair and Hirst [17] obtained similar results. They divided the pressure zone into four regions and solved the system of equations numerically for each zone. Stephenson and Osterle [18] used the direct method. They prescribed a film thickness and calculated pressure distribution from it.

The results obtained up to the present assumed isothermal conditions. Therefore, they are limited to rollers carrying out a pure rolling motion. If, in addition, there is a forced sliding motion, that is, a macroscopic sliding at the contact area, it is no longer permissible to ignore the thermal influences

such as heat conductivity in the lubricant and heat transfer at the surfaces. Papers on this subject have been published by /17
Cheng [19, 20, 21], Wernick [22], Cheng and Sternlight [23]; Dowson and Whitaker [24] and Liesegang [25] have written on this topic. It was found that the direct iterative solution [18] is only applicable for small loads. The so-called inverse path must be used for larger loads, which was first described in [13]. The influence of temperature was found to be extremely small on the magnitude of the film thickness in the contact zone. However, temperature does considerably influence the shape of the pressure profile.

Herrebruch [26] made another attempt for solving this problem. He assumed isothermal conditions and combined the hydrodynamic and elastic equations into an integral equation assuming constant viscosity. He then solved this equation numerically.

2.1.2 Point contact

The problem referred to here has the somewhat inaccurate name of "point contact". This is the elastohydrodynamic lubrication problem of circular and elliptical Hertz contact areas. The theoretical investigations are only just beginning. Howlett [27] and later on Kapitsa [28] were the first to apply the Reynolds equation to the lubrication between a sphere and a plane. Kapitsa assumed simplifying boundary conditions in 1955 and did not consider elastic deformations. Assuming constant viscosity, he arrived at the result

$$\frac{h_0}{R_x} = 113.5 \cdot \left[\frac{U' \cdot \eta_0'}{F/R_x}\right]^2 . \qquad (2.5)$$

Recently Lutz [29] wrote a paper in which substitutions were made for the crack height and the hydrodynamic pressure in the Reynolds equation. This equation was then replaced by a new differential equation which can be solved in closed form for the the sphere-plane problem, assuming small loads and constant lubricant viscosity. Archard and Cowking [30] used the well known results /18 for line contact to develop a first simplifying elastohydrodynamic theory for point contact. They first compared the classical solutions for point and line contacts for rigid bodies, and from this they derived a factor ψ for the lateral oil flow. It is defined as follows

$$\psi = \left[1 + \frac{2 \cdot R_x}{3 \cdot R_y}\right]^{-1} . \tag{2.6}$$

This factor was applied to the well known elastohydrodynamic formulas for line contact. Therefore they consider the problem of elliptical contact surfaces as a series of line contacts. In each case, the pressure is reduced by the constant factor ψ because of the sideways oil flow. They thus arrived at the formula

$$\frac{h_o}{R} = 2{,}04 \cdot \psi^{0.740} \cdot \left[\frac{\alpha \cdot \eta_o' \cdot U'}{R}\right]^{0.740} \cdot \left[\frac{F}{E' \cdot R^2}\right]^{-0.074} . \tag{2.7}$$

For simplifying boundary conditions, they also found the following solution for circular contact areas

$$\frac{h_o}{R} \sim \left[\frac{\alpha \cdot \eta_o' \cdot U'}{R}\right]^{3/4} \cdot \left[\frac{F}{E' \cdot R^2}\right]^{-1/12} . \tag{2.8}$$

Both solutions are based on the models of Ertel-Grubin according to which the surface contour is not modified by the lubricant film.

Using the same assumptions Cameron and Gohar [31] arrived at the following result for low load levels and for circular contact area

$$\frac{h_o}{R} = 5.81 \cdot \frac{\alpha \cdot \eta_o' \cdot U'}{R} \cdot \left[\frac{F}{E' \cdot R^2}\right]^{-1/3} . \qquad (2.9)$$

Cheng [32] gave another way of determining the elastohydrodynamic lubricant film thickness in 1970. He solved the coupled system of equations separately by first calculating the deformations using the Hertz equations. He then applied the Reynolds equation to this geometry. This means that he used the Ertel-Grubin model. He did not consider a change in the lubricant density. He assumed an exponential law for the viscosity change, which can be applied for oils based on naphtha. (See chapter 4.2). He then found the result

/ 19

$$\left[\frac{h_o}{R_x}\right]^{2-n^*} = 12 \cdot C^* \cdot \frac{\alpha \cdot \eta_o' \cdot U'}{R_x} \cdot \frac{b}{R_x} \cdot \left[\frac{3F}{2\pi \cdot E' \cdot a \cdot R_x}\right]^{-n^*} \qquad (2.10)$$

or for elliptical areas

$$\frac{h_o}{R_x} = \left[12 \cdot C^* \cdot \frac{\alpha \cdot \eta_o' \cdot U'}{R_x}\right]^{\frac{1}{2-n^*}} \cdot \left[\frac{b}{R_x}\right]^{\frac{1-n^*}{2-n^*}} \cdot \left[\frac{p_o}{E'}\right]^{\frac{-n^*}{2-n^*}} . \qquad (2.11)$$

The constants were found numerically as a function of the axis ratio a/b (Table 2.1).

TABLE 2.1. FACTORS IN EQUATION (2.11) OF CHENG

a/b	C*	n*
0.5	0.065	0.548
1.0	0.088	0.620
2.0	0.095	0.642
5.0	0.098	0.648

The film thickness found decreases with increasing R_x/R_y, in proportion to the thickness for line contact. However, the difference is extremely small up to $R_x/R_y = 1$ (circular contact area).

2.2 Experimental investigations

2.2.1 Measurement methods

Since the first publications on elastohydrodynamic theories by Ertel and Grubin, a number of research centers have attempted to experimentally determine the lubricant film thickness between two rollers. The experiments were mostly done for line contact, but the measurement methods used can be used for the general case as well.

2.2.1.1. Measurement of the ohmic resistance

The oldest method is the simple resistance measurement, which was applied in 1952 by Lane and Hughes [33] for the first time, using a measurement voltage of 0.2 V. This voltage was later on reduced to 10-25 mV, in order to avoid the nonlinearity of the resistance, which is characterized by the non-ohmic nature of the oil for large currents and voltages. The most extensive study in this area was made by Crook [34] in 1957. He found that the resistance fluctuates so greatly with the humidity content of the oil, that it is not possible to give quantitative results. He also showed that the temperature has a considerable influence on the resistance and therefore on the measurement results. This dependence on the humidity content can be prevented by working in an absolutely dry atmosphere or by adding components which reduce the resistance in a corresponding way. This then eliminates this deviation. El-Sisi and Shawki [35] made such an attempt. / 20

Another difficulty with this measurement method is the fact that the ohmic resistance depends on pressure and temperature. It is assumed that the resistance depends on the number of charge carriers and their mobility.

The last paper using this measurement method was written by Furey [36]. The percentage fraction of the maximum resistance which appears on an oscillograph is a measure for the separation of both contact surfaces caused by the lubricant.

/21

2.2.1.2 Measurement of voltage arcing

In another method, the voltage and current intensity were measured for which voltage arcing occurs for a certain film thickness. Cameron [37] in his investigations found that at current intensities up to 0.5 A, oil behaves like an ohmic resistor to a good degree of approximation. The measurements were found to be quite independent of the type of oil, because the current is primarily carried by CH_{2-} and CH_{3-} molecules, and their fraction does not differ much for the various oil types. Even small parts of water in the oil do not influence the measurement results. In later papers by Siripongse, Rogers, Cameron [38], and Mac Conochie, Cameron [39], the measurement methods were improved.

Crook [40] described the inaccuracies associated with this method compared with other methods.

2.2.1.3. Optical measurement methods

Transparent rollers and optical measurement methods were used in another method for determining the film thickness. Bell [41] used transparent gelatin bodies and determined the film thickness from the light absorption of the lubricant films. Archard and Kirk [42] used crossed cylinders made of plexiglass and determined the film thickness from the different colorings of the interference rings. Gohar and Cameron [43] pressed a rotating steel sphere against the glass plate with an extremely high index of refraction. In this case the film thickness was determined

with the aid of the Newton rings.

There are considerable difficulties associated with the optical measurement methods. First of all, most transparent material, such as for example glass, have an index of the fraction which is very close to that of normal lubricants, so that it is not easy to establish any difference. In addition, it is difficult to store glass. On the other hand, when plexiglass / 22
or other plastic materials were used, the elasticity modulus is so small that the pressure-viscosity effect does not occur. However, one advantage is that with this method, it is possible to determine the film thickness as well as the shape of the lubricant film.

2.2.1.4 Measurements with x-rays

Another method which provides both qualitative results on the smallest lubricant film thicknesses in addition to the possibility of determining the shape of the oil film was developed in 1961 by Sibley and Orcutt [44]. It consists of directing a parallel, monochromatic bundle of x-rays tangentially with respect to the contact point of the lubricated rollers. The number of x-rays which penetrate through the crack are measured with a Geiger counter and is a measure for the thickness of the oil film. The wavelength of the x-rays was selected so that the lubricant is completely penetrated, but the metallic surfaces absorb the rays. In this measurement method, the ray bundle is fixed and the machine with the rotating bodies is moved slowly and parallel to the axes. The exact alignment of the apparatus is one difficulty with this method.

In a recent publication by Bell and Kannel [45], this method was also applied for disks with curved surfaces, to simulate the roller bodies.

The method provides good results. However, it is quite costly because of the expensive measurement installations and the extensive safety devices.

2.2.1.5 Capacitive measurements

One additional method of determining the film thickness consists of measuring the capacitive resistance between two roller surfaces, which are separated by a lubricant film which acts like a dielectric. This principle was first developed by Lewicki [46]. He stated the advantages of this method over the resistance measurements in his paper. /23

Crook [40] carried out extensive capacity measurements for low load levels. Crook used a method which is independent of the deformation of the cylinders. He took advantage of the fact that the oil continues to adhere to the surfaces when it passes the crack. Crook used stationary slides which had low load levels and which were immersed in these oil films. He determined the capacity between the slides and the metallic rollers. From these results he calculated the amount of oil between the bodies and estimated the film thickness at the maximum pressure point.

Christensen [47, 48] presented an interesting variation of this slide technique. The amount of oil and therefore the film thickness were measured as a function of the slide displacement using an inductive transducer.

The direct capacity measurements between two surfaces carried out by Archard and Kirk [49], Hashimoto [50] and Dyson, Naylor and Wilson [51] gave more accurate results, especially for larger loads and for point contact. Many attempts have been made to determine the local film thickness during a contact pass using capacitive measurement methods. For example Kodnir [52] determined the capacity between an isolated electrode and a body of revolution made of bakelite and whose surface was covered with a thin tin foil. The capacity increases when the electrode is activated. Therefore, this is a measure for the distance between the two disks.

In Crook's [53] experiments, a glass disk was rotated which had a thin chromium thread on the surface. It was rotated together with a steel disk. A similar method was used by Cheng and Orcutt [54]. They used a thin platinum thread on a glass disk and a steel disk as the electrodes.

/ 24

Except for the laborious measurements using x-rays, the capacity method provides the best results. The direct measurement between the surfaces is especially appropriate when installed in real machines. However, the capacity values determined must be carefully converted to distance values, especially when the deformation of the surfaces must be taken into account for higher load levels.

2.2.2 Measurement results

2.2.2.1 Line contact

There are a large number of publications on lubricant film thickness measurements for elastohydrodynamic contact with line contact. First of all there are reports from four research institutes, which have extensively concerned themselves with these

type of measurements:

a) Research Laboratory, Associated Electrical Industries, Aldermaston, Berkshire, England:

The first systematic measurements were carried out by Crook [12, 40] in 1961. He used a two disk test stand and measured the lubricant film thickness using the capacitive resistance between disks and slides. Crook established that reasonable results can only be obtained if the lubricant film viscosity η_o at the surface temperature is taken into consideration. With this assumption, he found the following load-dependent result for loads between 7.15 kp/mm up to 20.4 kp/mm and for a disk diameter of 76.2 mm:

$$h_o^* \ [\mu m] = 0.08 \cdot (U^* \ [cm/sec] \cdot \eta^* \ [P])^{0.5} . \qquad (2.12)$$

With these dimensions, we arrive at the following result /25

$$\frac{h_o}{R} = 4.2 \cdot 10^{-6} \cdot (U \cdot \eta)^{0.5} . \qquad (2.13)$$

The velocity was varied between 0.03 up to 10 m/sec and the viscosity was varied between 14 to 119 cP. All measurement results agreed with the formula given above with an accuracy of ± 15%.

b) Battelle Memorial Institute, Columbus Ohio, USA:

Sibley and Orcutt [44] used x-rays in their investigations for measuring the lubricant film thickness between two disks. They arrived at the result

$$\frac{h_o}{R} = 0.112 \cdot \left[\frac{a \cdot \eta_o' \cdot U'}{R}\right]^{0,727} \cdot \left[\frac{F}{1 \cdot E' \cdot R}\right]^{-0,364} . \qquad (2.14)$$

c) Technical University, Trondheim, Norway:

Using the slide displacement method, Christensen [48] determined the following formula which uses the oil flow rate. The smallest film thickness between two rotating disks with a diameter of 80 mm is given by

$$h_o^* \,[\mu m] = 0.7 \cdot (F^* [dyn/cm])^{-0.2} \cdot (\eta^* [P] \cdot U^* [cm/sec])^{0.83} . \qquad (2.15)$$

When transformed, we find

$$\frac{h_o}{R} = 1,4 \cdot 10^{-6} \cdot \left(\frac{F}{I}\right)^{-0.2} \cdot (\eta_o \cdot U)^{0.83} . \qquad (2.16)$$

The experiments were carried out at velocities between 0.6 and 6.7 m/sec and loads between 2.5 and 20.4 kp/mm with a constant oil viscosity of η_o = 13 cP.

d) Shell Research, Thornton, Chester, England:

In the very expensive experiments of Dyson, Naylor and Wilson [51] the capacity was directly measured between two 76.2 mm diameter disks. The following result was found for various oil types for velocities between 0.4 and 6 m/sec and for loads between 2.2 and 26 kp/mm

$$\frac{h_o}{R} = 0.029 \cdot (U \cdot \eta_o)^{0.65} \cdot (\alpha^* [cm^2/dyn])^{0.56} \cdot \left[\frac{F}{1 \cdot E' \cdot R}\right]^{-0,15} . \qquad (2.17)$$

/26

Again we obtained the result

$$\frac{h_o}{R} = 9,707 \cdot 10^{-7} \cdot (U \cdot \eta_o)^{0.65} \cdot \alpha^{0.56} \cdot \left[\frac{F}{1 \cdot E' \cdot R}\right]^{-0,15} . \qquad (2.18)$$

2.2.2.2. Point contact

Only few measurement results are available for point contact. These are almost exclusively measurements with circular contact areas of both rollers.

Cameron and Gohar [31] determined the film thickness between a steel sphere (25.4 mm diameter) and a glass plate using interference rings. They compared the measurement results for maximum Hertz pressures up to 50 kp/mm^2 and for velocities up to 0.5 m/sec with the theoretically determined dimensionless equation (2.9),

$$\frac{h_0}{R} = 5{,}81 \cdot \frac{\alpha \cdot \eta_0' \cdot U'}{R} \cdot \left[\frac{F}{E' \cdot R^2}\right]^{-1/3} ,$$

and found good agreement between the exponents with a maximum deviation in absolute film thickness of ± 50%.

Tallian, Brady, McCool and Sibley [55] did not arrive at a single unique formula. They found that the film thickness is an exponential function of velocity. For partially elastohydrodynamic lubrication, this exponent changes with the load and lubricant. For complete lubrication we have

$$h \sim (\eta_0 \cdot U)^{x^*} . \qquad (2.19)$$

Archard and Kirk [49] used two crossed cylinders with the same diameter and making an angle of 90° in their experiments. They attempted to simulate point contact with circular contact surfaces. When the two velocities U* of the rollers are the same, the /27
average circumferential velocity is

$$U = \frac{\sqrt{2}}{2} \cdot U^* \qquad (2.20)$$

The authors used various measurement methods. They obtained the following formula for the direct capacity measurement between the two cylinders.

$$h\,[cm] = 0.203 \cdot (\alpha \cdot \eta_o\,[sec])^{0.57} \cdot (U\,[cm/sec])^{0.55} \cdot (R\,[cm])^{0.62} \qquad (2.21)$$

The experiments were carried out for

$$R = 3 \div 40 \text{ mm},$$
$$U^* = 0{,}01 \div 5 \text{ m/sec}$$

and

$$\alpha \cdot \eta_o = (0.8 \div 10) \cdot 10^{-9} \text{ sec}.$$

This can be rewritten as follows

$$h_o = 1{,}24 \cdot 10^{-5} \cdot (\alpha \cdot \eta_o)^{0.57} \cdot U^{0.55} \cdot R^{0.62} . \qquad (2.22)$$

In later experiments [30], they varied the diameter of the two cylinders, in order to investigate the influence of an elliptical contact surface. By using the ellipticity factor ψ defined in equation (2.6) in order to consider the sideways oil flow

$$\psi = \left[1 + \frac{2 \cdot R_x}{3 \cdot R_y}\right]^{-1} ,$$

and for one oil viscosity value and for the velocities

$$U = 0{,}09 \text{ m/sec} \quad \text{and} \quad U = 0{,}675 \text{ m/sec}$$

the formula

$$h_{Ellipse} \approx 1{,}6 \cdot \psi^{0.93} \cdot h_{circle} \qquad (2.23)$$

R_x/R_y was varied between 0.295 to 11.9, so that the factors varied between $\psi = 0.112$ up to $\psi = 0.835$.

2.3 Collection of results

The theoretical results can be expressed in terms of three-dimensional groups. Table 2.2 gives a summary of the various exponents.

TABLE 2.2. THEORETICAL RESULTS

a) Line contact

$$\frac{h_o}{R} = A_1 \cdot [\alpha \cdot E']^{A_2} \cdot \left[\frac{\eta_o' \cdot U'}{E' \cdot R}\right]^{A_3} \cdot \left[\frac{F}{1 \cdot E' \cdot R}\right]^{A_4}$$

	A_1	A_2	A_3	A_4
Ertel/Grubin (Eq.2.2)	1.95	0.73	0.73	-0.091
Crook (Eq.2.3)	2.14	0.75	0.75	-0.125
Dowson etc. (Eq.2.4)	2.0	0.6	0.7	-0.13

b) Circular contact area

$$\frac{h_o}{R} = A_1 \cdot [\alpha \cdot E']^{A_2} \cdot \left[\frac{\eta_o' \cdot U'}{E' \cdot R}\right]^{A_3} \cdot \left[\frac{F}{E' \cdot R^2}\right]^{A_5}$$

	A_1	A_2	A_3	A_5
Archard etc. (Eq.2.7)	1.40	0.74	0.74	-0.074
Cameron etc. (Eq.2.9)	5.81	1	1	-0.33
Cheng (Eq.2.11)	2.21	0.725	0.725	-0.058

When the maximum Hertz pressure P_o is introduced in the experimental investigations instead of the load defined in various ways, the results can be given in terms of a common formula. Table 2.3 gives a summary of the results and the corresponding parameters.

TABLE 2.3: EXPERIMENTAL RESULTS

$$h_0 = A_6 \cdot \alpha^{A_7} \cdot \eta_0^{A_8} \cdot U^{A_9} \cdot R^{A_{10}} \cdot p_0^{A_{11}}$$

	A_6	A_7 Range F $\alpha \left[\frac{mm^2}{kp}\right]$	A_8 Range F η_0 [cP]	A_9 Range F $U \left[\frac{m}{sec}\right]$	A_{10} Range F R [mm]	A_{11} Range F $p_0 \left[\frac{kp}{mm^2}\right]$
a) Line contact						
Crook (Eq. 2.13)	$8.0 \cdot 10^{-5}$	0 -	0.5 14-119	0.5 0.03-10	0 19.05	0 37-63
Sibley etc. (Eq. 2.14)	$1.58 \cdot 10^{-3}$	0.73 0.07-0.2	0.73 5-22	0.73 7.6-25.4	0 18.29	-0.73 70-126
Christensen (Eq. 2.16)	$8.0 \cdot 10^{-5}$	0 -	0.83 13	0.83 0.6-6.7	0 20.0	-0.4 21-62
Dyson etc. (Eq. 2.18)	$2.87 \cdot 10^{-4}$	0.56 0.1-0.34	0.65 7-310	0.65 0.4-6	0 19.05	-0.3 21-71
b) Point contact (circular contact area)						
Cameron etc. (Eq. 2.9)	$3.17 \cdot 10^{-5}$	1 -	1 180-800	1 0-0.5	0 12.7	-1 0-50
Archard etc. (Eq. 2.22)	$1.24 \cdot 10^{-5}$	0.57 8-98		0.55 0.01-5	0.62 3-40	0 -

/30

3. PROBLEM FORMULATION

A review of the known literature shows that the elastohydrodynamic lubrication problem has already been treated in experiments and in theory in some detail, for the case of line contact, that is, for cylindrical bodies having a large length in which the oil flow to the side can be ignored. Up to the present, no extensive investigations on roller bodies having arbitrary curvatures have been made, that is, no investigations of elliptical Hertz contact surfaces have been carried out. In this paper we will investigate the case which mostly occurs in technology, which is the case of

high loads. There is usually an elliptical contact surface for roller supports as well as for roller gears.

All the theoretical work will use the model of Ertel-Grubin. It is therefore assumed that the elastic deformation of the rollers is not changed when a lubricant is introduced. This very simple model will be tested by a coupled treatment of the system of equations. Mathematically, the problem is defined as follows:

Two bodies having arbitrary radii of curvature R_1 and R_3 or R_2 and R_4, respectively, which are separated by a lubricant film have the circumferential velocities $U_1 = U_2 = U$ in the x direction. This means that they are not subjected to a forced slip during the rolling process. There is no velocity component V in the y direction. There is a load F which is applied perpendicular to the lubricant film. It is an equilibrium with the resultant of the pressure distribution $p(x,y)$. This pressure distribution produces an elastic deformation $w(x,y)$ in the body. The lubricant is assumed to be a compressible medium with variable viscosity, i.e. the density $\rho(x,y)$ and the viscosity $\eta(x,y)$ are also influenced by the pressure distribution. The lubrication crack geometry $h(x,y)$ and the pressure distribution $p(x,y)$ are to be calculated for the problem under discussion. The solution /31 will be found using numerical methods because it seems that it is impossible to find a closed form of mathematical treatment, due to the complicated relationships in the equations and the large number of parameters.

The experiments described in Chapter 2.2.2.2 are only experiments carried out under low loads. The Equation (2.9) based on interference measurements and which applies for circular contact areas is the result of investigations carried out at extremely low velocities to 0.5 m/sec and Hertz pressures up to 50 kp/mm^2. It cannot be immediately applied to cases

which occur in practice. The equation (2.22) did not consider the influence of the loads, and is based on capacitive measurements. Therefore, the measured capacities can be recalculated in a relatively simple way without considering the elastic deformation. Contact areas having various shapes and sizes are produced by crossed cylinders which cross at various angles. The large slip component produced by this arrangement is not considered.

This means that experimental investigations on highly loaded rollers having arbitrary shapes do not exist. For this purpose, a test stand will be developed so that the lubrication film thickness can be determined using a suitable measurement technique and for loads which extend up to the elastic deformation limits. The most important parameters such as oil viscosity, load and circumferential velocity will be varied. Due to the high load, it is necessary to consider the elastic deformations of the surfaces and the pressure dependences of the density and viscosity of the lubricating agent. / 32

4. TECHNICAL-PHYSICAL PROPERTIES OF THE INVESTIGATED ROLLER BODIES AND LUBRICANTS

The roller bodies and lubricants had to be selected so that they would be suitable for the experiments. In order to be able to make a comparison, we also used this data for the mathematical treatment of the problem.

4.1 Roller bodies

4.1.1 Hertz equations

The general case of the processes which occur during contact of bodies having a curvature in all directions and which are not separated by a lubricant is described by the theory of Hertz

[56]. These are processes which occur under purely elastomechanical processes. For the following assumptions:

- small pressure area compared with the surface area of both bodies,
- isotropic and homogeneous material,
- the proportionality limits are not exceeded
- locally limited displacements and stresses
- forces only perpendicular to the pressure surface,

Hertz found that the pressure variation has the shape of a semi-ellipsoid (Figure 4.1).

This means that the pressure at an arbitrary point is given by

$$p(x,y) = p_o \cdot \sqrt{1-\left(\frac{x}{b}\right)^2-\left(\frac{y}{a}\right)^2} \quad . \tag{4.1}$$

Here b is the semiaxis of the elliptical pressure area in the roll direction (x-direction).

The maximum pressure becomes

$$p_o = \frac{3 \cdot F}{2\pi \cdot a \cdot b} \quad . \tag{4.2}$$

The average pressure is /33

$$p_m = \frac{2}{3} \cdot p_o \quad . \tag{4.3}$$

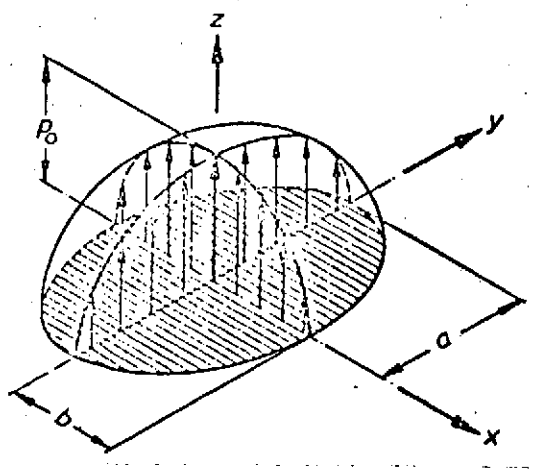

Figure 4.1. Pressure distribution over the elliptical contact area.

The semiaxes are given by

$$a = \xi \cdot \sqrt[3]{\frac{3 \cdot F \cdot R(1-\nu^2)}{E}} , \quad (4.4)$$

$$b = \eta \cdot \sqrt[3]{\frac{3 \cdot F \cdot R(1-\nu^2)}{E}} . \quad (4.5)$$

R is the replacement radius which is formed from the principal radii, that is, the maximum and minimum radii of curvature of two bodies as a contact point. R_1 and R_2 are defined as the radii of the two bodies in a plane perpendicular to the generator (x-z plane) and R_3 and R_4 are the radii of the two bodies in a plane perpendicular to the roll direction (y-z plane). Figure 4.2 shows the principal radii for the example of contact between a sphere and a cylinder.

We have the following equation for the replacement radius /34

$$\frac{1}{R} = \frac{1}{R_x} + \frac{1}{R_y} , \quad (4.6)$$

where

$$\frac{1}{R_x} = \frac{1}{R_1} + \frac{1}{R_2} \text{ and } \frac{1}{R_y} = \frac{1}{R_3} + \frac{1}{R_4} \quad (4.7)$$

The total approach of the two bodies is

$$\delta = 1{,}5 \cdot \frac{2K}{\pi \cdot \xi} \cdot \frac{1-\nu^2}{E \cdot a} \cdot F = 1{,}5 \cdot \frac{2K}{\pi \cdot \xi} \cdot \sqrt[3]{\frac{(1-\nu^2)^2}{E^2} \cdot \frac{F^2}{3R}} . \quad (4.8)$$

The factors ξ, η and $2K/(\Pi \cdot \xi)$ required to calculate the semi-axes and the deformation are given in a table as a function of an auxiliary variable $\cos\vartheta$ which is determined by the following equation [57]

$$\cos\vartheta = \frac{\sqrt{\left(\frac{1}{R_1} - \frac{1}{R_3}\right)^2 + \left(\frac{1}{R_2} - \frac{1}{R_4}\right)^2 + 2\left(\frac{1}{R_1} - \frac{1}{R_3}\right)\left(\frac{1}{R_2} - \frac{1}{R_4}\right)\cos 2\omega}}{\frac{1}{R_1} + \frac{1}{R_2} + \frac{1}{R_3} + \frac{1}{R_4}} \quad . \tag{4.9}$$

The plane containing the radii of curvature R_1 and R_3 and the plane containing the radii of curvature R_2 and R_4 make an angle ω. For the case under discussion here in which the principal radii lie in two mutually perpendicular planes, we have $\omega = 0$ and the equation can be simplified as follows:

$$\cos\vartheta = \frac{\frac{1}{R_1} + \frac{1}{R_2} - \frac{1}{R_3} - \frac{1}{R_4}}{\frac{1}{R_1} + \frac{1}{R_2} + \frac{1}{R_3} + \frac{1}{R_4}} \quad ; \tag{4.10}$$

and $\cos\vartheta$ is positive for $a>b$, according to definition (Figure 4.3).

/36

For hardened steel we have:

Modulus of elasticity $E = 2.12 \cdot 10^4$

Poisson constant $\nu = 0.3$

This means that we find

$$a = \xi \cdot 0.0505 \cdot \sqrt[3]{F \cdot R} \quad , \tag{4.11}$$

$$b = \eta \cdot 0.0505 \cdot \sqrt[3]{F \cdot R} \quad , \tag{4.12}$$

$$p_o = \frac{187.2365}{\zeta \cdot \eta} \cdot \sqrt[3]{\frac{F}{R^2}} \quad , \tag{4.13}$$

$$\delta_{ges} = 1.275 \cdot 10^{-3} \cdot \frac{2 \cdot K}{\pi \cdot \xi} \cdot \sqrt[3]{\frac{F^2}{R}} \quad . \tag{4.14}$$

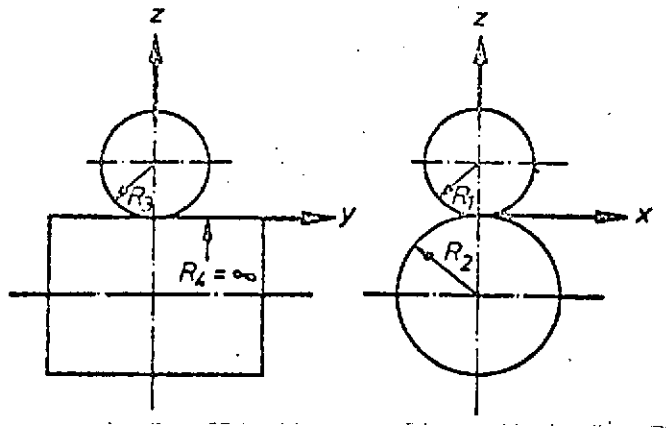

Figure 4.2. Definition of the principal radii of two rollers.

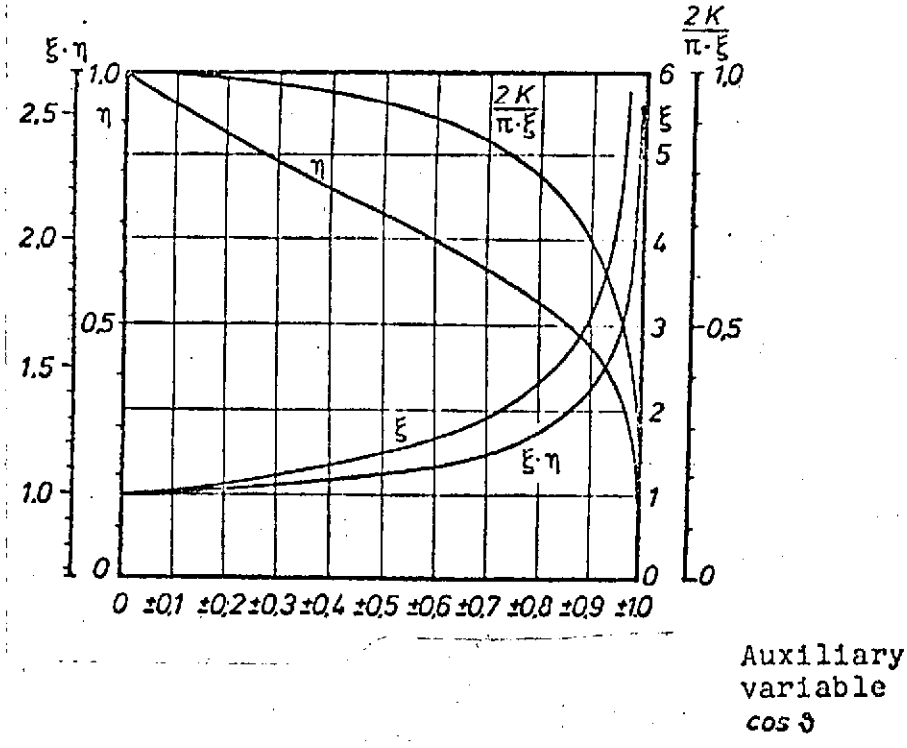

Figure 4.3. Coefficients of Hertz

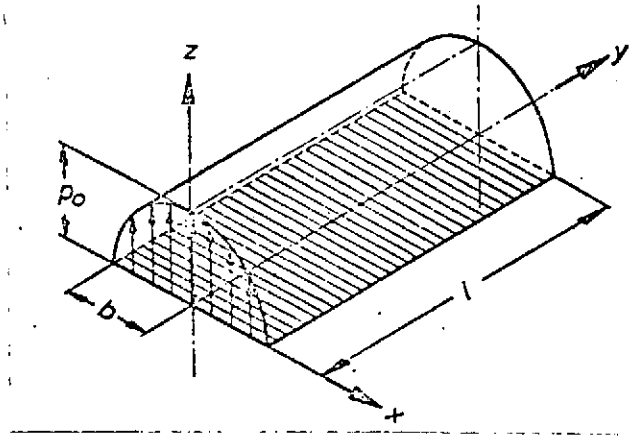

Figure 4.4. Pressure distribution over a rectangular contact area.

For the special case of pure line contact, Figure 4.4, we have the following corresponding equations

$$p(x) = p_o \cdot \sqrt{1-\left(\frac{x}{b}\right)^2} \quad , \tag{4.15}$$

$$p_o = \frac{2 \cdot F}{\pi \cdot b \cdot l} \quad , \tag{4.16}$$

$$p_m = \frac{p_o}{1,27} \quad , \tag{4.17}$$

$$b = \sqrt{\frac{8 \cdot F \cdot R(1-\nu^2)}{\pi \cdot E \cdot l}} \quad . \tag{4.18}$$

/37

For hardened steel we have $p_o = 86,114 \cdot \sqrt{\frac{F}{2 \cdot R \cdot l}}$, (4.19)

$$b = 0,010455 \cdot \sqrt{\frac{F \cdot R}{l}} \quad . \tag{4.20}$$

4.1.2 Geometry and materials

The investigations will determine the thickness of the oil film which forms in the contact zone between two roller bodies having arbitrary shape. This means that the test bodies used must have different curvatures, so that the size and shape of the Hertz contact areas can be varied and so that their influence on the development of the lubrication film and therefore on the elastohydrodynamic lubrication can be determined. / 37

TABLE 4.1: LIST OF TEST BODIES USED*

Principal radii of curvature	R_1	R_2	R_3	R_4	L
Spheres, barrel rollers and cylindrical rollers made of 100 Cr 6	20,625		20,625		
	29,0		29,0		
	14,5		82,0		29,0
	20,5		105,0		38,0
	20,0		118,5		38,0
	19,5		161,0		50,0
	25,5		193,0		45,0
	13,5		294,0		33,0
	13,0		∞		37,0
	16,0		∞		28,5
	20,0		∞		36,0
Opposing body made of 20 Mn Cr 5		47,5		∞	60,0
		47,5		50,0	60,0

* Translator's note: Commas represent decimal points

/38

It is possible to obtain contact areas with almost circular shape up to rectangular shape using the test bodies mentioned in Table 4.1. We only considered the technically interesting cases, in which the semiaxis b in the roll direction is smaller than the semiaxis a. Figure 4.5 shows the combinations investigated.

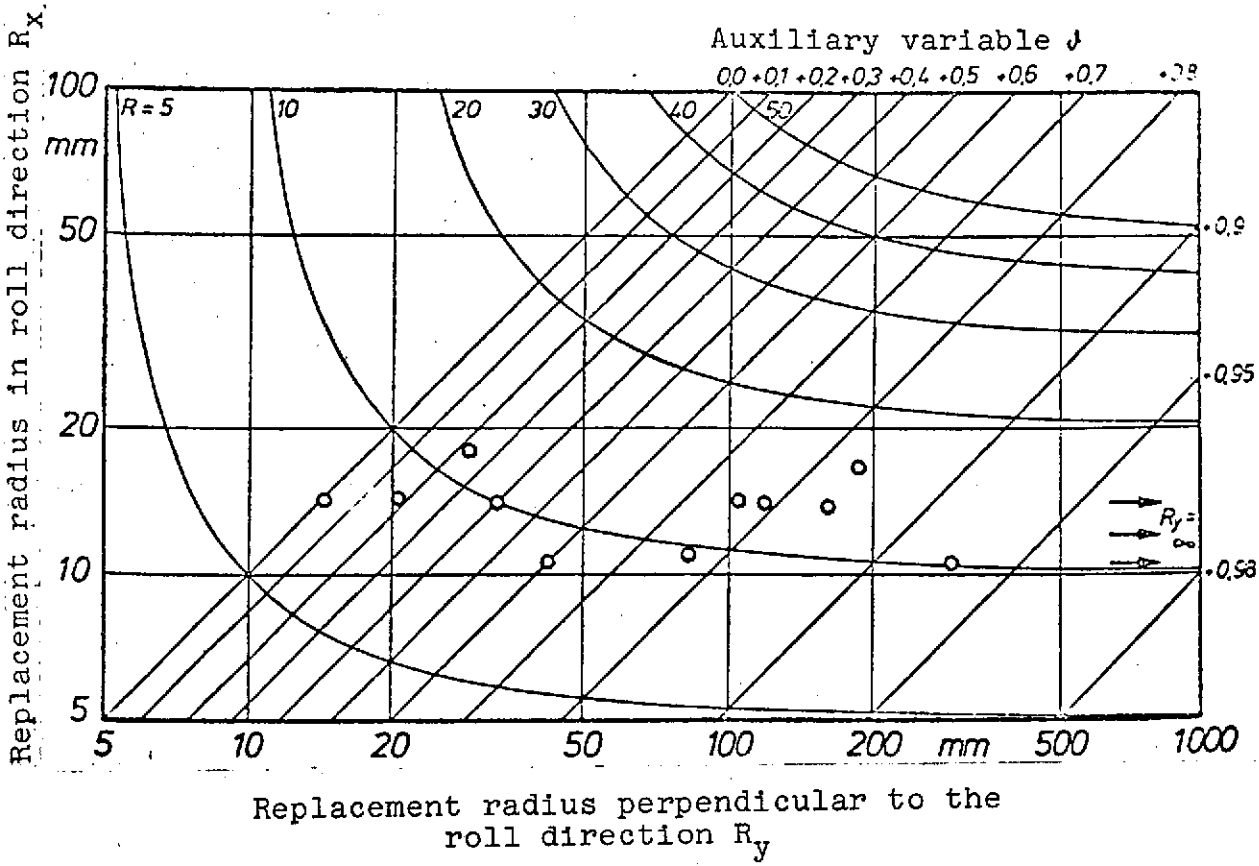

Figure 4.5. Summary of the investigated roller pairs.

We used precision spheres according to DIN 5401 and barrel and cylindrical rollers according to DIN 5402 made of roller bearing steel (100 Cr 6) which were combined with hardened rollers made of 20 Mn Cr 5 having cylindrical or barrel-shaped contours. All test bodies had a hardness of $HR_C \geq 62$. The surfaces were polished and the roughness depth was $R_t \leq 0.2$ µm c.l.a.

We were only able to establish an influence of the surface roughness during the starting up process. After a few minutes, we were not able to find any differences in regard to lubrication film thickness even when the surface characteristics were different, so that we could assume that the surface roughnesses decayed because of the influence of the relatively high loadings.

4.1.3 Loading capacity

During the investigations we wanted to increase the load to the limits of elastic deformation. The transition to the plastic range is not characterized by a sharp boundary. Instead, the permissible area pressure and the osculation surface depend on the specific plastic deformation δ_b/d_w, i.e. the plastic deformation δ_b which occurs at a contact point divided by the roller body diameter d_w. The power law determined empirically which characterizes this dependence is given by [58]
for point contact

$$(p_o)_{zul} = 431 \cdot c_p^{1/3} \cdot \left(\frac{\delta_b}{d_w}\right)^{1/5} \qquad (4.21)$$

and for line contact

$$(p_o)_{zul} = 181 \cdot c_p^{1/2} \cdot \left(\frac{\delta_b}{d_w}\right)^{1/5} . \qquad (4.22)$$ /40

The permissible load for this specific plastic deformation is assumed to be 0.002%. This is a value which is used in the roller bearing industry for calculating the static carrying coefficient for bearings which must run extremely quietly.

The osculation conditions are characterized by the area pressure constant c_p. For point contact we have the following equation

$$c_p = \sqrt[3]{\frac{p_o^3 \cdot d_w^2}{F}} . \qquad (4.23)$$

Using the Hertz relationship given by Equation 4.13,

$$p_o = \frac{187,24}{\xi \cdot \eta} \cdot \sqrt[3]{\frac{F}{R^2}} ,$$

we find

$$c_p = \frac{297,22}{\xi \cdot \eta} \cdot \sqrt[3]{\left(\frac{R_1}{R}\right)^2} . \qquad (4.24)$$

We therefore find the following permissible area pressures for the investigated test bodies

For example:

a) Sphere 41.25 mm diameter and roller 95 mm diameter,

$$c_p = 534.2\ [kp/mm^2]^{2/3} \rightarrow (p_o)_{zul} = 401.7\ kp/mm^2;$$

b) Barrel roller 13.5 mm diameter and roller 95 mm diameter,

$$c_p = 234.5\ [kp/mm^2]^{2/3} \rightarrow (p_o)_{zul} = 305.3\ kp/mm^2.$$

The corresponding formula for the area pressure constant c_p is as follows for line contact

$$c_p = \sqrt{\frac{p_o^2 \cdot d_w \cdot l}{F}} \quad . \tag{4.25}$$

Using the Hertz relationship given by equation (4.19), /41

$$p_o = 86.11 \cdot \sqrt{\frac{F}{2 \cdot R \cdot l}} \quad ,$$

in this case we find

$$c_p = 86.11 \cdot \sqrt{\frac{R_1}{R}} \quad . \tag{4.26}$$

For the example of the cylindrical roller with a diameter of 26 mm and a roller with a diameter of 95 mm, the values are

$$c_p = 97.2\ [kp/mm^2]^{1/2} \rightarrow (p_o)_{zul} = 205.0\ kp/mm^2.$$

4.2 Lubricants

We used Shell-Tellus oil in the experiments. These oils had differing viscosities, so that we had a range of 10-200 cP available for the measurements. These are the paraffin-based oils Tellus 23, Tellus 29, Tellus 41 and Tellus 69. The viscosity index VI is about 95. The oils contain aging additives.

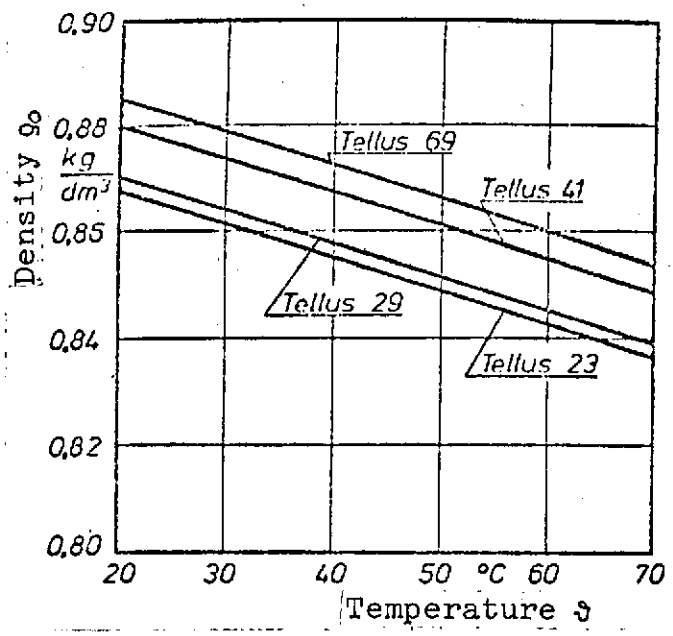

Figure 4.6. Density of the mineral oils used as a function of temperature.

4.2.1 Density

Figure 4.6 shows the dependence of density of these oils on temperature for atmospheric pressure. At the high pressures which exist in the lubricating film, the liquid can no longer be considered as an incompressible medium, i.e. in addition to the temperature dependence, we must also consider the dependence of the density on the pressure. The authors Dowson, Higginson and Whitaker [16] gave the following empirical formula

$$\frac{\varrho}{\varrho_0} = 1 + \frac{0.0057 \cdot p}{1+0.0165 \cdot p} \quad . \tag{4.27}$$

More accurate results were found from formulas which are based on experimental results in ASME investigations [59].

In these experiments, the density and viscosity up to 10,000 atm and up to 220°C were measured for 40 different lubricating oils. /42

Bradbury, Mark and Kleinschmidt [60] summarized these measurements with the following empirical formula:

$$\frac{1}{\varrho} = \frac{1}{\varrho_0}\left[\frac{1}{1-C^*\cdot\Delta T^*} - \frac{1}{n^*}\cdot \ln\left(\frac{p}{m^*/n^*}+1\right)\right] \qquad (4.28)$$

where

$$m^* = m_0^*\left(1+a^*\cdot\Delta\frac{1}{T^*}\right),$$

$$n^* = n_0^*\left(1+b^*\cdot\Delta\frac{1}{T^*}\right).$$

If the density ϱ_0 is known at each temperature, that is, if $\Delta T^* = 0$, the formula, can be simplified to

$$\frac{\varrho}{\varrho_0} = \frac{1}{1-\frac{1}{n_0^*}\cdot\ln\left(\frac{p}{m_0^*/n_0^*}+1\right)}. \qquad (4.29)$$

/43

The average values for the constants are

$$m_0^* = 168.2\ \mathrm{kp/mm^2}$$

and

$$n_0^* = 11.5.$$

We therefore find the following final formula

$$\frac{\varrho}{\varrho_0} = \frac{1}{1-0.087\cdot\ln(0.0684\cdot p+1)}. \qquad (4.30)$$

Hartung [61] found the following dependence based on the ASME investigations:

$$\frac{\varrho}{\varrho_0} = \left[1+\frac{42.8\cdot10^{-6}\cdot\Delta p^*}{(p^*)^{0.25}\cdot\nu^{0.0385}}\right]\cdot\left[1+\frac{\left(\frac{23.2}{(T)^{0.25}}+0.421\right)\cdot10^{-4}\cdot\Delta\vartheta^*}{\varrho_0^{\,2}\left(1+\frac{42.8\cdot10^{-6}\cdot\Delta p^*}{(p^*)^{0.25}\cdot\nu^{0.0385}}\right)}\right]^{-1}. \qquad (4.31)$$

Here we have

p^* = pressure in psi,

$\Delta p^* = p^* - p_0^*$ in psi ,

$\Delta \vartheta^* = \vartheta^* - \vartheta_0^*$ in °F ,

ϑ^*_0 = initial temperature (between 50 and 120°F)

ν = viscosity in cSt for 100 °F ≙ 38 °C .

Since the temperature is assumed to be constant, ϱ_0 can be directed such that $\Delta \vartheta^*$ is equal to zero. For $\Delta p^* \approx p^*$ we find the following simplified equation

$$\frac{\varrho}{\varrho_0} = 1 + \frac{42.8 \cdot 10^{-6} \cdot (p^*)^{0.75}}{\nu^{0.0385}} \qquad (4.32)$$

or

$$\frac{\varrho}{\varrho_0} = 1 + \frac{9.73 \cdot 10^{-3} \cdot p^{0.75}}{\nu^{0.0385}} \qquad (4.33)$$

where p in kp/mm^2 and ν in cSt at 38° C.

This formula (equation 4.33) will be used in the following and a graph is given in Figure 4.7.

4.2.2 Viscosity

Figure 4.8 shows the dependence of viscosity on temperature for the oils used at atmosphere pressure. Here the influence of pressure is considerably greater than for the density. Measurement results only exist up to a pressure of 100 kp/mm^2 and it is necessary to extrapolate for higher loads. The often used exponential law

$$\frac{\eta}{\eta_0} = e^{\alpha \cdot p}$$

gives satisfactory values only for naphthene-based oils (aniline point < 90° C). For this case, Wooster [62] found the following for the pressure coefficient

$$\alpha = 0.06 + 0.0965 \cdot \log \eta_0 \quad ; \qquad (4.35)$$

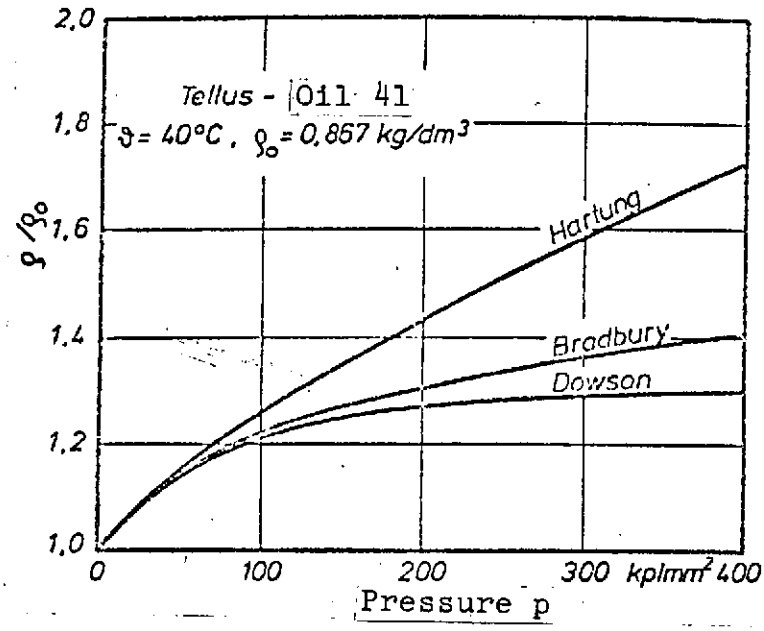

Figure 4.7. Density ratio of mineral oils as a function of pressure.

The viscosity η_0 in cP is to be substituted. For most paraffin-based mineral oils, the exponential law gives values which are much too high. Our results can also be applied to these oils.

Based on the extensive investigations of the ASME [59,63], Chu and Cameron [64] found the following relationship for these oils

$$\frac{\eta}{\eta_0} = (C^* \cdot p + 1)^{n^*} \quad . \tag{4.36}$$

Here we have

$$n^* = 16 \quad ,$$

$$C^* = 0.088 \cdot 10^{a^*} \cdot \eta_0^{-0.062} \quad \text{where } \eta_0 \text{ in cP,}$$

$$a^* = -(0.48 + \frac{1.8 \cdot \vartheta}{400}) \quad \text{where } \vartheta \text{ in } ^\circ\text{C.}$$

Finally, Cameron [65] formulated a law which agrees the best with the experimental results:

$$(\log \eta)^{3/2} = m^*(p + a^*) \quad . \tag{4.37}$$

For $1 < \eta_0 < 6$ cP we have the following equation for m*

$$m^* = (1.3 + 7.1 \cdot \log \eta_0) \cdot 10^{-2} \quad ,$$

for $\eta_0 > 6$ cP we have

$$m^* = 0.076 \cdot \log \eta_0 \quad .$$

The constant a* is found from the initial conditions at atmospheric pressure

$$a^* = 13.2 \cdot \sqrt{\log \eta_0} \quad ,$$

so that this equation for $\eta_0 > 6$ cP is given by

$$\log \eta = 0.18 \cdot (\log \eta_0)^{2/3} \cdot (1.422 \cdot p + 13.2 \cdot \sqrt{\log \eta_0})^{2/3} . \tag{4.38}$$

We will use this formula in the following dimensionless form

$$\frac{\eta}{\eta_0} = \frac{1}{\eta_0} \cdot \exp\left[0.16478 \cdot p \cdot \ln \eta_0 + \sqrt{(\ln \eta_0)^3}\right]^{2/3} \tag{4.39}$$

Figure 4.9 shows a graph. /47

5. BASIC EQUATIONS FOR MATHEMATICAL SOLUTION OF A PROBLEM

The presented elastohydrodynamic lubrication problem for elliptical contact areas is described by the following equations:

a) The Reynolds equation considers the hydrodynamic influences.

b) The deformation equation establishes the relationship between the load and the elastic deformation of the roller bodies.

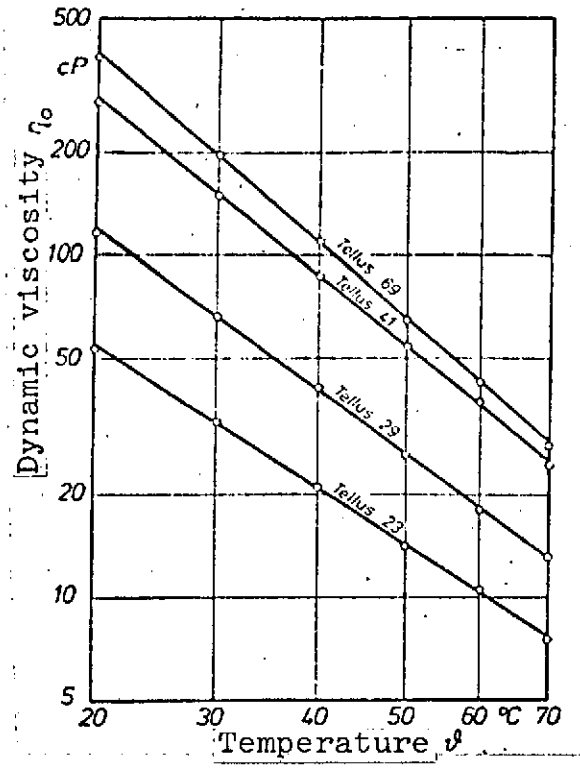

Figure 4.8. Dynamic viscosity of the mineral oils used as a function of temperature

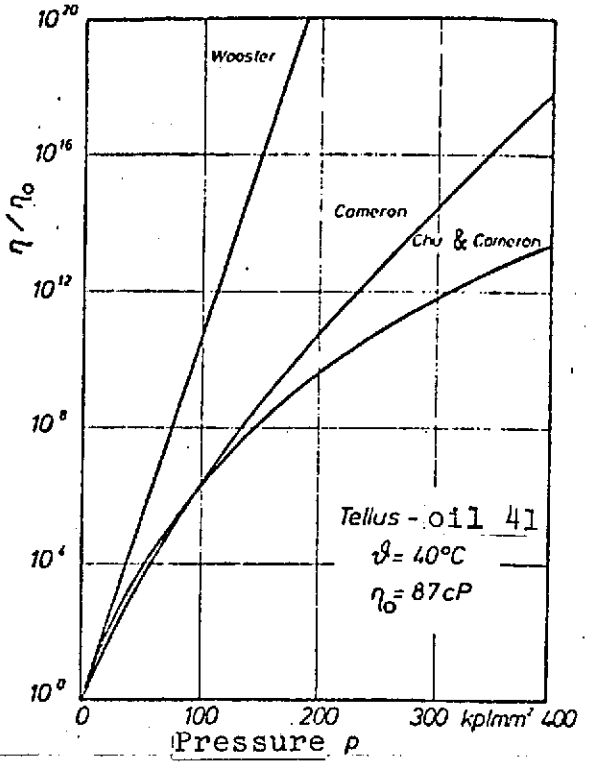

Figure 4.9. Viscosity ratio of mineral oils as a function of pressure

c) The geometric equation describes the various body contours.

d) The state equations of the lubricant describe how the density and the viscosity depend on temperature and pressure, as discussed in Chapter 4.2.

It is not necessary to introduce an energy equation for considering the thermodynamic influences, for the case of pure rolling without forced slipping. Since there is no velocity drop here, there is no heat energy which is produced by

friction energy, so that we can assume isothermal conditions. This hypothesis has already been confirmed in calculations and experiments many times [21, 25, 66].

5.1 Reynolds equation of motion

Assuming that the lubricant has a Newton behavior which is a good approximation for mineral oils [67], and for laminar flow, we may use the Navier-Stokes equations of motion.

These have been given by various authors (for example [65, 68]) and with the notation of Figure 5.1 they are: /48

$$\left.\begin{aligned}
\rho\cdot\frac{Du}{Dt} &= X-\frac{\partial p}{\partial x}+\frac{\partial}{\partial x}\left[2\eta\,\frac{\partial u}{\partial x}-\frac{2}{3}\,\eta\left(\frac{\partial u}{\partial x}+\frac{\partial v}{\partial y}+\frac{\partial w}{\partial z}\right)\right]\\
&\quad+\frac{\partial}{\partial y}\left[\eta\left(\frac{\partial u}{\partial y}+\frac{\partial v}{\partial x}\right)\right]+\frac{\partial}{\partial z}\left[\eta\left(\frac{\partial w}{\partial x}+\frac{\partial u}{\partial z}\right)\right],\\
\rho\cdot\frac{Dv}{Dt} &= Y-\frac{\partial p}{\partial y}+\frac{\partial}{\partial y}\left[2\eta\,\frac{\partial v}{\partial y}-\frac{2}{3}\,\eta\left(\frac{\partial u}{\partial x}+\frac{\partial v}{\partial y}+\frac{\partial w}{\partial z}\right)\right]\\
&\quad+\frac{\partial}{\partial z}\left[\eta\left(\frac{\partial v}{\partial z}+\frac{\partial w}{\partial y}\right)\right]+\frac{\partial}{\partial x}\left[\eta\left(\frac{\partial u}{\partial y}+\frac{\partial v}{\partial x}\right)\right],\\
\rho\cdot\frac{Dw}{Dt} &= Z-\frac{\partial p}{\partial z}+\frac{\partial}{\partial z}\left[2\eta\,\frac{\partial w}{\partial z}-\frac{2}{3}\,\eta\left(\frac{\partial u}{\partial x}+\frac{\partial v}{\partial y}+\frac{\partial w}{\partial z}\right)\right]\\
&\quad+\frac{\partial}{\partial x}\left[\eta\left(\frac{\partial w}{\partial x}+\frac{\partial u}{\partial z}\right)\right]+\frac{\partial}{\partial y}\left[\eta\left(\frac{\partial v}{\partial z}+\frac{\partial w}{\partial y}\right)\right].
\end{aligned}\right\}\qquad(5.1)$$

The left side of the equations include the inertia forces. We have

$$\frac{D}{Dt}=\frac{\partial}{\partial t}+u\cdot\frac{\partial}{\partial x}+v\cdot\frac{\partial}{\partial y}+w\cdot\frac{\partial}{\partial z}\,.\qquad(5.2)$$

On the right sides, we consider the external forces X, Y, Z acting on the fluid, as well as the pressure and the viscosity. The following assumptions are made to solve the problem:

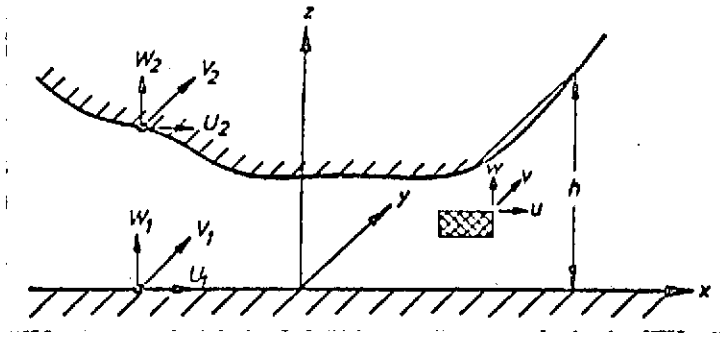

Figure 5.1. Coordinate system and velocities.

1. Other forces are ignored. This assumption is applicable for non-conducting media such as lubricants, because gravitational and magnetic forces do not have any influence. /49

2. Inertia forces are not considered. This simplification is not important for normal conditions. Even for Reynolds numbers larger than 1,000, the error is less than 5%. In the experiments which we carried out, the Reynolds number is smaller by several orders of magnitude.

3. The pressure change in the z direction is ignored because the film thickness is several powers of ten smaller than the size of the pressure zone.

4. The viscosity η is constant in the z direction. This is because isothermal conditions were assumed and because of assumption 3.

5. The density ρ is also constant in the z direction.

6. There is no slip at the limiting surfaces, i.e. the liquid has the same velocity at the edge as the surface of the body in motion.

7. The changes in the velocities u and v in the x and y directions are ignored compared to the changes in the z direction.

8. The velocity difference which is the result of shortened radii caused by deformation at a constant angle of velocity is not considered.

9. We only consider steady conditions.

With these assumptions the equations of motion of Navier-Stokes are simplified as follows: /50

$$\left.\begin{aligned} \frac{\partial p}{\partial x} &= \eta \cdot \frac{\partial^2 u}{\partial z^2} \,, \\ \frac{\partial p}{\partial y} &= \eta \cdot \frac{\partial^2 v}{\partial z^2} \,, \\ \frac{\partial p}{\partial z} &= 0 \,. \end{aligned}\right\} \qquad (5.3)$$

Using the boundary conditions according to assumption 6, these equations can be solved for the velocity distributions u(z) and v(z).

The relationship is given by the continuity of the equation, which is as follows for a volume element

$$\frac{\partial \varrho}{\partial t} + \frac{\partial(\varrho \cdot u)}{\partial x} + \frac{\partial(\varrho \cdot v)}{\partial y} + \frac{\partial(\varrho \cdot w)}{\partial z} = 0 \,. \qquad (5.4)$$

Considering the motion conditions prescribed

$V_1 = V_2 = 0$ (no body motion perpendicular to the roll direction),

$U_1 = U_2 = U$ (pure rolling without slip)

we find the following equation developed by Reynolds [69] which carries his name

$$\frac{\partial}{\partial x}\left(\frac{\rho \cdot h^3}{\eta} \cdot \frac{\partial p}{\partial x}\right) + \frac{\partial}{\partial y}\left(\frac{\rho \cdot h^3}{\eta} \cdot \frac{\partial p}{\partial y}\right) = 12 \cdot U \cdot \frac{\partial}{\partial x}(\rho \cdot h) \quad . \tag{5.5}$$

5.2 Elastic deformation equation

The general case of two bodies with arbitrary curvature which are pressed against each other was analyzed by Timoshenko [70]. Assuming that the pressure area A is small with respect to the body dimensions and that the contact area represents the limits of one body which extends to infinity in the other direction, we find the following for the sum of deformations at any arbitrary point

$$w_1 + w_2 = \left(\frac{1-\nu_1^2}{\pi \cdot E_1} + \frac{1-\nu_2^2}{\pi \cdot E_2}\right) \cdot \iint_{(A)} \frac{p \cdot dA}{r} \quad . \tag{5.6}$$

/51

If the materials are the same we have

$$\nu_1 = \nu_2 = \nu \quad ,$$
$$E_1 = E_2 = E \quad ,$$

i.e. the deformation is distributed equally to both bodies and the total deformation becomes, Figure 5.2,

$$w = \frac{2(1-\nu^2)}{\pi \cdot E} \cdot \iint_{(A)} \frac{p \cdot dA}{r} \tag{5.7}$$

or at a certain point (x,y)

$$w(x,y) = \frac{2(1-\nu^2)}{\pi \cdot E} \cdot \iint_{(A)} \frac{p \cdot dx_1 \cdot dy_1}{r} \quad . \tag{5.8}$$

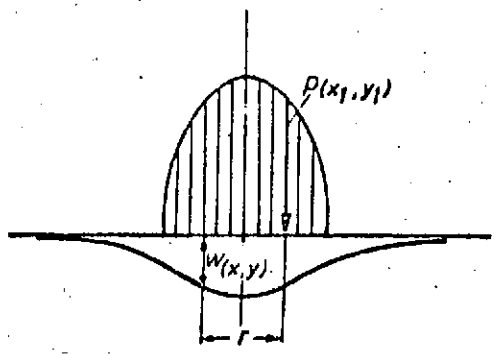

Figure 5.2. Elastic deformation of a semi-infinite body.

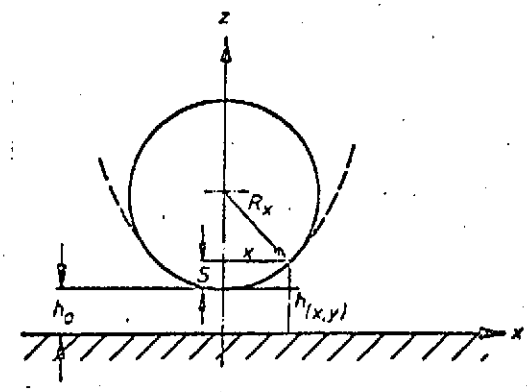

Figure 5.3. Distance between a deformed body and a plane.

In this equation $p.dx_1 \cdot dy_1$ are the point loads at any arbitrary point and r is the distance between this point and the desired point (x,y), that is

$$r = \sqrt{(x-x_1)^2+(y-y_1)^2} \quad . \tag{5.9}$$

With Equation (5.8) it is possible to calculate the deformation for any arbitrary pressure distribution.

5.3 Geometric equations

/52

Both bodies between which the lubricant film thickness is being determined can be replaced mathematically in Equation (4.7) by a plane and a body with the radii R_x and R_y. If the smallest distance between the body and the plane is called h_o, then according to Figure 5.3 we find the following for any arbitrary point

$$h(x,y) = h_o + s_x + s_y \quad . \tag{5.10}$$

From the geometric relationships we find

$$\left.\begin{aligned} x^2 &= s_x(2\cdot R_x - s_x) \quad , \\ y^2 &= s_y(2\cdot R_y - s_y) \quad . \end{aligned}\right\} \tag{5.11}$$

Since for the problem under discussion we have

$$2R_x \gg s_x \quad \text{and} \quad 2R_y \gg s_y \quad ,$$

the expressions can be simplified to

$$\left.\begin{aligned} x^2 &\approx 2\cdot R_x \cdot s_x \quad , \\ y^2 &\approx 2\cdot R_y \cdot s_y \quad , \end{aligned}\right\} \tag{5.12}$$

/53

i.e. the circular contour of the body is replaced by the parabolic contour for the relatively small contact area. The error can be ignored. It is given by

$$f = \frac{R_x - \sqrt{R_x^2 - x^2} - \frac{x^2}{2\cdot R_x}}{R_x - \sqrt{R_x^2 - x^2}} \quad , \tag{5.13}$$

$$f = 0.5\left(1 - \sqrt{1-\left(\frac{x}{a}\right)^2}\right) \quad ; \tag{5.14}$$

In other words, for example, for

$\frac{x}{R} = 0.1$ the error is f - 0.25%,

or for

$\frac{x}{R} = 0.01$ the error becomes f = 0.0025%.

Therefore the distance satisfies

$$h(x,y) = h_0 + \frac{x^2}{2\cdot R_x} + \frac{y^2}{2\cdot R_y} \quad . \tag{5.15}$$

If we also consider the elastic deformation, Figure 5.4, we finally find

$$h(x,y) = h_0 + \frac{x^2}{2\cdot R_x} + \frac{y^2}{2\cdot R_y} + w(x,y) - w_0 \quad . \tag{5.16}$$

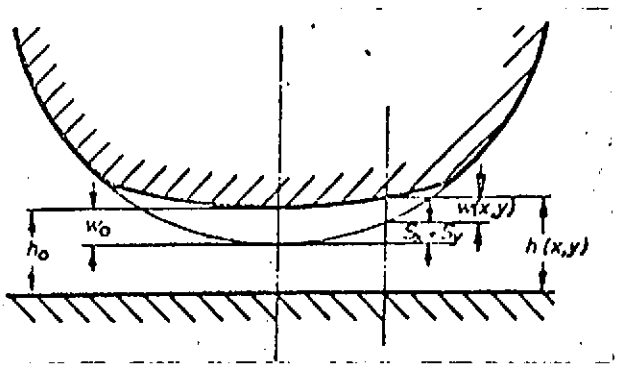

Figure 5.4. Distance between a deformed body and a plane

5.4 System of equations

Summarizing, we find the following coupled system of equations for solving the problem:

a) Reynolds equation

$$\frac{\partial}{\partial x}\left(\frac{\rho \cdot h^3}{\eta} \cdot \frac{\partial p}{\partial x}\right) + \frac{\partial}{\partial y}\left(\frac{\rho \cdot h^3}{\eta} \cdot \frac{\partial p}{\partial y}\right) = 12 \cdot U \cdot \frac{\partial}{\partial x}(\rho \cdot h) \quad , \tag{5.5}$$

b) Elastic deformation equation

$$w(x,y) = \frac{2(1-\nu^2)}{\pi \cdot E} \iint_{(A)} \frac{p \cdot dx_1 \cdot dy_1}{r} \quad . \tag{5.8}$$

c) Geometric equation

$$h(x,y) = h_0 + \frac{x^2}{2 \cdot R_x} + \frac{y^2}{2 \cdot R_y} + w(x,y) - w_0 \quad . \tag{5.16}$$

In addition, we have the following lubricant state equations described in Chapter 4.2

d) Density

$$\frac{\rho}{\rho_0} = 1 + \frac{9.73 \cdot 10^{-3} \cdot p^{0.75}}{\nu^{0.0385}} \quad . \tag{4.33}$$

e) Viscosity

$$\frac{\eta}{\eta_0} = \frac{1}{\eta_0} \cdot \exp\left[0.16478 \cdot p \cdot \ln \eta_0 + \sqrt{(\ln \eta_0)^3}\right]^{2/3} \quad . \tag{4.39}$$

6. NUMERICAL SOLUTION OF THE SYSTEM OF EQUATIONS

6.1 Solution path

It is not possible to give an exact mathematical calculation of the nonlinear and coupled system of equations described in Chapter 5.4. Therefore, a numerical differencing method is introduced for solving the problem. The prevailing pressure distribution is replaced by a network grid, and the desired variables are calculated at its nodes.

Starting with a selected pressure distribution, we first calculate the corresponding elastic deformation, the smallest crack with h_o and from this the crack contour. An improved pressure distribution is found by iteration in the boundary areas, i.e. the initial pressure is changed until all equations are satisfied at every grid point. Then a new crack contour is calculated. This method fails in the Hertz pressure zone. Here we can use another solution method. Using the Reynolds equation, a new calculation of the crack contour is made instead of a calculation of the pressure distribution. This is then compared with the shape determined based on the deformation. Then the pressure distribution is changed until there are no more deviations.

Finally, it is necessary to recalculate the deformation with the improved pressure. This calculation is repeated until there are no more noticeable changes in all the variables. The method of solution is shown in the program flow diagram given in Figure 6.1.

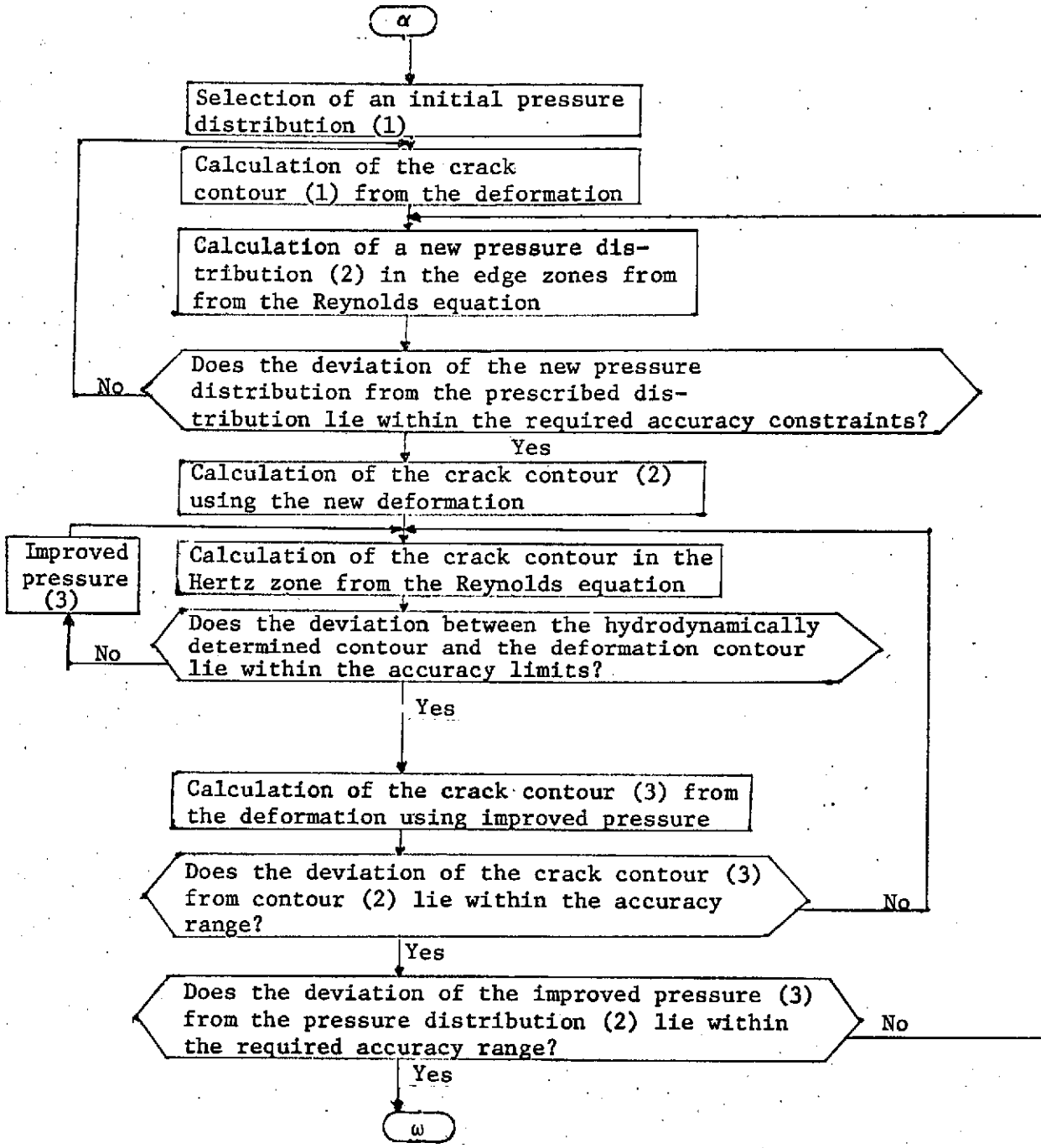
α
Selection of an initial pressure distribution (1)
Calculation of the crack contour (1) from the deformation
Calculation of a new pressure distribution (2) in the edge zones from from the Reynolds equation
Does the deviation of the new pressure distribution from the prescribed distribution lie within the required accuracy constraints?
No
Yes
Calculation of the crack contour (2) using the new deformation
Improved pressure (3)
Calculation of the crack contour in the Hertz zone from the Reynolds equation
Does the deviation between the hydrodynamically determined contour and the deformation contour lie within the accuracy limits?
No
Yes
Calculation of the crack contour (3) from the deformation using improved pressure
Does the deviation of the crack contour (3) from contour (2) lie within the accuracy range?
No
Yes
Does the deviation of the improved pressure (3) from the pressure distribution (2) lie within the required accuracy range?
No
Yes
ω

Figure 6.1. Program flow diagram

6.2 Selection of the grid and initial pressure distribution

The field which is to be expected due to the influence of the elastohydrodynamic processes is specified in the roll direction by

$$-2 \cdot b \leq x \leq 1.5 \cdot b$$

/57

and perpendicular to the roll direction by

$$-1.5 \cdot a \leq y \leq 1.5 \cdot a \quad .$$

Because of the symmetry with respect to the x axis, we must only consider one-half of the field. By dividing this region into a considerable number of grid points, we find the step length s. The division of the semiaxis b is used as a measure.

$$s = \frac{b}{i^*} \quad . \tag{6.1}$$

The factor f is introduced in order to be able to multiply the step length in the y direction in the case of very elongated ellipses, so that there is flexibility in the selection of the network grid. In this way, we obtain a grid corresponding to Figure 6.2 with the following exceptions

$$\left.\begin{aligned} i_{min} &= -2 \cdot i^* \quad , \\ i_{max} &= \text{whole no.}(1.5 \cdot i^* + 0.5) \quad , \\ j_{min} &= 0 \quad , \\ j_{max} &= \text{whole no.}\left(\frac{1.5 \cdot a}{s \cdot f} + 0.5\right) \quad . \end{aligned}\right\} \tag{6.2}*$$

The number of grid points is specified by the factors i* and f, so that the maximum storage capacity of the available computer /58 installation can be used.

It is necessary to now select a suitable initial pressure distribution so that for each grid point there will be a pressure value available. For this purpose, we first use the Hertz pressure distribution as a first approximation. It is supplemented

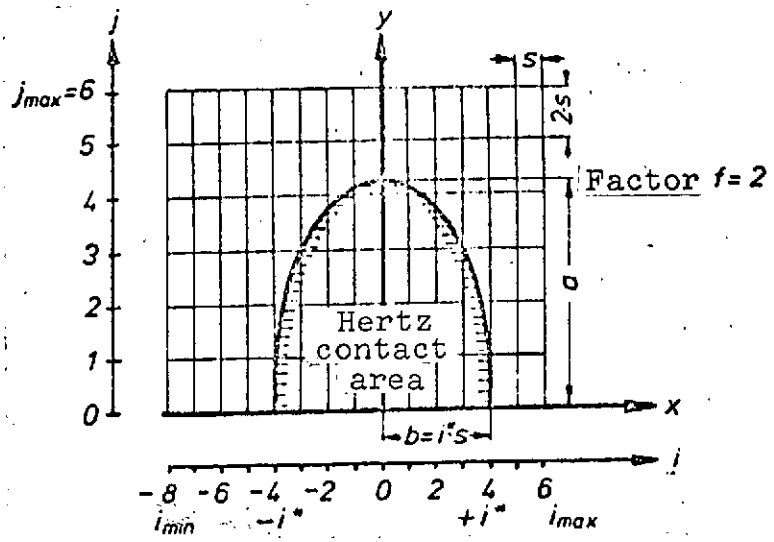

Figure 6.2. Structure of the net grid for numerical calculation

by appropriate additions in the boundary area. All values are used in dimensionless form, i.e. they are referred to the Hertz pressure p_o.

6.3 Calculation of the elastic deformation

According to equation (5.8) we have the following equation for the deformation of a semi-infinite body.

$$w[x,y] = \frac{2\cdot(1-\nu^2)}{\pi\cdot E}\cdot\iint_{(A)}\frac{p\cdot dx_1\cdot dy_1}{\sqrt{(x-x_1)^2+(y-y_1)^2}}\quad .$$

The deformation at any arbitrary point is given by the following expression for the pressure field under discussion and considering the symmetry according to Figure 6.3.

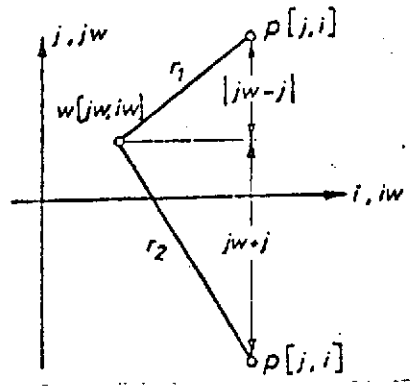

Figure 6.3. Numerical calculation of deformation

$$w[jw,iw] = \frac{2\cdot(1-\nu^2)}{\pi\cdot E}\cdot\left\{\sum_{\substack{i=imin\\ j=0}}^{\substack{j=0\\ i=imax}} \frac{p[j,i]\cdot s\cdot s\cdot f}{r_1} + \sum_{\substack{i=imin\\ j=1}}^{\substack{j=jmax\\ i=imax}} \left[p[j,i]\cdot s\cdot s\cdot f\cdot\left(\frac{1}{r_1}+\frac{1}{r_2}\right)\right]\right\}. \qquad (6.3)$$

/59

Using the dimensionless values from the pressure field we obtain

$$w[jw,iw] = \frac{2\cdot(1-\nu^2)}{\pi\cdot E}\cdot s\cdot p_0\cdot\left\{\sum_{\substack{i=imin\\ j=0}}^{\substack{j=0\\ i=imax}} \frac{P[j,i]}{\sqrt{(jw-j)^2+\left(\frac{iw-i}{I}\right)^2}} + \sum_{\substack{i=imin\\ j=1}}^{\substack{j=jmax\\ i=imax}} \left[P[j,i]\cdot\left(\frac{1}{\sqrt{(jw-j)^2+\left(\frac{iw-i}{I}\right)^2}}+\frac{1}{\sqrt{(jw+j)^2+\left(\frac{iw-i}{I}\right)^2}}\right)\right]\right\}. \qquad (6.4)$$

The deformation calculated with this equation becomes infinite at the point j = jw, i = iw. This can be avoided if a constant pressure is assumed for the corresponding area element and the equation is integrated within these limits, that is

$$w' = \frac{2\cdot(1-\nu^2)}{\pi\cdot E}\cdot p_o\cdot P[j-jw,i-iw]\cdot \int_{y=-f\cdot s/2}^{+f\cdot s/2}\int_{x=-s/2}^{+s/2}\frac{dx\cdot dy}{\sqrt{x^2+y^2}} \quad . \tag{6.5}$$

Integration with respect to x results in

$$\int_{x=0}^{s/2}\frac{dx}{\sqrt{x^2+y^2}} = \ln\frac{\frac{s}{2}+\sqrt{(\frac{s}{2})^2+y^2}}{y} = A^* \quad , \tag{6.6}$$

and subsequent integration with respect to y using the substitution

$$z^* = -\sqrt{(\tfrac{s}{2})^2+y^2}$$

leads to the result /60

$$\int_{y=0}^{+f\cdot s/2} A^*\cdot dy = \frac{s}{2}\left[\sqrt{1+f^2}\cdot\ln\frac{\sqrt{1+f^2}}{\sqrt{1+f^2}-1}+\ln(\sqrt{1+f^2}-1)\right]. \tag{6.7}$$

Finally we obtained the following for the deformation of the two bodies at this point

$$w' = \frac{2\cdot(1-\nu^2)}{\pi\cdot E}\cdot p_o\cdot P[j-jw,i-iw]\cdot 2\cdot s\left[\sqrt{1+f^2}\cdot\ln\frac{\sqrt{1+f^2}}{\sqrt{1+f^2}-1}+\right.$$
$$\left.+\ln(\sqrt{1+f^2}-1)\right] . \tag{6.8}$$

The total deformation is obtained as a sum of w[jw,iw] and w'.

As detailed investigations have shown, the deformation is practically independent of the selected step lengths. There are no substantial deviations even for the smallest possible step length within the available storage capacity.

6.4 Calculation of the smallest crack width h_o

In the remainder of the calculation, we must first obtain the approximate value for h_o from the estimated initial pressure

distribution. Using the substitution

$$\rho \cdot h = h^*$$

the Reynolds equation (5.5) for the symmetry line y = 0 is simplified as follows:

$$\frac{h^{*3}}{\eta \cdot \rho^2} \cdot \left(\frac{\partial^2 p}{\partial x^2} + \frac{\partial^2 p}{\partial y^2} - \frac{2}{\rho} \cdot \frac{\partial \rho}{\partial x} \cdot \frac{\partial p}{\partial x} - \frac{1}{\eta} \cdot \frac{\partial \eta}{\partial x} \cdot \frac{\partial p}{\partial x}\right) + \frac{\partial h^*}{\partial x} \cdot \left(\frac{3 \cdot h^{*2}}{\eta \cdot \rho^2} \cdot \frac{\partial p}{\partial x} - 12 \cdot U'\right) = 0 \quad . \tag{6.9}$$

Using numerical methods, a point [y=0, $x=x_a$] is found for which the first bracket becomes zero, that is

$$\left(\frac{\partial^2 p}{\partial x^2}\right)_a + \left(\frac{\partial^2 p}{\partial y^2}\right)_a - \frac{2}{\rho_a} \cdot \left(\frac{\partial \rho}{\partial x}\right)_a \cdot \left(\frac{\partial p}{\partial x}\right)_a - \frac{1}{\eta_a} \cdot \left(\frac{\partial \eta}{\partial x}\right)_a \cdot \left(\frac{\partial p}{\partial x}\right)_a = 0 \quad . \tag{6.10}$$

This occurs in the initial zone. /61

At this point we then find the following Reynolds equation

$$\frac{3 \cdot h_a^{*2}}{\eta_a \cdot \rho_a^2} \cdot \left(\frac{\partial p}{\partial x}\right)_a - 12 \cdot U' = 0 \quad , \tag{6.11}$$

and the film thickness here becomes

$$h_a = 2 \cdot \sqrt{\frac{U' \cdot \eta_a}{\left(\frac{\partial p}{\partial x}\right)_a}} \quad . \tag{6.12}$$

Using the geometric relationships from Chapter 5.3, this value can be recalculated for the origin of the coordinate system. This leads to a first estimation of the lubricant film thickness h_o.

6.5 Calculation of the crack contour from the deformation

According to equation (5.16), the crack contour at any arbitrary point of the field is calculated according to

$$h[x,y] = h_0 + \frac{x^2}{2 \cdot R_x} + \frac{y^2}{2 \cdot R_y} + w[x,y] - w[0,0]$$

or using the field variables, we have

$$h[j,i] = h_0 + \frac{s^2}{2} \cdot \left[\frac{i^2}{R_x} + \frac{(j \cdot f)^2}{R_y}\right] + w[j,i] - w[0,0]. \qquad (6.13)$$

6.6 Approximation of the pressure distribution in the boundary area

Using the Reynolds equation, the pressure distribution in the boundary areas of the field can be approximated by iteration, Figure 6.4.

The following chapters will describe the required calculation of the pressure matrix coefficients, the way in which this matrix is established and the solution. If the initial pressure is cleverly selected, the deviation will be less than 1% already after a few steps. /62

Unfortunately, this relatively fast and elegant method fails for the Hertz contact zone itself. As other authors have established (for example Archard, etc [17] and Dowson, etc. [24]), this method no longer converges at higher pressures. The desired result is not obtained even if the pressure distribution is approximated in steps. However, this method is important for the solution of the overall problem, because it provides the missing pressure values for the boundary regions, which are then used to build up the remainder of the solution. /63

6.6.1 Calculation of the coefficients

After carrying out the partial differentiation, we obtained the Reynolds equation in the following form

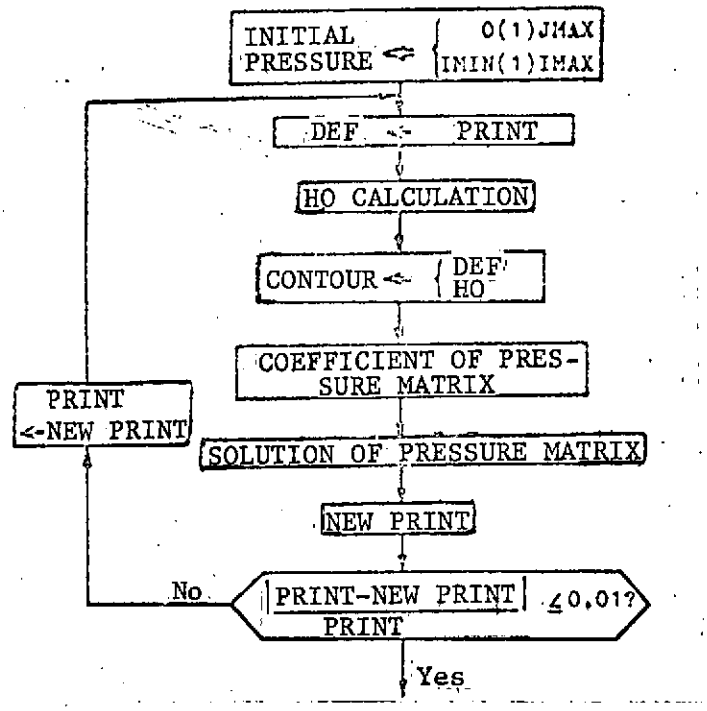

Figure 6.4. Flow diagram for approximating the flow distribution

$$\frac{\partial^2 P}{\partial x^2} + \frac{\partial^2 P}{\partial y^2} + F_1 \cdot \frac{\partial P}{\partial x} + F_2 \cdot \frac{\partial P}{\partial y} = F_3 \qquad (6.14)$$

with

$$\left.\begin{aligned} F_1 &= \frac{1}{\rho} \cdot \frac{\partial \rho}{\partial x} - \frac{1}{\eta} \cdot \frac{\partial \eta}{\partial x} + \frac{3}{h} \cdot \frac{\partial h}{\partial x} \quad , \\ F_2 &= \frac{1}{\rho} \cdot \frac{\partial \rho}{\partial y} - \frac{1}{\eta} \cdot \frac{\partial \eta}{\partial y} + \frac{3}{h} \cdot \frac{\partial h}{\partial y} \quad , \\ F_3 &= \frac{12 \cdot U' \cdot \eta'}{p_o \cdot h^2} \cdot \left(\frac{1}{\rho} \cdot \frac{\partial \rho}{\partial x} + \frac{1}{h} \cdot \frac{\partial h}{\partial x} \right) \quad . \end{aligned}\right\} \qquad (6.15)$$

The differential quotients are replaced by difference quotients according to a Taylor series expansion (for example Stiefel [71], Willers [72]) i.e. the value of a function G is expressed in terms of the derivatives at the point under consideration, Figure 6.5.

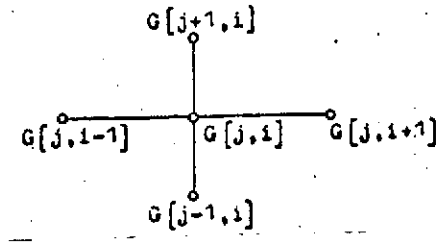

Figure 6.5. System of neighboring node points

For example, then we have

$$G[j,i+1] = G[j,i] + s \cdot \frac{\partial G[j,i]}{\partial x} + \frac{s^2}{2!} \cdot \frac{\partial^2 G[j,i]}{\partial x^2} + \frac{s^3}{3!} \cdot \frac{\partial^3 G[j,i]}{\partial x^3} + \dots \quad (6.16a)$$

$$G[j,i-1] = G[j,i] - s \cdot \frac{\partial G[j,i]}{\partial x} + \frac{s^2}{2!} \cdot \frac{\partial^2 G[j,i]}{\partial x^2} - \frac{s^3}{3!} \cdot \frac{\partial^3 G[j,i]}{\partial x^3} + \dots \quad (6.16b)$$ /64

This means that the first derivative with respect to x becomes

$$G[j,i+1] - G[j,i-1] = 2 \cdot s \cdot \frac{\partial G[j,i]}{\partial x} + \text{Rem.},$$

$$\frac{\partial G[j,i]}{\partial x} = \frac{G[j,i+1] - G[j,i-1]}{2 \cdot s} + \text{Rem.}, \quad (6.17)$$

and the second derivative is

$$G[j,i+1] + G[j,i-1] = 2 \cdot G[j,i] + \frac{2 \cdot s^2}{2!} \cdot \frac{\partial^2 G[j,i]}{\partial x^2} + \text{Rem.}, \quad (6.18)$$

$$\frac{\partial^2 G[j,i]}{\partial x^2} = \frac{G[j,i+1] - 2 \cdot G[j,i] + G[j,i-1]}{s^2} + \text{Rem.}$$

The difference quotient with respect to y is formed in a similar way.

The coefficients F_1, F_2 and F_3 can be calculated for any node point in this way. According to Equation (4.33) we find the following for the density

$$\frac{\rho}{\rho_0} = 1 + A^* \cdot p^{0.75}$$

where

$$A^* = \frac{9.73 \cdot 10^{-3}}{\nu^{0.0385}} \cdot p_0^{0.75} \quad .$$

The corresponding difference quotient is then

$$\frac{1}{\rho} \cdot \frac{\partial \rho}{\partial x} = \frac{0.75 \cdot A^*}{P[j,i]^{0.25} + A^* \cdot P[j,i]} \cdot \frac{P[j,i+1] - P[j,i-1]}{2 \cdot s} \quad . \qquad (6.19)$$

According to Equation (4.39) the viscosity was given by

$$\eta = e^{(D^* \cdot P + E^*)^{2/3}}$$

with

$$D^* = 0.16478 \cdot \ln \eta_0 \cdot p_0 \quad ,$$

$$E^* = \sqrt{(\ln \eta_0)^3} \quad .$$

In this case we then have

$$\frac{1}{\eta} \cdot \frac{\partial \eta}{\partial x} = \frac{D^*}{1.5 \cdot (D^* \cdot P[j,i] + E^*)^{1/3}} \cdot \frac{P[j,i+1] - P[j,i-1]}{2 \cdot s} \quad , \qquad (6.20)$$

/65

and finally we obtain the following from the crack contour

$$\frac{1}{h} \cdot \frac{\partial h}{\partial x} = \frac{h[j,i+1] - h[j,i-1]}{h[j,i] \cdot 2 \cdot s} \quad . \qquad (6.21)$$

The difference quotions with respect to y are always formed in a corresponding way and the factor f should be used for changing the step length.

6.6.2 Establishment of the system of equations

After transforming the differential quotient, Equation (6.14) becomes

$$\frac{P[j,i+1]-2\cdot P[j,i]+P[j,i-1]}{s^2}+\frac{P[j+1,i]-2\cdot P[j,i]+P[j-1,i]}{s^2\cdot f^2}+$$
$$+F_1\cdot\frac{P[j,i+1]-P[j,i-1]}{2\cdot s}+F_2\cdot\frac{P[j+1,i]-P[j-1,i]}{2\cdot s\cdot f}=F_3 \quad . \tag{6.22}$$

By rearrangement we find

$$P[j,i+1]\cdot F_{11}+P[j,i-1]\cdot(2\cdot f^2-F_{11})+$$
$$+P[j+1,i]\cdot F_{22}+P[j-1,i]\cdot(2-F_{22})+ \tag{6.23}$$
$$+P[j,i]\cdot(-2\cdot f^2-2)=F_{33} \quad .$$

where

$$F_{11}=(1+F_1\cdot\tfrac{s}{2})\cdot f^2 \quad ,$$
$$F_{22}=1+F_2\cdot\tfrac{s}{2}\cdot f \quad , \tag{6.24}$$
$$F_{33}=s^2\cdot f^2\cdot F_3 \quad .$$

Figure 6.6 shows the scheme for establishing the coefficient matrix. The boundary conditions state that the pressure at the boundaries of the field is zero and that there is symmetry with respect to the line $j = 0$, that is

$$P[-1,i]=P[+1,i] \quad .$$

/66

This means that for the unknown pressures there is an equal number of linear equations available. This means that this can be established and can be solved. Figure 6.7 shows the corresponding matrix for an example of a pressure field with 24 unknowns. A maximum of five unknowns occur in each line (equation) because each considered node point is connected with a maximum of four neighboring points. All unused fields have a value of zero. The solution vector B is written in the

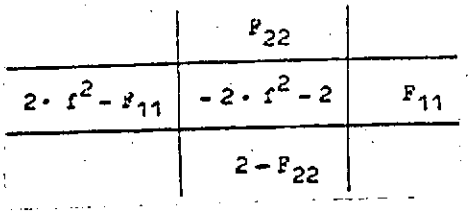

Figure 6.6. Diagram for establishing the coefficient matrix.

right column.

6.6.3 Solution of the system of equations

The system of equations can be solved using the Gauss algorithm. This is the continuous elimination of unknowns (Zurmühl [73]). Programs already exist in the program library of the computer center of the Technical University at Braunschweig. However, the required accuracy in the calculation of the elastohydrodynamic lubrication problem means that a relatively small step length must be used. This means that there is a large number of grid points. Since every time the step length is divided in half, this produces a requirement for 16 times the storage requirement for the coefficient matrix, and the capacity of 30,000 storage points is rapidly exceeded. This is also because in order to solve the system, an equal number of storage locations is also required.

New methods had to be developed for reducing the size of the matrix. It was not appropriate to divide it into smaller matrices, because the numerous required matrix multiplications would again cancel the gain in capacity. In the problem under discussion, we are dealing with a matrix A of large order in which all non-zero elements lie to both sides of the main diagonal in a small band. Therefore, we can use the transformation according to the law

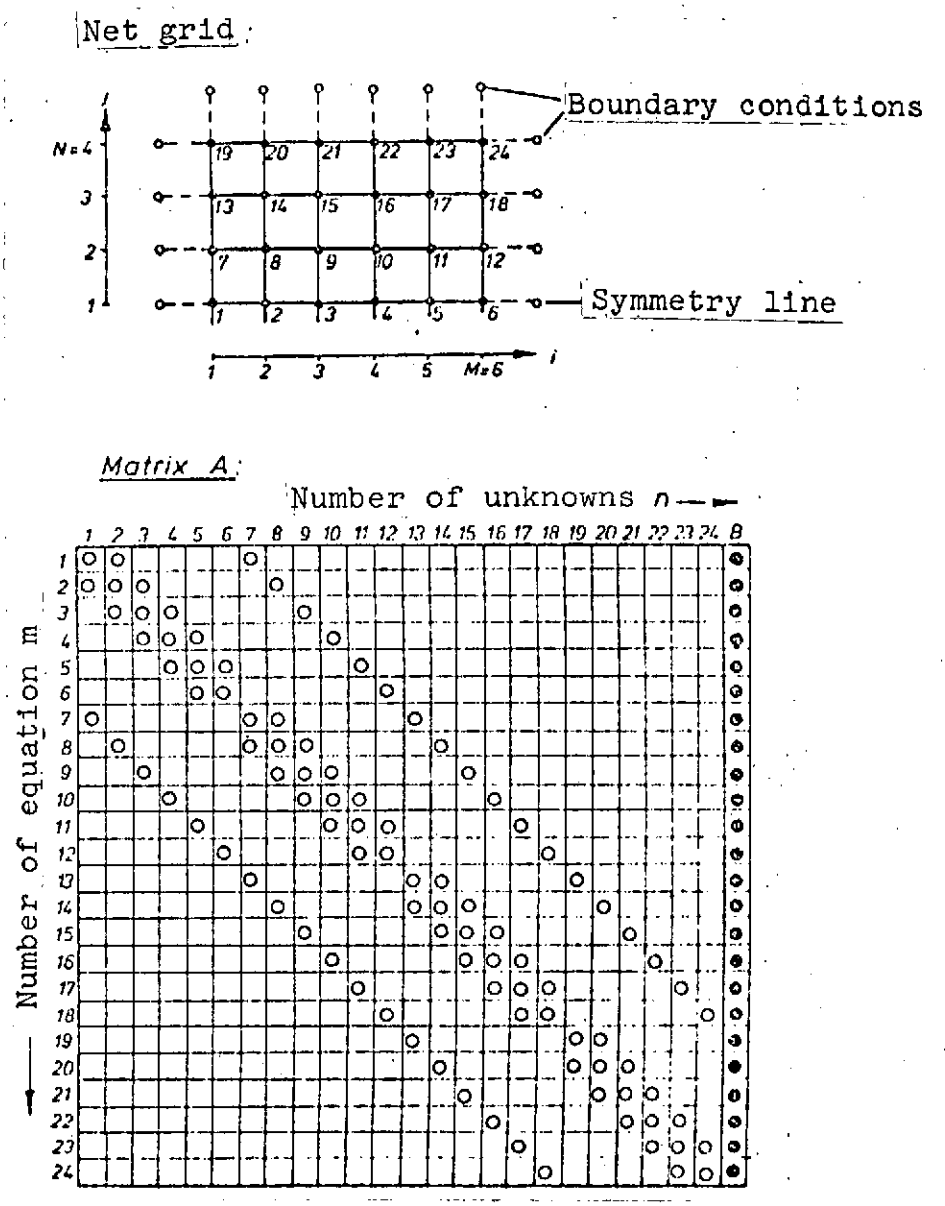

Figure 6.7. Coefficient matrix for a field with 24 grid points.

$$A[m,n] \cdot C[m,n-n+N^*+1] \qquad (6.25)$$

This means that the elements are displaced one after another in such a way that a band matrix having the width $2 \cdot N^* + 1$ is produced as shown in Figure 6.8. This means that most of the zero fields are eliminated. For example, the storage location savings is over 95% for a pressure field with 600 grid points. This means that in this way we can use substantially lower step lengths within the framework of the available capacity. /68

When the matrix is established, we must make sure that the direction of a lower number has a priority when running through the grid points. In this way we obtain the minimum band width.

The matrix C is solved using the "BANDSOLVE" procedure, shown in Figure 6.9. This is established so that only one band piece is processed during the solution. The contents of field C are destroyed by a solution process, which is carried out using Gauss elimination with series exchange, followed by back-substitution (Zurmühl [73]).

6.7 Pressure approximation in the Hertz zone /71

In the Hertz contact zone, a solution is obtained by comparing the elastically-deformed body contour with the crack contour established based on the prevailing hydrodynamic laws. For this, the pressure is changed until the deviation between both contours lies within the required accuracy range. This accuracy range must be selected small because small differences already lead to considerable pressure deviations. One of the most important things for rapid convergence is the proper selection of a suitable criterion for the required pressure corrections.

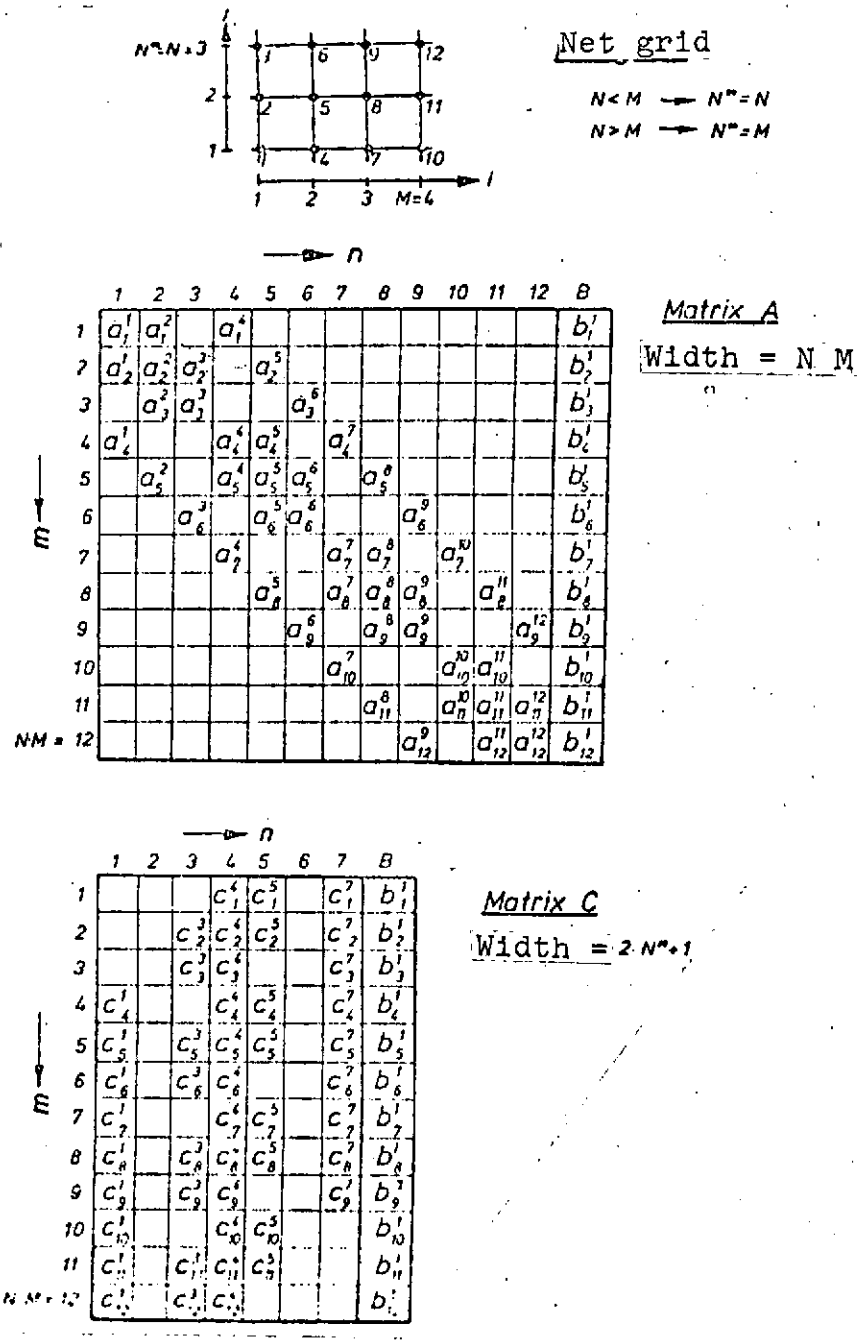

Figure 6.8. Conversion of a sqaure matrix A into a band matrix C

```
    'PROCEDURE'BANDS(C,V,N,M,LF);
BLOCK    21
      'VALUE'N,LF,M;
      'INTEGER'N,LF,M;
      'ARRAY'C,V;
      'BEGIN' 'INTEGER'JM,LR,I,PIV,L,R,J;  'REAL'T;
        LR:=(M+1)/2;
        'FOR'R:=1'STEP'1'UNTIL'LR-1'DO'
        'FOR'I:=1'STEP'1'UNTIL'LR-R'DO'
        'BEGIN''FOR'J:=2'STEP'1'UNTIL'M'DO'
        C[R,J-1]:=C[R,J];
        C[R,M]:=C[N+1-R,M+1-I]:=0
        'END';
        'FOR'I:=1'STEP'1'UNTIL'N-1'DO'
        'BEGIN'PIV:=I;
          'FOR'R:=I+1'STEP'1'UNTIL'LR'DO'
          'IF'ABS(C[R,1])'GREATER'ABS(C[PIV,1])'THEN'
          PIV:=R;
          'IF'PIV'NOTEQUAL'I'THEN'
           'BEGIN'
          'FOR'L:=1'STEP'1'UNTIL'LF'DO'
            'BEGIN'T:=V[I,L];
             V[I,L]:=V[PIV,L];
             V[PIV,L]:=T;
            'END';
            'FOR'J:=1'STEP'1'UNTIL'M'DO'
            'BEGIN'T:=C[I,J];
             C[I,J]:=C[PIV,J];
             C[PIV,J]:=T
            'END'
          'END';
        'FOR'L:=1'STEP'1'UNTIL'LF'DO'
        V[I,L]:=V[I,L]/C[I,1];
        'FOR'J:=2'STEP'1'UNTIL'M'DO'
        C[I,J]:=C[I,J]/C[I,1];
        'FOR'R:=I+1'STEP'1'UNTIL'LR'DO'
        'BEGIN'T:=C[R,1];
          'FOR'L:=1'STEP'1'UNTIL'LF'DO'
          V[R,L]:=V[R,L]-T*V[I,L];
          'FOR'J:=2'STEP'1'UNTIL'M'DO'
          C[R,J-1]:=C[R,J]-T*C[I,J];
          C[R,M]:=0
        'END';
        'IF'LR'NOTEQUAL'N'THEN'LR:=LR+1
      'END';
        'FOR'L:=1'STEP'1'UNTIL'LF'DO'
        V[N,L]:=V[N,L]/C[N,1];
      JM:=2;
        'FOR'R:=N-1'STEP'-1'UNTIL'1'DO'
       'BEGIN' 'FOR'J:=2'STEP'1'UNTIL'JM'DO'
        'FOR'L:=1'STEP'1'UNTIL'LF'DO'
        V[R,L]:=V[R,L]-C[R,J]*V[R+1-J,L];
       'IF'JM'NOTEQUAL'M'THEN'JM:=JM+1
      'END'
    'END';
```

Figure 6.9. "BANDSOLVE" procedure for solving a band matrix

In principle, the method is similar to the one described in Chapter 6.6. It also leads to the result with a coefficient determination, establishment of the matrix and solution of the system of equations.

Another possible method, that is of finding the pressure by changing the crack, does not lead to convergence. In addition, it is very difficult to calculate the deformation from a given crack contour.

6.7.1 Calculation of the crack contour from the Reynolds equation

If the partial differential equation (6.14) is solved with respect to h, we find

$$\frac{\partial h}{\partial x}\cdot\left[\frac{3\cdot h^2\cdot\frac{\partial p}{\partial x}}{K^*}-\frac{12\cdot U'\cdot\eta'}{p_0\cdot K^*}\right]+\frac{\partial h}{\partial y}\cdot\left[\frac{3\cdot h^2\cdot\frac{\partial p}{\partial y}}{K^*}\right]= -h^3+h\cdot\frac{12\cdot U'\cdot\eta'\cdot\frac{1}{\rho}\cdot\frac{\partial\rho}{\partial x}}{p_0\cdot K^*} \tag{6.26}$$

where

$$K^*=\frac{\partial^2 p}{\partial x^2}+\frac{\partial^2 p}{\partial y^2}+\frac{\partial p}{\partial x}\cdot\left(\frac{1}{\rho}\cdot\frac{\partial\rho}{\partial x}-\frac{1}{\eta}\cdot\frac{\partial\eta}{\partial x}\right)+ +\frac{\partial p}{\partial y}\cdot\left(\frac{1}{\rho}\cdot\frac{\partial\rho}{\partial y}-\frac{1}{\eta}\cdot\frac{\partial\eta}{\partial y}\right) \tag{6.27}$$

In this we obtain the system of equations /72

$$h[j,i+1]\cdot H_{11}+h[j,i-1]\cdot(-H_{11})+h[j+1,i]\cdot H_{22}+ +h[j-1,i]\cdot(-H_{22})+h[j,i]=H_{33} \tag{6.28}$$

	H_{22}	
$-H_{11}$	1	H_{11}
	$-H_{22}$	

Figure 6.10. Diagram for establishing the coefficient matrix

with

$$\left.\begin{aligned} H_{11} &= \frac{3 \cdot h^2 \cdot \frac{\partial p}{\partial x}}{2 \cdot s \cdot K^*} - \frac{12 \cdot U' \cdot \eta'}{2 \cdot s \cdot p_o \cdot K^*} \\ H_{22} &= \frac{3 \cdot h^2 \cdot \frac{\partial p}{\partial y}}{2 \cdot s \cdot f \cdot K^*} \\ H_{33} &= -h^3 + h \cdot \left[1 + \frac{12 \cdot U' \cdot \eta' \cdot \frac{1}{p} \cdot \frac{\partial p}{\partial x}}{K^* \cdot p_o}\right] \end{aligned}\right\} \qquad (6.29)$$

The differential quotients are transformed into difference quotients using the method described in Chapter 6.6. The method of establishing the coefficient matrix is shown in Figure 6.10.

The transformation into a band matrix and a solution is the same as described in Chapter 6.6.

6.7.2 Change of the pressure

By solving the system of equations we find a contour (h"), which is the result of hydrodynamic laws and will first deviate from the deformation contour (h'). In order to obtain agreement, the pressure must be changed according to the differences which occur. Since the field under consideration is two-dimensional, it takes a great deal of time to find the correct pressure. A simple comparison of the two contours, that is

$$\left|\frac{h'' - h'}{h'}\right| \leq \varepsilon \qquad (6.30)$$

does not lead to the results, because the differential quotients contained in the system of equations have a greater influence on the equations. This is why we selected the additional criteria

$$\left|\frac{\frac{\partial h''}{\partial x}-\frac{\partial h'}{\partial x}}{\frac{\partial n'}{\partial x}}\right| \leq \varepsilon \quad \text{and} \quad \left|\frac{\frac{\partial h''}{\partial y}-\frac{\partial n'}{\partial y}}{\frac{\partial n'}{\partial y}}\right| \leq \varepsilon \tag{6.31}$$

and we continuously changed the pressures at the individual grid points corresponding to the results. The corrections are selected smaller and smaller until the deviations no longer exceed a certain measure. The entire field must always be considered because all points have an influence on each other.

After approach has been achieved, the deformation is calculated again with the improved pressure and the process is repeated.

/74

7. EXECUTION OF THE NUMERICAL CALCULATION AND RESULTS

The numerical method described in Chapter 6 makes it possible to calculate the elastohydrodynamic lubricant film thickness for any arbitrary roller body pair without slip. In order to save money and computer time, we will not carry out a systematic variation of the individual parameters. Instead, a few characteristic examples will be calculated with the corresponding experimental data, and the resulting lubricant film thicknesses will be compared with the experimental results. The discussion of the individual parameters will be carried out in the experimental part (Chapter 11).

7.1 Computer installation

The required computer operations were programmed in the problem-oriented language Algol, (for example Herschel [74]).

The calculations were carried out on the computer installation ICL-1907 of the computer center at the Technical University at Braunschweig. The available core storage capacity of 32 K limits the size of the matrices and therefore the possible step length s.

The operational systems George 2 and George 3 (ICL handbook [75]) make it possible to submit test runs with a maximum running time of 150 seconds two to three times a day. Production runs require between one and two days. The maximum running time is 30 minutes and therefore limits the number of loops which can be calculated and the associated accuracy.

7.2 Calculation sequence

The data on the material and the lubricant, the circumferential velocity and the load are specified for a certain roller body geometry. From this the Hertz values for the pressure and size of the contact area are first calculated, and an appropriate step length is determined. From an appropriate initial selected pressure distribution, one obtains a dimensionless pressure referred to the Hertz pressure P_o for each grid point of the prescribed field. Atmospheric pressure prevails at the edge of the field. /75

The special point at which the first approximation solution for the lubricant film thickness h_o can be found lies within the inlet zone in the vicinity of the inflection point of the pressure distribution. During the subsequent calculation, it is necessary to correct h_o according to the results obtained. Only one value of h_o provides the desired pressure distribution, and when h_o is made smaller, the pressure volume is enlarged. The reverse is also true. The first solution for the crack contour is obtained from the deformation, the geometry of the roller body and h_o.

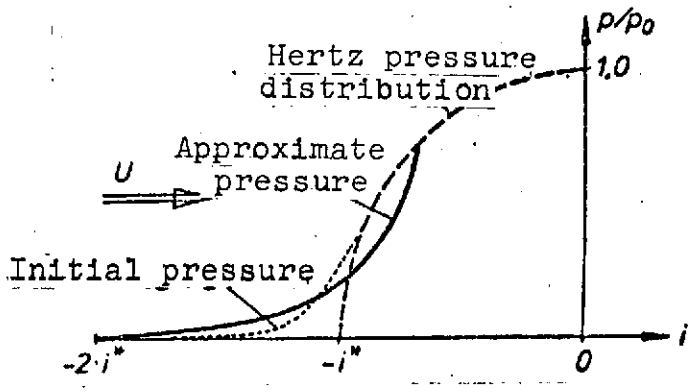

Figure 7.1. Pressure approximation in the edge zone

Figure 7.1 shows the approximation for the pressure in the edge zones. /76

A typical example will show how the iteration proceeds.

For a field containing 420 grid points, the first 99% of all points considered in the edge zone deviated from the specified pressure by more than 1%. After the second loop, there were only 48%, after the third loop 6% remained and after the fourth loop the deviations were less than the permissible range for all points.

This means that the pressure approximation in the edge regions will rapidly and certainly lead to the desired result.

As already mentioned, this direct path cannot be used in the Hertz zone itself. In this region, the solution is obtained by a comparison with the contour which is the result of the hydrodynamic pressure in the lubricant and the contour determination based on the contact pressure in the elastically deformed roller bodies. Since the change in the pressure has a different

effect at every point, the magnitude of deviation between both contours cannot be used as a measure for the pressure correction. Only a systematic method of searching for the smallest difference will lead to the results. The pressure at each individual point is changed, corresponding to the tendency of the result to change in the same direction or in the opposite direction by small amounts.

How much the pressure itself reacts to the smallest crack changes can be seen from the fact that no noticeable pressure changes occur anymore when the contour deviation is less than 0.001%. The number of required iteration loops is a random variable and depends on how fast the optimum values can be found for the individual points.

The entire approximation method had to be repeated several times, until an additional calculation of the deformation with the improved pressure no longer resulted in any change of the result.

7.3 Results

/77

The results of the numerical computation procedure will be discussed using a characteristic example:

For two rollers with the radii R_1 = 20.5 mm, R_2 = 47.5 mm, R_3 = 105 mm and R_4 = ∞, the deformation and crack contour first approximations are given in Figure 7.2, for a Hertz pressure of p_o = 75 kp/mm^2 and an appropriately selected initial pressure distribution. The film thickness is assumed to be h_o = 1.594 µm, which is obtained as an initial value for a circumferential velocity of U = 5 m/sec and an oil viscosity of η_o = 85 cP.

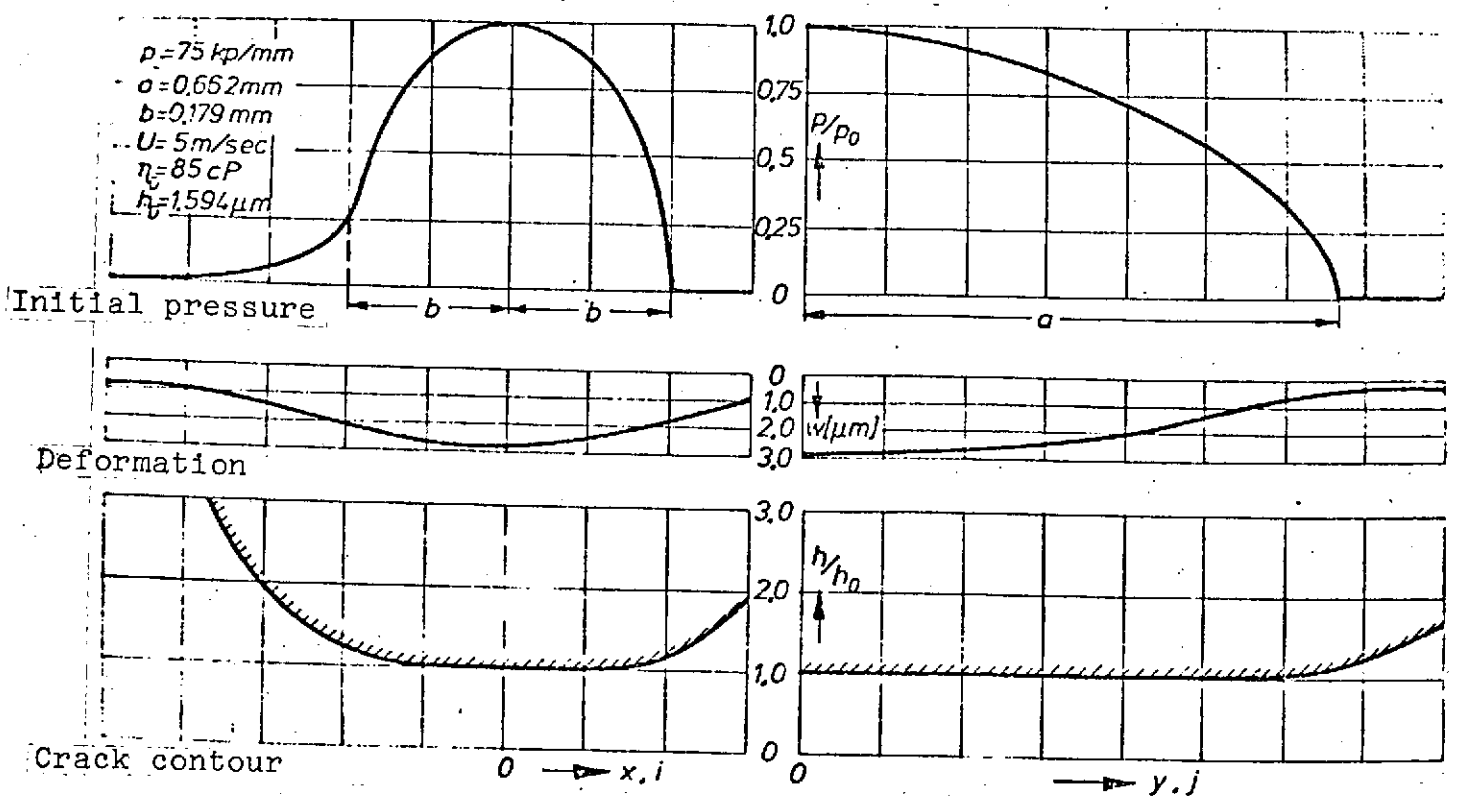

Figure 7.2. Initial pressure, deformation and crack contour at the beginning of the numerical calculation.

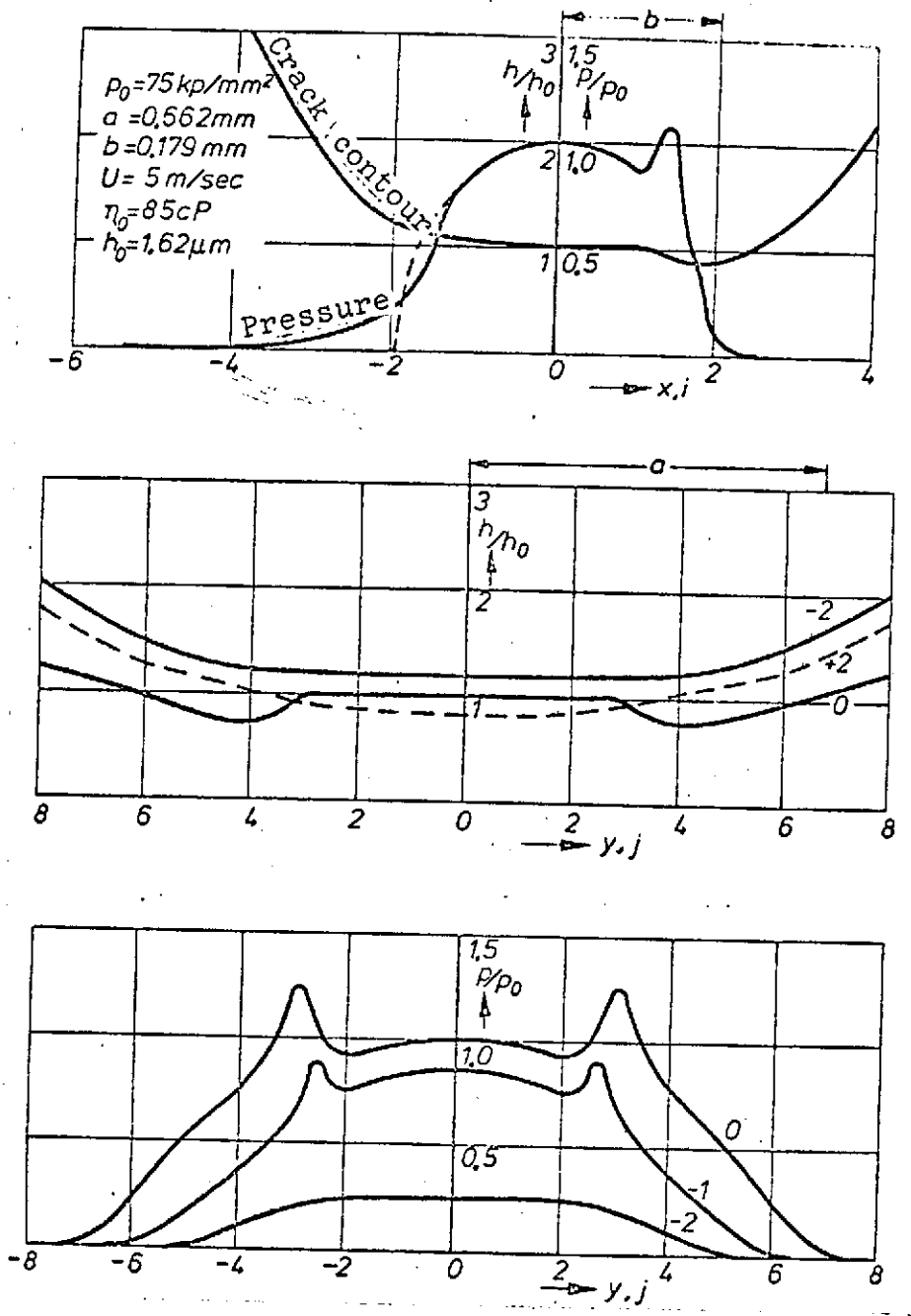

Figure 7.3. Crack contour and pressure distribution for elastohydrodynamic lubrication for elliptical contact areas

The results of the elastohydrodynamic lubrication problem are shown in Figure 7.3. Just like for line contact, the crack contour is mostly parallel. The crack contraction which occurs at the outlet is characteristic for all results. This can be compared with the reduction in the film thickness which occurs for line contact. However, in our case, this does not occur at a straight line, but is shaped in the form of a horseshoe in the direction of the inlet.

The pressure distribution is very close to the Hertz distribution in the region of greatest load, and is only flatter in the inlet zone. However, there is a strong arc-shaped peak within the pressure distribution corresponding to the crack contraction, which can be compared with the "pressure peak" for line contact.

The crack contraction and the related pressure increase can be explained using the continuity condition. The crack is approximately parallel within the Hertz zone. However, after the zone, the contours diverge greatly, i.e. the crack suddenly increases in size. At this point there is a large negative pressure gradient, which changes the oil flux

$$q_x = u \cdot h - \frac{h^3}{12 \cdot \eta} \cdot \frac{\partial p}{\partial x} \qquad (6.32)$$

to a considerable degree. Continuity is only maintained under these conditions when the crack becomes narrower here. The same thing holds for the sideways oil flux /78

$$q_y = -\frac{h^3}{12 \cdot \eta} \cdot \frac{\partial p}{\partial y} \quad . \qquad (6.33)$$

so that the curved force of the contraction becomes understandable. On the other hand, this produces a steep pressure increase. Because of the finite step length of the computation method, it is difficult to determine the actual pressure increase magnitude. However, it seems that this does not have any influence on the other results.

8. TEST INSTALLATION /81

In addition to the theoretical investigations, experimental measurements will give information on the formation of the elasto-hydrodynamic lubrication film. The purpose of these experiments is to determine the thickness of the oil film in the contact zone between two roller bodies. For this purpose we built an experimental installation with which it is possible to vary the parameters which determine the crack thickness, such as load, velocity, lubrication oil properties, as well as the size and shape of the pressure area. We selected the capacitive measurement method from those described in Chapter 2.2.1, because it provides the best results for the amount of effort involved. The entire test installation is shown in Figure 8.1.

8.1 Test stand

The main element in the test stand is the measurement gear complex, shown in Figure 8.2. It consists of a precision sphere or roller with a hole, two rollers and a double-conical pressure roller. The lubricant film thickness is always measured between the sphere (or roller) and the roller. Between these parts there is pure rolling motion, and there are only normal force loads. /83 Both rollers are supported in glass-fiber reinforced fluorine-Simrit boxes, which are electrically insulated. The driveshaft is also electrically separated from the motor because the bearing cover and coupling are made of a high quality insulating material. The pressure roller is guided from the side in an adjustable guide strip. The measurement gear is driven by a direct current, shunt-wound electric motor, which is controlled up to the nominal rotation rate by means of an armature resistor. Above this it is controlled by field attenuation. The rotation rate can be varied in this way between zero and 4300 rpm in a continuous fashion. The rotation rate can be reversed by

Reproduced from best available copy.

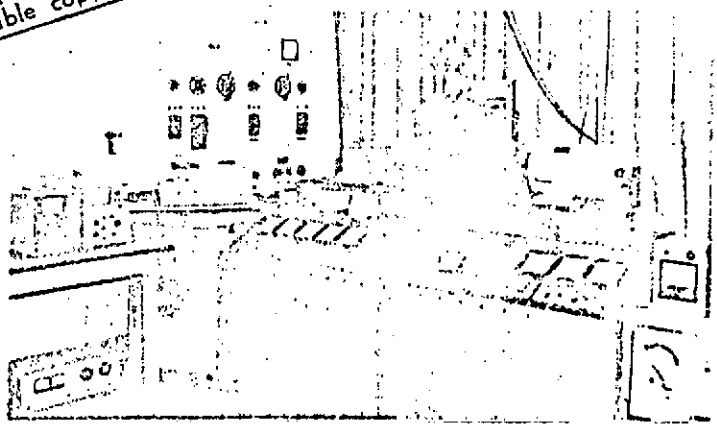

Figure 8.1 Test installation

exchanging the field coil connections. There are several safety installations to turn off the motor automatically if there are disturbances or overloads.

The load is applied mechanically with a spindle to the pressure roller. Plate spring units are used for damping. The loads were selected so that the maximum Hertz pressure p_o is applied continuously with consideration of the dead weight.

We were very careful to have absolutely clean conditions. We also carefully monitored the viscosity of the lubrication oil. The oil is maintained at a constant temperature with a thermostat. It reaches the measurement gear through a filter and then a microfilter. There it is sprayed into the lubrication crack. The amount of lubricant can be controlled with a throttle. It is monitored by means of a flux measurement device.

8.2 Measurement arrangement

A measurement system was built which makes it possible to measure the lubricant film thickness with a capacitive measurement as a function of the following parameters: load, circumferential velocity and physical oil properties. Figure 8.2 shows the

1 Spindle
2 Force measurement box
3 Pressure roller
4 Adjustable guide rod
5 Sphere or roller
6 Flexible shaft
7 Drive shaft
8 Cylinder roller
9 Teflon box
10 Mercury - measurement flux converter
11 Rotation rate transducer

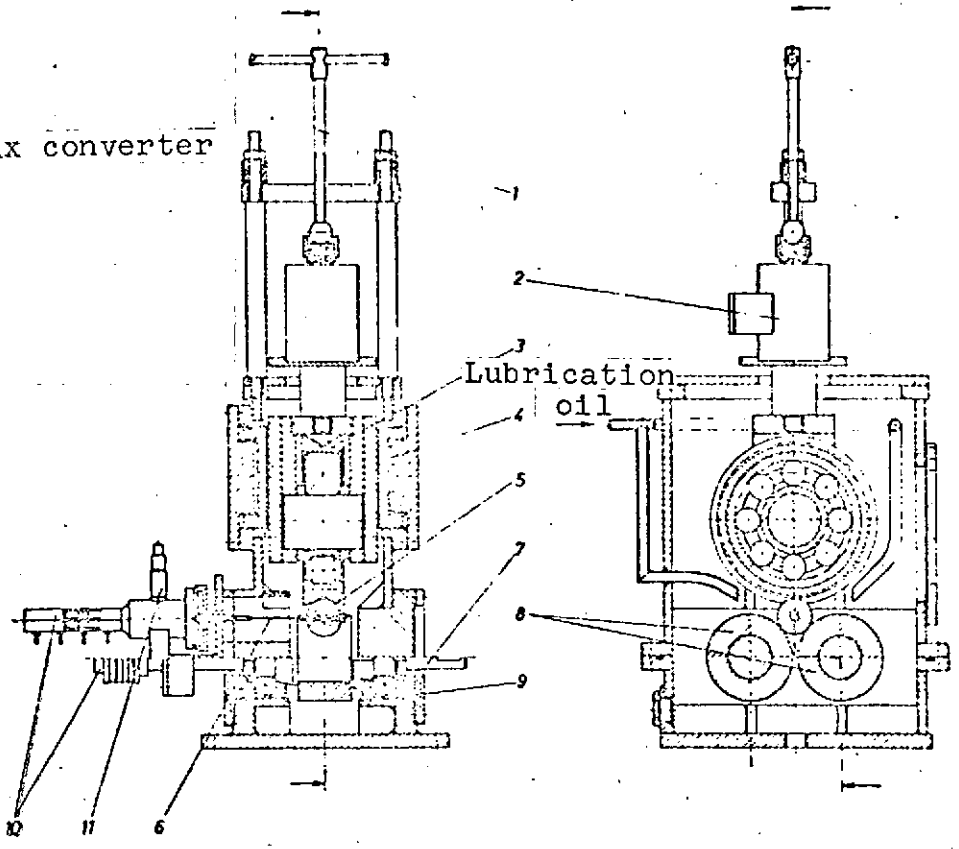

Figure 8.2 Measurement drives

entire measurement arrangement. /85

8.2.1 Measurement of the lubricant film thickness

The lubricant film thickness is measured by establishing the capacitive resistance change. A low voltage alternating current is used. This measurement method is very sensitive and is very suitable for rapid processes. The principle is as follows: the roller body in the center contacts the two cylindrical rollers and the pressure roller when at rest. The lubricant film in between during the rolling process acts like a dielectric, so that one condensor each is produced. The sphere is one electrode of the condensor and is connected to the mass through a mercury-measured current transfer unit. Both rollers make up the second electrode in each case. They are completely electrically insulated and are also connected to the measurement unit through a mercury-measurement current transfer unit. The pressure roller and the housing are grounded and in this way shields the measurement system with respect to the outside. The entire measurement installation is built as a two-channel system. Each channel consists of a measurement point, a capacitive equalization unit, carrier frequency measurement amplifier and an oscillograph, Figure 8.4. The oscillator of the measurement amplifier supplies the measurement point with high frequency alternating current through the capacitive equilization unit. It is possible to balance the magniture and phase of the entire system with the electrical resistors in the capacitive equalization unit. The measurement /86
signals are picked off the rotating shafts with mercury measurement current transfer units so that a constant transfer resistance is established, which is not influenced by changes in the rotation rate. This is not the case for sliding ring transfer units.

Reproduced from best available copy.

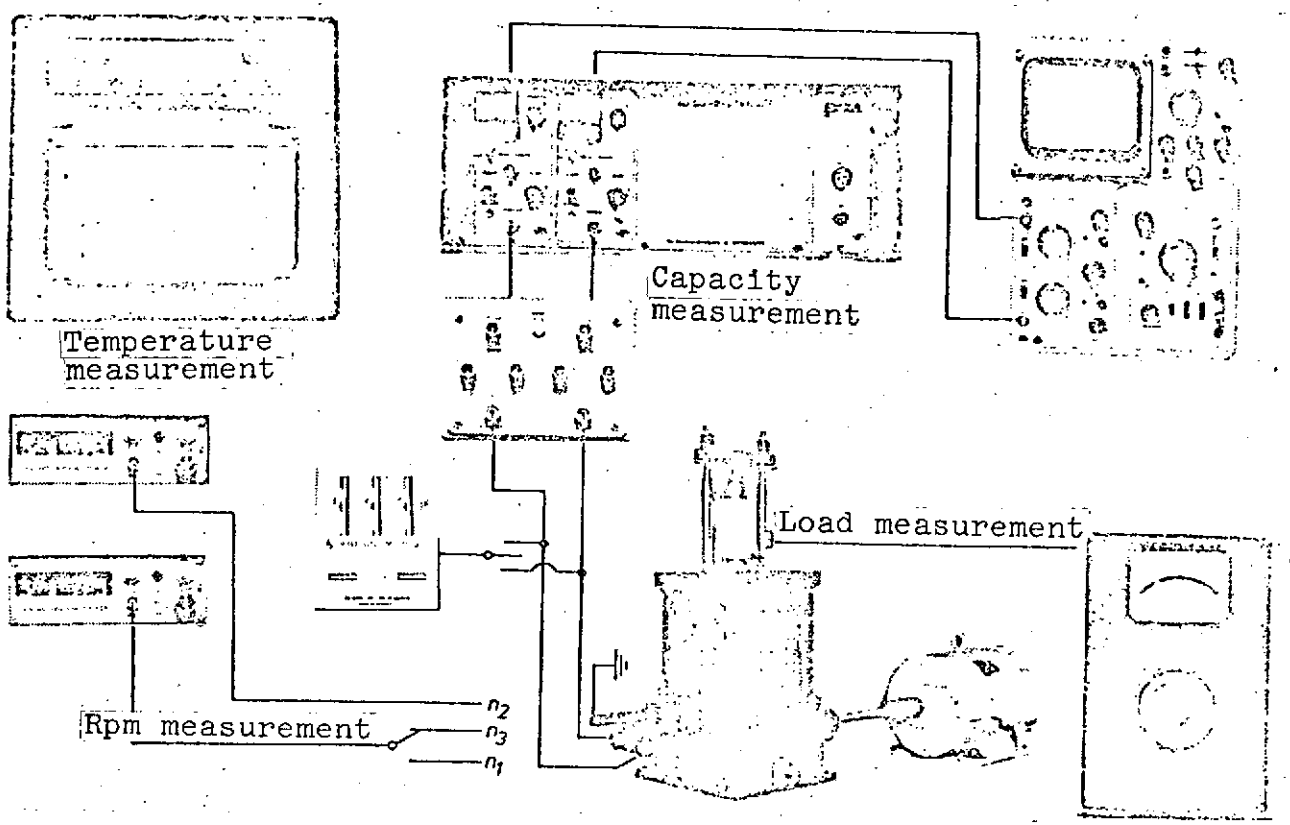

Figure 8.3 Measurement arrangement

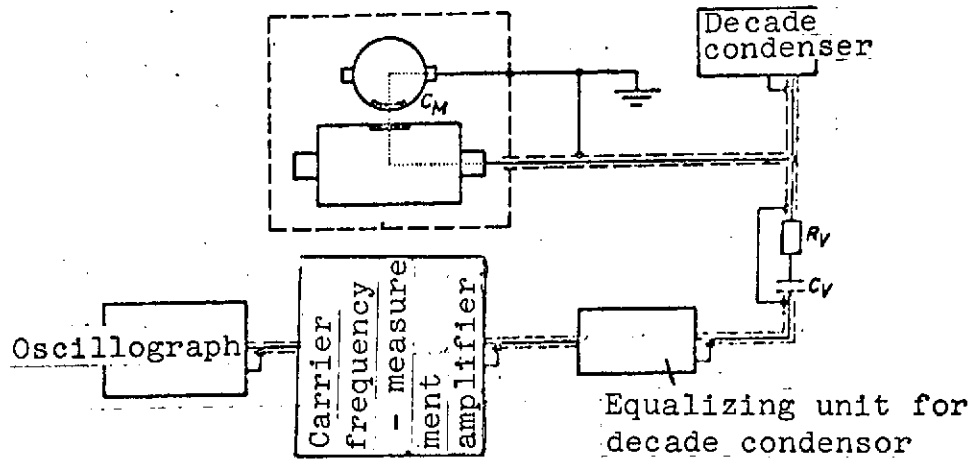

Figure 8.4. Measurement of capacitive resistance

A capacitive and an ohmic resistance is produced at the measurement point because of the lubricant film. We have the following formula for the current through the system

$$I = \sqrt{I_C^2 + I_R^2} \quad . \tag{8.1}$$

$$I = U \cdot \sqrt{(\omega \cdot C)^2 + (\frac{1}{R})^2} \quad . \tag{8.2}$$

Because of the high carrier frequency of 465 kHz, we have

$$\omega \cdot C \gg \frac{1}{R} \quad .$$

If we ignore the ohmic resistance, we have

$$I \approx U \cdot \omega \cdot C \quad . \tag{8.3}$$

During the measurement the carrier voltage U remains constant. This means that a capacity change at the measurement point brings about a change in the current intensity. This is the input signal to the carrier frequency measurement amplifier. There it is transformed into an analog direct voltage, amplified and then is made visible with a storage oscillograph.

With this arrangement we measured a maximum voltage of 9.54 V at the measurement point. Since the thickness of lubricant films is on the order of microns, capacitive measurements can lead to voltage arcing. Therefore it was necessary to switch in suitable resistors, which would make the voltage at the measurement point as small as possible but without reducing the sensitivity of the measurement system too much. This is why various combinations of ohmic and capacitive resistors were switched in series with the system. The condensors have the purpose of making the short circuit current infinitely large when the sphere contacts the roller. This could lead to damage to the units. Figure 8.5 shows the result of these test series. We define the sensitivity as the ratio of the largest possible amplification and the amplification required to obtain the same current intensity. As the diagram shows, it is not possible to satisfy the two conditions, very low voltage and large sensitivity, at the same time. Apparently the envelope curve will provide the optimum results. We selected the following final series resistors

/87

$$R_V = 3{,}3\ k\Omega \quad \text{and} \quad C_V = 47\ pF$$

which meant that the maximum voltage at the measurement point was reduced to 0.9 V.

This system for the capacitive measurement of the lubricant film thickness is extremely sensitive and therefore produces very exact results. However, it is necessary to have carefully laid stable connections and a shielding of the entire installation with respect to disturbing fields.

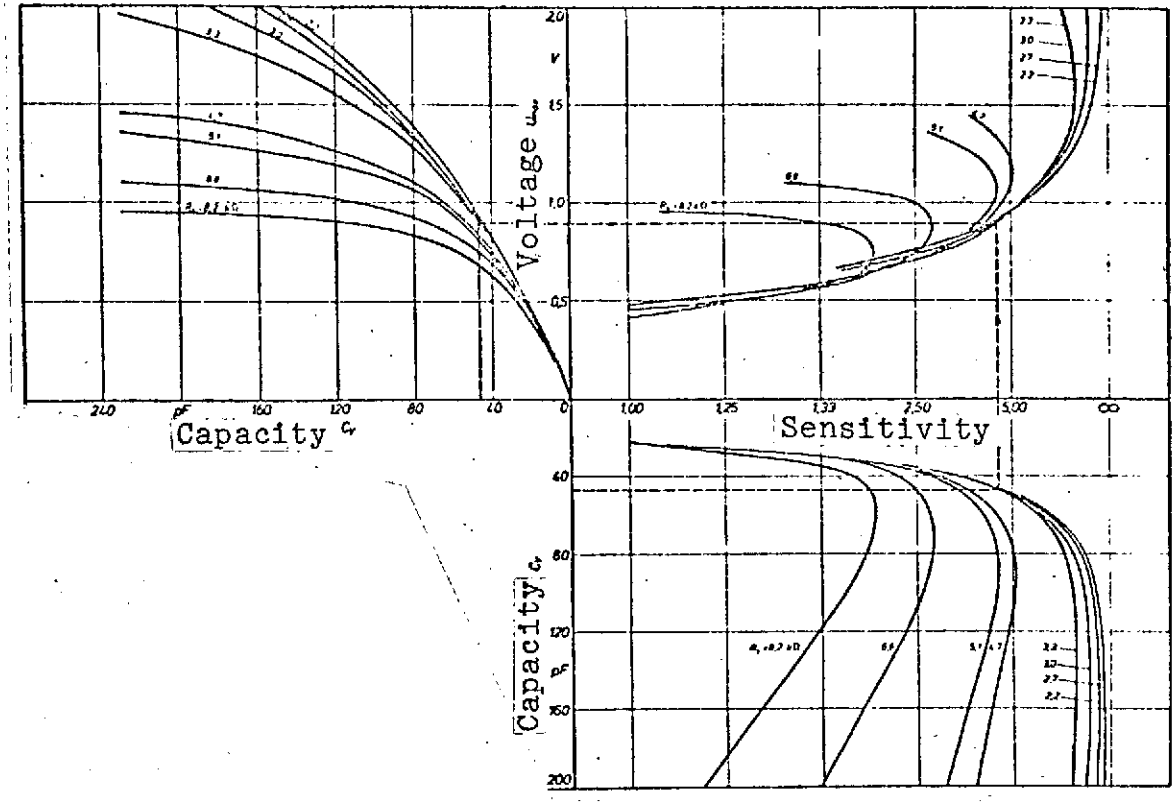

Figure 8.5. Measurement voltage and sensitivity of the measurement system as a function of series resistance.

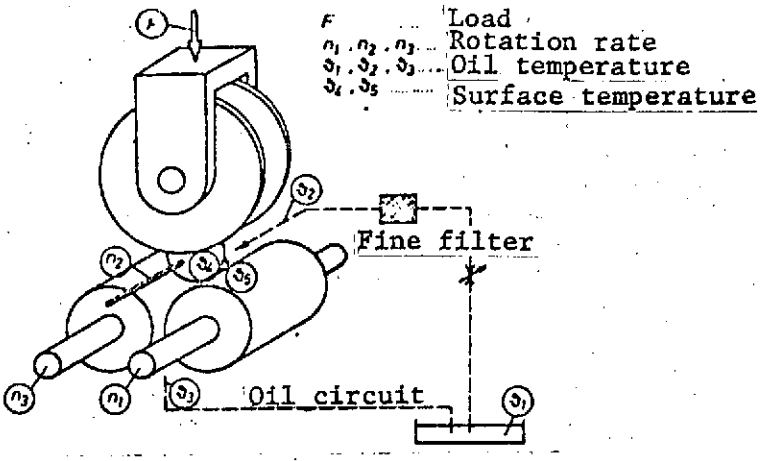

Figure 8.6. Measurement of the influence variables

8.2.2 Measurement of the parameters

In order to describe the various parameters, it is necessary to measure the load, rotation rate, oil temperature and surface temperature of the rollers. Figure 8.6 shows this. The adjusted load force F is controlled using strain gauges and a carrier frequency measurement amplifier. The temperature-compensated strain gauges are located in a force measuring box. This is calibrated at the operational conditions.

In order to determine the rotation rate, we measured the rotation rates n_1 and n_3 of the two rollers and the rotation rate n_2 of the sphere or barrel roller. Some of these measurements are done with magnetic pulse transducers and some of them, with photoelectrical units by using light-dark markings. This will keep disturbing capacitive influences away from the measurement point.

The pulses of the individual measurement points are directed to digital counters. A two-channel counter is available for accurate slip measurements. A certain angular position is defined for all three shafts by a pulse which is about 20% larger, so that it is possible to establish a correspondence of each contact surface using a two-beam oscillograph. /89

In order to determine the lubricant viscosity in the crack, it is important to exactly measure the various temperatures. The oil temperature controlled with a thermostat is measured at various points of the circuit (ϑ_1 to ϑ_3) and is recorded with a multiple pen recorder. The surface temperatures ϑ_4 and ϑ_5 of the roller are measured right next to the contact point. /90

9. EXECUTION OF THE EXPERIMENTS

9.1 Calibration of the capacitive measurement installation

In order to calibrate the capacitive measurement installation, the two rollers are separated by means of an insulating material which is a plate five mm thick. In this way the distance compared with the lubricant film thickness is relatively large, which means that the capacity is practically zero compared with the measured capacity. After equalizing the system in this state, a number of exactly known condensors are switched in parallel to the lubrication crack. This means that if the voltage displayed on the oscillograph is the same during a calibration as during the test for a certain distance of the roller, the capacities are the same. A decade condensor is used for this calibration and is shown in Figure 8.4. It can be varied in the range between 1 to 1222 pF, in the smallest steps of 1_{pF}. The error in this very accurate normal standard is less than ± 0.2%. The calibration is carried out at the same frequency of 465 kHz as the tests were carried out. This means that it is not necessary to consider the capacity change of the condensor as

a function of frequency.

9.2 Measurement process

After all measurement units have been equalized and after a certain load has been adjusted, the rotation rate of the drive shaft is increased slowly until a partial lubricant film is formed in the contact zone of the rollers. The oscillograph will then have a reading, as shown in Figure 9.1, which is often interrupted by voltage arcing caused by metallic contact. The difference between the image display and the equalization level is a measure for the measured capacity and therefore for the lubricant film thickness being determined. As the rotation rate is increased, the number of voltage arcs decreases, until there is a final complete separation of the surfaces. /92

Since the viscosity of the oil has a considerable influence on the lubricant film thickness, it is necessary to know the temperatures which occur exactly. The viscosity in the crack is primarily determined by the surface temperatures of the rolling rollers. In order to obtain as exact values as possible, these temperatures must be the same as the oil temperature during all measurements. In this way we can avoid disturbing effects of heat differences. All experiments were repeated three times.

9.3 Measurement results

The test program consisted of investigating the combinations shown in Table 4.1 for various circumferential velocities and loads. In addition, we varied the type of oil and the temperature in order to establish the influence of viscosity. We carried out a total of 10,000 measurements. The appendix gives a selection

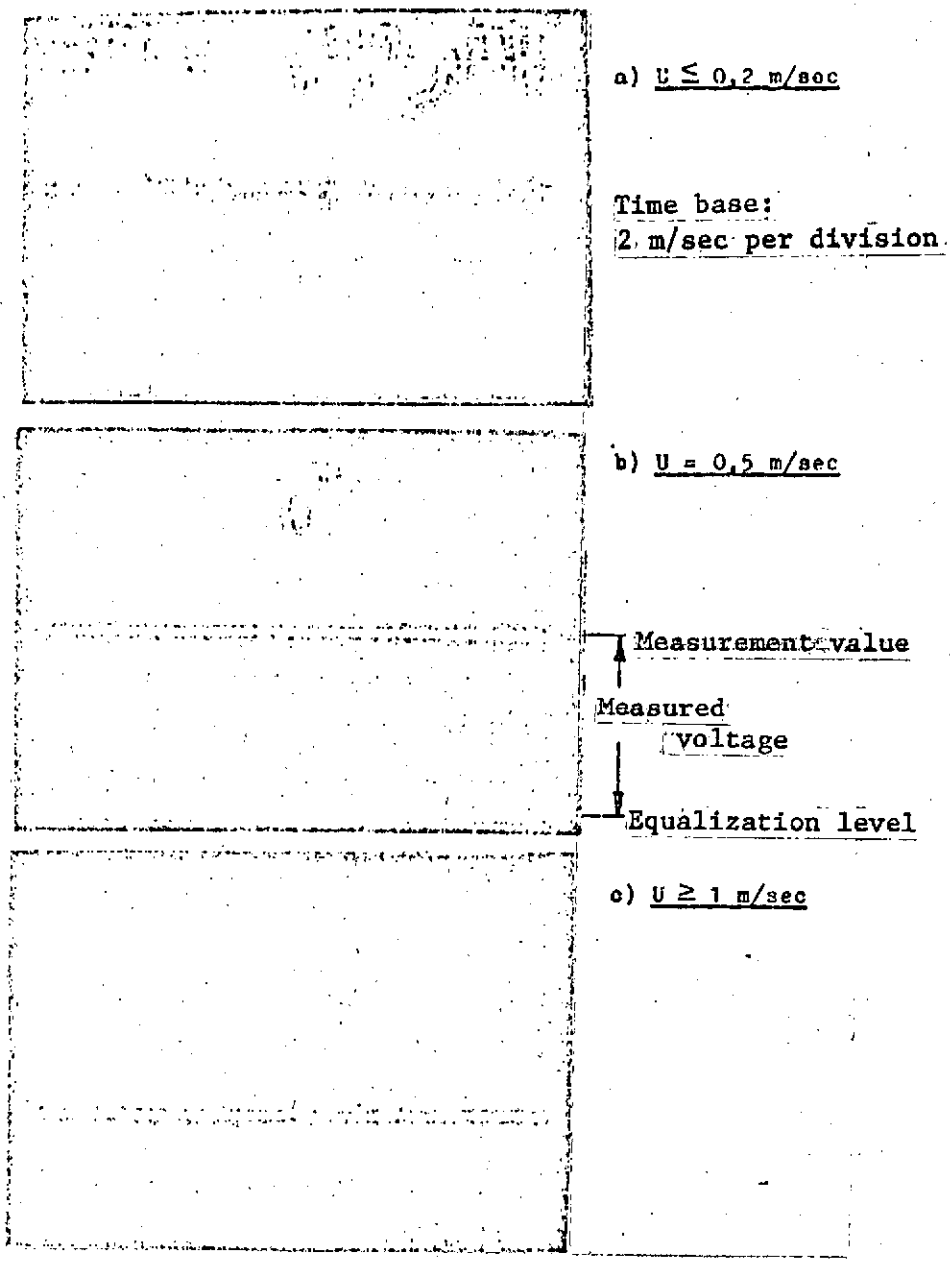

Figure 9.1. (Illegible) as a function of velocity

of measurement results.

Figures 14.1, 14.2, 14.3, and 14.4 show the influence of the roller geometry on the lubricant crack capacity under otherwise identical conditions. Figures 14.5, 14.6 and 14.7 show the important influence of the temperature. When the oil temperature and the surface temperature are increased from 30° C to 40° C, and finally to 50° C, there is a considerable increase in the capacity. A similar effect can be obtained by reducing the basic viscosity of the mineral oil as shown by Figures 14.8, 14.9 and 14.10.

9.4 Reproducibility of the measurement results

The lubricant film thickness measurements using the capacitive resistance change were found to be very reproducible. The errors which occurred were relatively small if this highly sensitive measurement method was applied carefully, especially if the temperature was maintained exactly. Two types of errors can be distinguished:

/93

a) Systematic errors

Systematic errors are produced by the measurement instruments or by the changing experimental conditions. They falsify the measurement results in one direction. For example, there is the erroneous adjustment of the load or of the amplification, erroneous equalization of the measurement system, zero point displacements of the measurement devices and temperature deviations of the roller surfaces or of the mineral oil. The error sources in this group can be eliminated for the most part, i.e. they can be avoided by careful procedures or they can be immediately found during the evaluations, if one measurement series deviates

from another by a constant amount.

b) Random errors

Random errors are distributed randomly. They can be negative or positive and are produced by various random and coincidental influences, which are not under the control of the observer, such as reading errors, rotation rate fluctuations, or recalculation errors.

Only the random errors can be described in terms of the error theory.

In the sense of statistics, the three measurement results C_i ($i = 1, 2, 3$) which are obtained for each load for a certain circumferential velocity can be considered as a sample from the totality of all equivalent and independent experiments for determining the capacity C.

The random nature of the measurement errors is characterized by the following assumptions:

Positive and negative errors with the same magnitude are equally frequent.

As the magnitude of the error increases, the frequency of the currents decreases monotonically. The frequency distribution /94 has a maximum for zero error.

Since the true value of the capacity is unknown, an estimated value $\bar{C}$ is determined to be the value with a maximum probability density for the measurement series being considered as a sample.

The average error is then

$$m_C = \sqrt{\frac{\sum_{i=1}^{3} (C_i - \bar{C})^2}{n\,(n-1)}} \,. \qquad (9.1)$$

The relative error is

$$m_r = \frac{m_C}{\bar{C}} \cdot 100\ [\%] \qquad (9.2)$$

For example, for a load of 175 kp/mm^2 it was a maximum of 1.9% for various circumferential velocities and viscosities. The average value was 1.2%. This means that the results can be considered good. /95

10. RECALCULATION OF THE LUBRICANT CRACK CAPACITY INTO FILM THICKNESSES

The measured lubricant crack capacities must be recalculated into film thicknesses using relationships between the capacity and the distance of the two bodies. Experimental calibrations cannot be used here because, on the one hand, the small distance of less than one µm is very difficult to measure, and also the important influence of the elastic deformation cannot be considered at all.

Hashimoto [50] used the following formula for the capacitive lubricant film thickness measurements between two rollers.

$$C = \varepsilon_{Oil} \cdot \varepsilon_0 \cdot 1 \cdot \int_{-R_1}^{+R_1} \frac{dx}{h_0 + \frac{x^2}{2R}} \,, \qquad (10.1)$$

i.e. he assumed non-deformed surfaces and assumed that the lubrication crack was completely filled with oil.

Dyson, Naylor and Wilson [51] considered a deformation in their measurements. They divided the region into three zones shown in Figure 10.1 and added the individual contributions to the

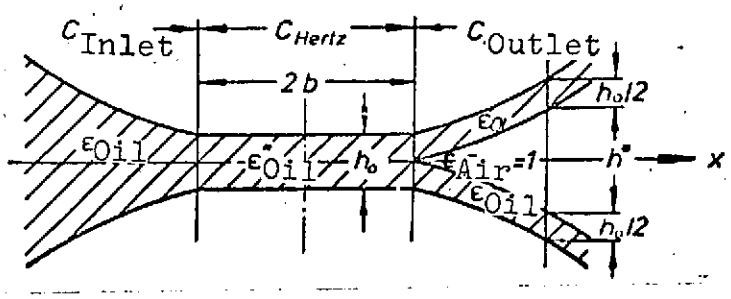

Figure 10.1. Lubrication crack model of Dyson, Naylor and Wilson.

total capacity

$$C = C_{inlet} + C_{Hertz} + C_{outlet} \tag{10.2}$$

According to our assumption, the inlet zone is completely filled with oil and according to equation (10.1) we have /96

$$C_{inlet} = \varepsilon_{oil} \cdot \varepsilon_o \cdot l \cdot \int_{-\infty}^{-b} \frac{1}{h} \cdot dx \ . \tag{10.3}$$

Considering the change in the dielectric constant with pressure, we have the following expression for the parallel central zone

$$C_{Hertz} = \varepsilon^*_{oil} \cdot \varepsilon_o \cdot l \cdot \frac{2b}{h_o} \ . \tag{10.4}$$

Finally for the outlet part we obtain

$$C_{outlet} = \varepsilon_o \cdot l \cdot \int_{+b}^{+\infty} \frac{dx}{h_o/\varepsilon_{Oil} + h^*/1} \ . \tag{10.5}$$

where we have assumed two dielectrics in series, one dielectric of oil with a thickness h_o and one dielectric of air with the thickness h*.

Archard and Kirk [49] used the following recalculation formula in their investigations for point contact and low loads

$$c = 2{,}14 \left(\ln \frac{R}{h_o} - 1\right) , \qquad (10.6)$$

and they assumed a 25-35% reduction because of incomplete oil filling. For larger loads, they assumed a constant distance for the Hertz contact surface A,

$$c = c^* = \varepsilon_{Oil} \varepsilon_o \cdot \frac{A}{h_o} . \qquad (10.7)$$

and they ignored the dependence of the remaining capacity C* on the load.

The recalculation methods described above contain many simplifications. This is especially true for point contact. This is why we will perform a differentiated analysis of the measured capacity for the case of contact between a cylindrical body and a sphere or a barrel roller, under discussion here. The accuracy of the method used will first be investigated without considering the dielectric and the deformation for the mathematically /97
accessible limiting case of a cylinder-cylinder or sphere-sphere combination. After this we will discuss the general case.

10.1 Calculation of the capacity between two cylinders

The field lines between two cylinders are circled if both bodies have the same radius. These all intersect at two points inside the cylinders. The center of these circles lies in the central plane between the cylinders because of symmetry. The electrical axes pass through the intersection points which in this case do not coincide with the geometric centers of the bodies. At these points we can assume constant charges, without changing the field. This is shown in Figure 10.2.

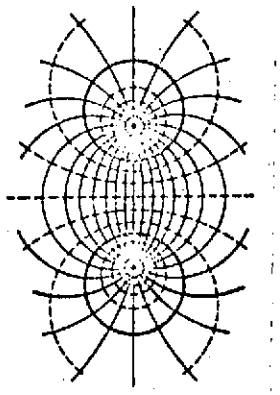

Figure 10.2. Variation of the field lines between the cylinders

The dashed equipotential surfaces are circular cylinders. They are all perpendicular to the field lines. If we replace the curved field lines by the straight connection of two adjacent surface points, it is possible to give an exact mathematical calculation of the capacity. The simplification obtained in this way is inconsequential for the results, as the following derivation will show.

With these assumptions, we obtain the following for the total capacity between two cylinders

$$C = 2 \cdot \varepsilon_0 \cdot l \cdot \int_0^R \frac{dx}{h} \quad . \tag{10.8}$$

The distance of two opposing points is

$$h = h_0 + 2(R - \sqrt{R^2 - x^2}) \quad . \tag{10.9}$$

Therefore we obtain

$$\frac{C}{\varepsilon_0 \cdot l} = 2 \cdot \int_0^R \frac{dx}{h_0 + 2R - 2R \cdot \sqrt{1 - (x/R)^2}} \quad . \tag{10.10}$$

With the substitution $\frac{x}{R}$ = cos y this leads to the result

$$\frac{C}{\varepsilon_0 \cdot l} = -\frac{\pi}{2} + \frac{2 + \frac{4}{h_0/R}}{\sqrt{1 + \frac{4}{h_0/R}}} \cdot \arctan \sqrt{1 + \frac{4}{h_0/R}} \; ; \tag{10.11}$$

Figure 10.3 shows a graphical representation. / 99

We will now give a few approximation formulas from electrical technology for capacity calculations between two long cylinders separated by a small distance. Roth [76] gives the following equation for this case

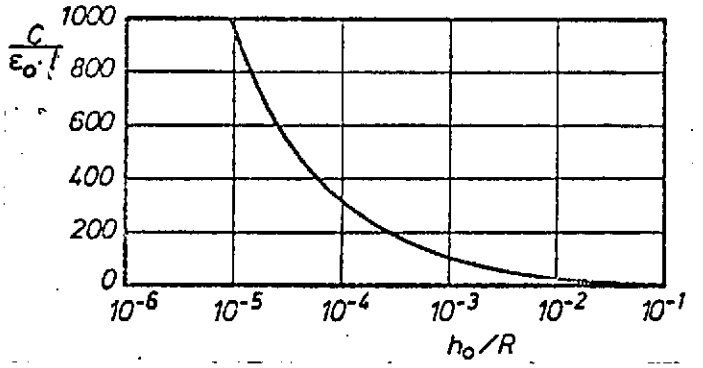

Figure 10.3. Capacity between two cylinders as a function of distance ratio h_o/R

$$\frac{C}{\varepsilon_o \cdot l} = \frac{\pi}{\ln\left[\frac{2 + h_o/R}{2} + \sqrt{\left(\frac{2 + h_o/R}{2}\right)^2 - 1}\right]} \quad (10.12)$$

Coursey [77] reached the same results, if his formula for two cylinders having different sizes is transformed. Schwaiger [78] finds the following approximate solution for the same case

$$\frac{C}{\varepsilon_o \cdot l} = \frac{2\pi}{\ln\frac{(2+h_o/R)^2 + \sqrt{(2+h_o/R)^4 - 4(2+h_o/R)^2}}{(2+h_o/R)^2 - \sqrt{(2+h_o/R)^4 - 4(2+h_o/R)^2}}} \quad (10.13)$$

All results differ only slightly from the representation shown in Figure 10.3.

If we integrate not over the entire surface but only up to a distance x from the origin, we can obtain an idea of the individual contributions to the total capacity. The formula is then as follows by carrying out the integrations

$$\frac{C}{\varepsilon_o \cdot l} = \arccos\frac{x}{R} - \frac{\pi}{2} + \frac{2 + \frac{4}{h_o/R}}{\sqrt{1 + \frac{4}{h_o/R}}} \cdot \arctan\left[\frac{1 - \sqrt{\frac{1-x/R}{1+x/R}}}{1 + \sqrt{\frac{1-x/R}{1+x/R}}} \cdot \sqrt{1 + \frac{4}{h_o/R}}\right] \quad (10.14)$$

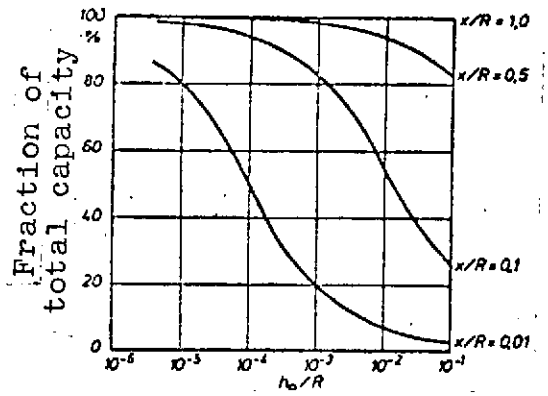

Figure 10.4. Percentage contribution of the range x/R to the total capacity.

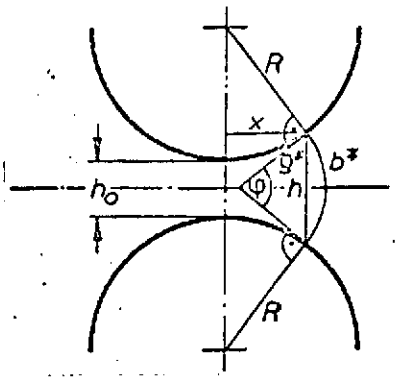

Figure 10.5. Linearization of the field line variation

We can see that for the range of interest $h_o/R < 10^{-4}$, over 90% of the total capacity is due to the range $-0.1 \leq \frac{x}{R} \leq +0.1$. This is shown in Figure 10.4.

This is why we can ignore the curved path of the field lines without introducing a large error. Since the field lines are perpendicular to the body surfaces, we have the following relationship for the arc length using the notation from Figure 10.5. /100

$$b^* = \varrho^* \cdot \widehat{\varphi} = \varrho^* \cdot 2 \cdot \arcsin \frac{h}{2 \cdot \varrho^*} \quad . \tag{10.15}$$

With

$$\varrho^* = \frac{R \cdot \frac{h}{2}}{x} \tag{10.16}$$

we find (Table 10.1)

$$\frac{h^*}{h} = \frac{R}{x} \cdot \arcsin \frac{x}{R} \quad . \tag{10.17}$$

TABLE 10.1: RATIO OF THE TRUE FIELD LINE LENGTH b* AND THE LINEAR CONNECTION h

x/R	0.01	0.1	0.5	1.0
b*/h	1.0000	1.0017	1.0472	1.5708

If we also considered the distribution of the total capacity according to Table 10.4, then the deviation from the assumed distance and therefore the error in the capacity calculation becomes negligibly small for $h_o/R < 10^{-3}$, as shown in Table 10.2. This means that in the problem under discussion, we are allowed to calculate with the straight distance of two opposing points.

TABLE 10.2: ERRORS CAUSED BY THE SIMPLIFIED CAPACITY CALCULATION OF TWO CYLINDERS*

h_o/R	10^{-5}	10^{-4}	10^{-3}	10^{-2}	10^{-1}
$\frac{\Sigma b^*}{\Sigma h}$	1,001	1,004	1,012	1,028	1,075
$\left\|\frac{\Delta C}{C}\right\|$	0,1 %	0,4 %	1,2 %	2,8 %	7,5 %

10.2 Calculation of the capacity between two spheres

The second limiting case for the problem being solved is the capacity between two spheres. In principle, we can apply the same reasoning as in Chapter 10.1. According to this, the capacity up to a distance x from the center is

$$C = \varepsilon_0 \cdot \int_0^x \frac{2 \cdot \pi \cdot x \cdot dx}{h_0 + 2R - 2 \cdot \sqrt{R^2 - x^2}} \quad . \tag{10.18}$$

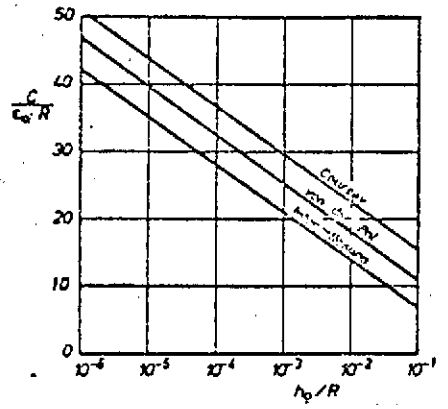

Figure 10.6. Capacity between two spheres as a function of distance ratio h_o/R

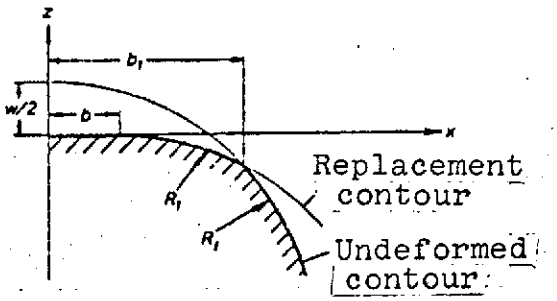

Figure 10.7. Replacement contour for capacity calculation

/102

$$\frac{C}{\varepsilon_o \cdot R} = \pi \cdot \left[\sqrt{1-(x/R)^2} + (h_o/2R+1) \cdot \ln \frac{h_o/R + 2 - 2 \cdot \sqrt{1-(x/R)^2}}{h_o/R} - 1 \right]. \qquad (10.19)$$

The total capacity is given by

$$\frac{C}{\varepsilon_o \cdot R} = \pi \cdot \left[(h_o/2R+1) \cdot \ln \frac{h_o/R+2}{h_o/R} - 1 \right]. \qquad (10.20)$$

Approximation formulas for the capacity calculations have been given by Coursey [77] for small distances

$$\frac{C}{\varepsilon_o \cdot R} = 2 \cdot \pi \cdot \left(1 + \frac{h_o/R}{\varepsilon}\right) \cdot \left(1{,}2704 + 0{,}5 \cdot \ln \frac{1}{h_o/R} + \frac{h_o/R}{45}\right). \qquad (10.21)$$

Also Clothier and Bairnsfather [80] gave the following formula based on Van Der Pol [79]:

$$\frac{C}{\varepsilon_o \cdot R} = 2 \cdot \pi \cdot \left(0{,}577 + 0{,}5 \cdot \ln \frac{1}{h_o/R}\right), \qquad (10.22)$$

Figure 10.6 shows a graphical representation.

The distribution of the capacity over the surface is similar to the cylinder-cylinder case. Here again we find that most of the total capacity comes from the immediate vicinity of the areas near the center.

10.3 Calculation of capacity between two arbitrary bodies

The capacity between two bodies having arbitrarily curved surfaces is calculated by summing the individual distances of two opposing points on the body surfaces. As shown in Chapter 10.1 it is possible to simplify the course of the field lines without introducing substantial errors. /103

On the other hand, the capacity is considerably changed by the elastic deformations. In the Equation (5.8) derived in Chapter 5.2

$$w(x,y) = \frac{2\cdot(1-\nu^2)}{\pi\cdot E}\cdot\iint_{(A)}\frac{p\cdot dx_1\cdot dy_1}{\sqrt{(x-x_1)^2+(y-y_1)^2}}$$

The integrand becomes infinite for $x = x_1$ and $y = y_1$. This difficulty can be avoided by transferring to polar coordinates. For example, with

$$dx_1\cdot dy_1 = r\cdot dr\cdot d\varphi \qquad (10.23)$$

the maximum deformation at the center of the pressure distribution becomes

$$w_o = \frac{2\cdot(1-\nu^2)}{\pi\cdot E}\cdot\int_0^{2\pi}\int_0^{r} p(r,\varphi)\cdot dr\cdot d\varphi \quad . \qquad (10.24)$$

Since the experiments are carried out with very large loads and for pure rolling conditions, we can assume the pressure distribution of Hertz in order to obtain sufficient accuracy in the recalculation. This distribution is given by the following formula in polar coordinates

$$p(r,\varphi) = p_o\cdot\sqrt{1-\left(\frac{r\cdot\cos\varphi}{b}\right)^2-\left(\frac{r\cdot\sin\varphi}{a}\right)^2} \quad . \qquad (10.25)$$

The elliptical pressure area is limited by

$$r_{max} = \sqrt{\frac{1}{(\frac{\cos\varphi}{b})^2 + (\frac{\sin\varphi}{a})^2}} \quad (10.26)$$

Thus we obtain the following deformation

$$w_o = \frac{8(1-\nu^2)}{\pi \cdot E} \cdot p_o \cdot \int_0^{\pi/2} \int_0^{r_{max}} \sqrt{1-(\frac{r\cdot\cos\varphi}{b})^2-(\frac{r\cdot\sin\varphi}{a})^2} \cdot dr \cdot d\varphi. \quad (10.27)$$

The numerical solution of this double integral is obtained by applying the Simpson rule twice

$$F \approx \frac{s}{3}\left[y_0+y_n+4(y_1+y_3\cdots+y_{n-1})+2(y_2+y_4\cdots+y_{n-2})\right]. \quad (10.28)$$

It is not necessary to find a replacement contour for the capacity calculation, which is as close as possible to the true distance of the deformed body surface.

For this purpose, we calculate the deformations of the bodies to a distance of up to 20 times the length of the ellipse semiaxes. The true distances are then determined by considering the body curvatures. We found that the pressure ellipse can be assumed to be a plane and the remainder of the replacement contour is tangential to this plane in all directions. This is shown in Figure 10.7.

The replacement contour intersects the undeformed contour at a distance b_1 from the center of the Hertz surface. This intersection point can be determined from the following quadratic equation /105

$$b_1^2(4b^2+w^2)-b_1(bw^2+4b^3)+w^2(\frac{w^2}{16}+\frac{b^2}{2}-R_1^2)+b^4=0 \quad (10.29)$$

The equation for the intersection point a_1 in the y direction is similar.

In order to numerically calculate the capacity, we assume the replacement contour up to the intersection point and after that the undeformed original contour. The error in the

capacity calculation because of the slight deviation from the exact shape of the surface is less than 1%.

Thus we find the following for the ellipse-shaped contact surface.

$$C_1 = \frac{\varepsilon_0 \cdot \pi \cdot a \cdot b}{h_0} \quad . \tag{10.30}$$

The capacity for the sphere-roller case and for the outer region from the intersection point up to the edge become

$$C_3 = 4 \cdot \varepsilon_0 \cdot \int_{y_1=0}^{y_2=R_1} \int_{x_1=b_1 \cdot \sqrt{1-(y/a_1)^2}}^{x_2=\sqrt{R_1^2-y^2}} \frac{dx \cdot dy}{h_0 - w_0 + h_1 + L_2} \quad . \tag{10.31}$$

The outer limits for the barrel roller are

$$\left.\begin{aligned} y_2 &= \frac{l}{2} \quad , \\ x_2 &= \sqrt{R_3^2 - y^2} + R_1 - R_3 \quad . \end{aligned}\right\} \tag{10.32}$$

the distances for the two bodies are

$$\left.\begin{aligned} h_1 &= R_1 - \sqrt{\left|\sqrt{R_3^2 - y^2} + R_1 - R_3\right|^2 - x^2} \quad , \\ h_2 &= R_2 - \sqrt{\left|\sqrt{R_4^2 - y^2} + R_2 - R_4\right|^2 - x^2} \quad . \end{aligned}\right\} \tag{10.33}$$

The equations simplify as follows for the special case of a sphere-cylinder roller combination

$$\left.\begin{aligned} h_1 &= R_1 - \sqrt{R_1^2 - y^2 - x^2} \quad , \\ h_2 &= R_2 - \sqrt{R_2^2 - x^2} \quad . \end{aligned}\right\} \tag{10.34}$$

/106

This outer region is divided even more for the calculation in order to be able to consider distances in the dielectric (see Chapter 10.4).

Finally we obtain the following for the central range from the edge of the contact surface to the intersection point

$$C_2 = 4 \cdot \varepsilon_0 \cdot \int_{y_1=0}^{y_2=a_1} \int_{x_1=b \cdot \sqrt{1-(y/a)^2}}^{x_2=b_1 \cdot \sqrt{1-(y/a_1)^2}} \frac{dx \cdot dy}{h_0 + h_1' + h_2'} \quad . \tag{10.35}$$

The distances h_1' and h_2' are determined by the fact that the replacement coutour is tangential to the elliptical contact surface.

This means that if air is the dielectric, the total capacity is

$$C = C_1(h_0) + C_2(h_0) + C_3(h_0) \quad . \tag{10.36}$$

10.4 Dielectric

The composition of the dielectric in the lubrication crack has a considerable influence on the recalculation. For this we first determined the dielectric coefficient for the mineral oils used according to the test guidelines VDE 0303, part 4/12.69. This is shown in Table 10.3. We were not able to establish any difference for the temperatures between 30° C to 50° C used in the experiments.

TABLE 10.3: DIELECTRIC COEFFICIENT ε_{OIL} FOR ATMOSPHERIC PRESSURE AND 30 TO 50° C*

	Tellus 23	Tellus 29	Tellus 41	Tellus 69
50 Hz	2,26	2,28	2,29	2,30
465 kHz	2,12	2,14	2,15	2,16

* Translator's note: Commas represent decimal points.

This means that the time between two oscillations is no longer sufficient for establishing a field for the measurement frequency of 465 kHz used so that the dielectric constant decreases. /107

It is necessary to consider three regions with different dielectrics in the capacity measurements between two rollers lubricated with oil:

The lubrication crack is completely filled with oil in the contact zone. Because of the high pressure, the dielectric constant deviates from the values given in Table 10.3. It varies with density in mineral oils according to the following law (for example Bondi [81])

$$\frac{\varepsilon_{Oil} - 1}{(\varepsilon_{Oil} + 2) \cdot \rho} = \text{const.} \tag{10.37}$$

This means that for higher pressures we have

$$\varepsilon'_{Oil} = \frac{\varepsilon_{Oil}}{\varepsilon_{Oil}} \frac{+ 2 + 2(\varepsilon_{Oil} - 1) \cdot \rho'/\rho_o}{+ 2 - (\varepsilon_{Oil} - 1) \cdot \rho'/\rho_o} \quad . \tag{10.38}$$

This means that we have the following relationship between the density ratio and the pressure according to Equation (4.33)

$$\frac{\rho'}{\rho_o} = 1 + \frac{9.73 \cdot 10^{-3} \cdot p_m^{0.75}}{v^{0.0385}} \quad .$$

In the vicinity of the contact zone, the crack is also completely filled with oil, but we do not have the increased pressure so that we can use the dielectric constant ε_{oil}.

In the edge zone, the dielectric consists of oil and air. Physically, these two media are in series, so that we have

$$\left.\begin{aligned} &\frac{1}{C_{Edge}} \cdot \frac{1}{C_{Air}} \cdot \frac{1}{C_{Oil}} \cdot \\ &\frac{\Sigma h}{\epsilon} \cdot \frac{\Sigma h_{Air}}{\epsilon_{Air}} \cdot \frac{\Sigma h_{Oil}}{\epsilon_{Oil}} \cdot \end{aligned}\right\} \qquad (10.39)$$

For $\epsilon_{Air} \cdot 1$ and $\Sigma h_{Air} \cdot \Sigma h - \Sigma h_{Oil}$ we have

$$\epsilon \cdot \frac{1}{1 + \Sigma h_{Oil} / \Sigma h \cdot (1/\epsilon_{Oil} - 1)} \cdot \qquad (10.40)$$

It is relatively difficult to make the division between air and oil and to determine the limits of the region completely filled with oil. We carried out extensive experiments in order to determine this. We performed static experiments with the calibration installation and dynamic experiments with the measurement gear.

The distance between two insulated bodies can be changed with a micrometer screw on the calibration device as shown in Figure 10.8.

Two inductive pass transducers are used to carry out measurements with an electronic length measurement unit, having an amplification factor of 1 : 50,000 (scale division 0.02 µm). The corresponding capacity is determined according to the method described in Chapter 8.2.1.

A test body (sphere or barrel roller) is fixed on the measurement gear at a defined distance from the rotating opposing body, using a special device.

With these two test installations, it was possible to determine the percentage of air in the edge zones with sufficient accuracy for the individual roll repairs. This is true because

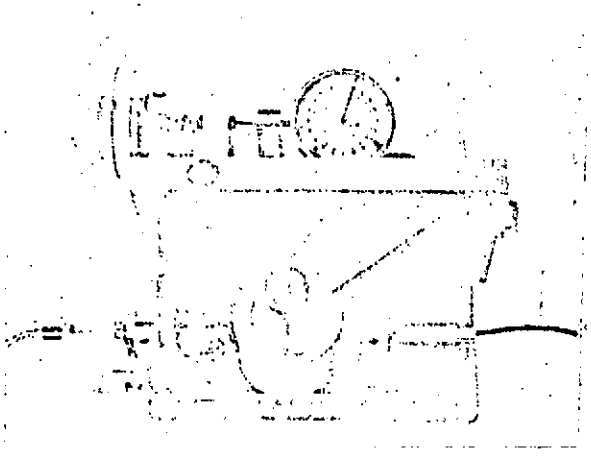

Figure 10.8. Calibration installation for investigating the dielectric

less than 10% of the total capacity is produced in this area. We were not able to establish any influence of the circumferential velocity of the body or of the amount of lubricant on the composition of the dielectric. /109

10.5 Recalculation curves

The total capacity between the individual roller combinations can be determined from the formulas derived from above. It is composed of

$$C = \varepsilon_{\ddot{O}il} \cdot C_1(h_o) + \varepsilon_{\ddot{O}il}\left[C_2(h_o) + C_{30}(h_o)\right] + \sum_{n=1}^{n}\left[\varepsilon_n \cdot C_{3n}(h_o)\right]. \qquad (10.41)$$

The distance is changed from h_o = 0.1 µm to h_o = 5 µm. After evaluating the numerical results, one obtains recalculation curves as shown in Figure 10.9 for an example of a barrel roller and a roller. The measured lubrication crack capacities C can be recalculated to the corresponding lubricant film thickness h_o using these curves.

11. TEST RESULTS

A selection from the numerous test results is contained in the appendix (Chapter 14). Because such a large number of measurements were performed, it is possible to determine the influence of the individual parameters and to investigate their importance for the lubricant film thickness. In the final analysis, all the varied quantities can be collected into an empirical common formula, which will give information on the

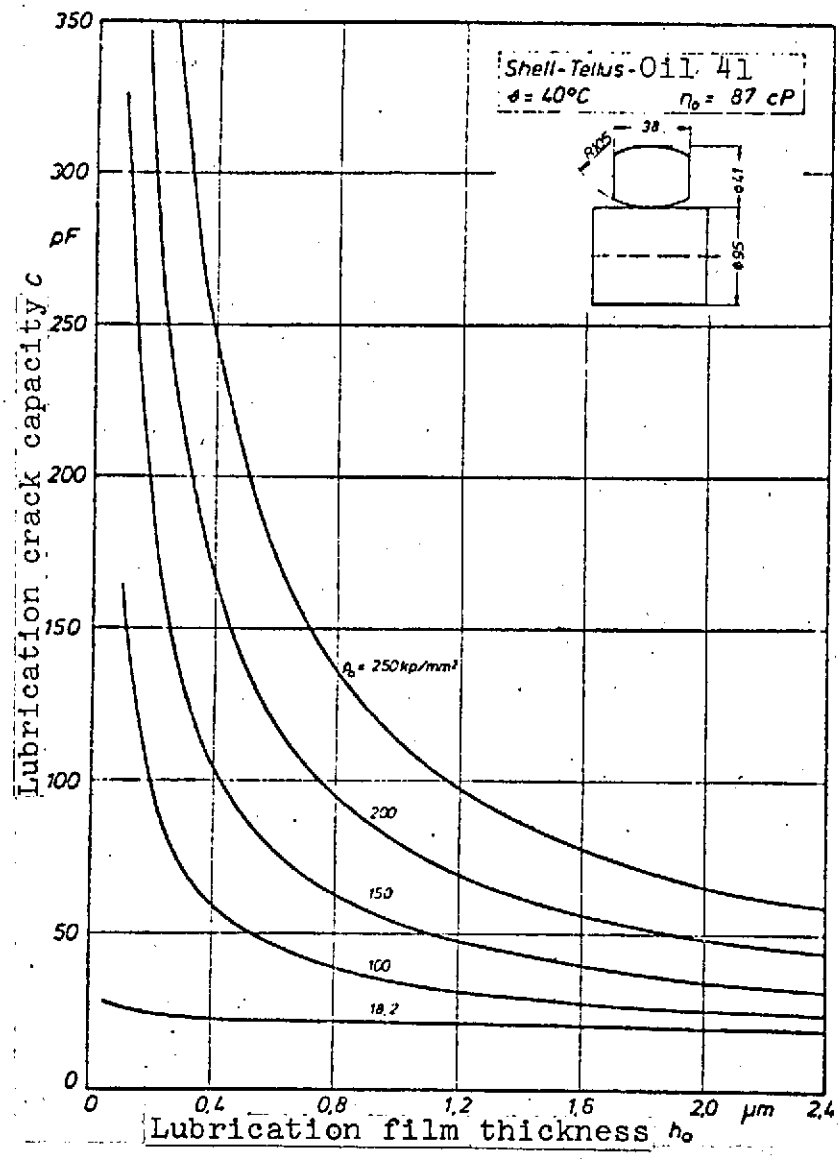

Figure 10.9. Lubrication crack capacity as a function of lubrication film thickness h_o

thickness of the lubricant film between two loaded roller bodies.

11.1 Influence on the circumferential velocity

The circumferential velocity U was varied in the range between 0 to 12 m/sec. We were able to verify the expected increase in the lubricant film thickness as the velocity was increased in all the measurements. Figure 14.11 shows a few of the measurement results. We always found a value of 0.72 for the velocity exponent, even for otherwise different conditions, i.e. a doubling in the circumferential velocity leads to an increase of 60% in the lubricant film thickness. The results are in the range of the experimental values contained in the literature for line contact, and within the range of the theoretical values for point and line contact.

Other measurements have shown that the exponent becomes smaller at higher circumferential velocities, so that the factor $U^{0.72}$ only seems to be valid for velocities up to 10 m/sec.

11.2 Influence of the load

The Hertz pressure p_o was selected as a measure of the load. This influence was found to be greater than expected for the extremely high loads investigated. Figure 14.12 shows that the decrease in the film thickness with increasing Hertz pressure is described to a good degree of approximation by the negative exponent 0.35. This corresponds to an exponent of minus 0.12 /112
for the load force F. This is a value which agrees with the published results for line contact. However, up to the present a lower value has been given for point contact. The lubricant film thickness decreases by only 8% when the normal force is doubled.

This also explains the fact that even the highest loads cause a closed oil film without metallic contact of the two surfaces for relatively small circumferential velocities. The elastohydrodynamic theory is therefore completely valid even for the highest loads in the elastic range which had not been investigated up to the present.

11.3 Influence of the shape of the Hertz contact area

The shape of the Hertz contact area was varied from an approximately circular shape to a rectangular shape. The technically interesting case of an ellipse perpendicular to the roll direction was investigated. In other words, the ellipse semiaxis b in the direction of the circumferential force was always smaller than the semiaxis a. The influence of the axis ratio was found to be small. Figure 14.13 shows that the lubricant film thickness is only slightly larger for elongated ellipses, that is for the so-called line contact case. This dependence can be characterized using the auxiliary variable $\cos \vartheta$ with the exponent 0.08 for the investigated range between 0.1 and 1.0.

This result was confirmed by Cheng [32], but in the case of Archard and Cowking [30], the lubricant film thickness increases faster for point contact. We expect that in this latter case, the increasing bore friction contribution caused by the test installation at small values of $\cos \vartheta$ decreases the lubricant film thickness and therefore leads to an apparently larger influence of the axis ratio.

11.4 Influence of oil viscosity /113

On the other hand, the viscosity of the lubricating oil used has a very substantial influence on the film thickness. As examples of Figure 14.14 show, the exponent 0.8 can be used here.

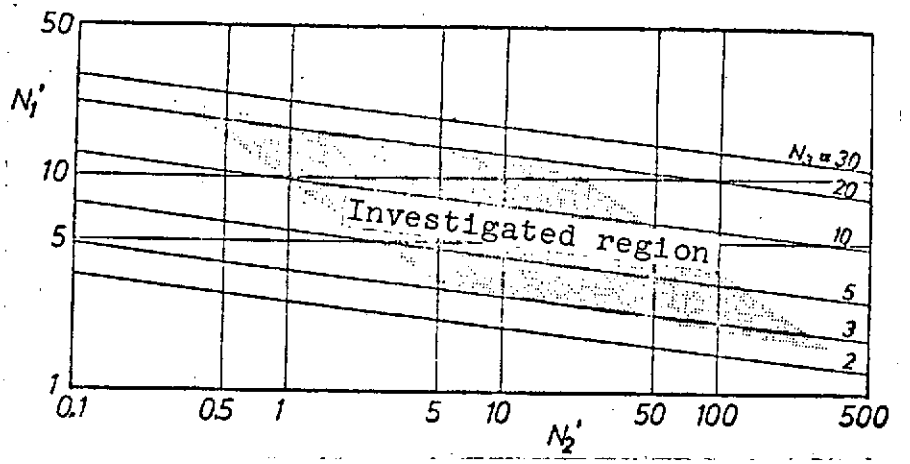

Figure 11.1. State diagram of the elastohydrodynamic lubrication film thickness for elliptical contact

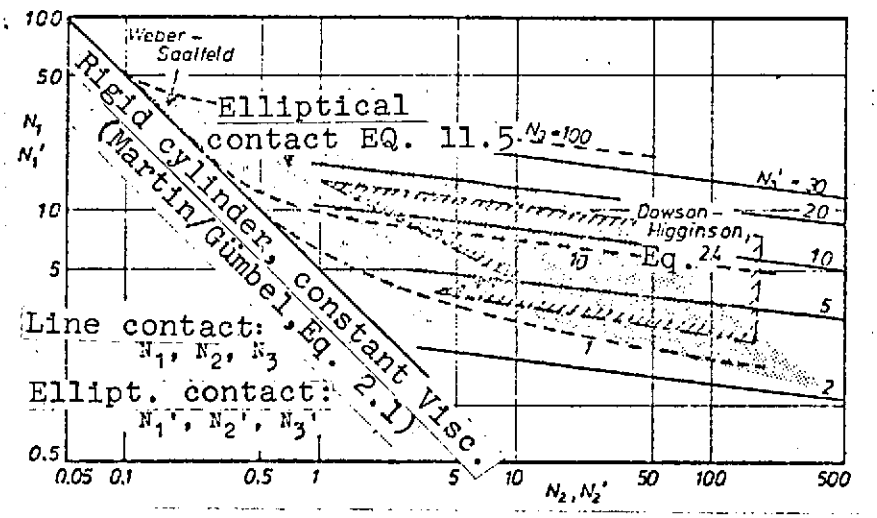

Figure 11.2. Comparison of elliptical contact and line contact on a Moes diagram

This means that for the case of the Tellus oils used, a temperature increase of 10° C decreases the lubricant film thickness by more than 30%. This fact shows that the measurements can only be reproduced if the temperatures are controlled very accurately. The oil temperature which prevails when there is a heat equilibrium between the rollers and the lubricants is characteristic for each test.

There are no differences for the various types of Tellus oil used. This means that a thicker oil at a high temperature produces the same values as a thinner oil at lower temperatures, if the viscosity η_o was the same. This means that we had a continuous range between 10 to 300 cP available for the experiments.

11.5 Influence of the pressure-viscosity behavior of the lubricating oil

As mentioned above, the pressure-viscosity behavior of the oil is very important in the calculation of the elastohydrodynamic lubrication problem. This is described by Equation (4.39)

$$\frac{\eta}{\eta_o} = \frac{1}{\eta_o} \cdot \exp\left[0{,}16478 \cdot p \cdot \ln \eta_o + \sqrt{(\ln \eta_o)^3}\right]^{2/3},$$

According to Figure 14.15, and for the pressures investigated in our experiments, this equation can be represented as follows with sufficient accuracy

$$\frac{\eta}{\eta_o} = (10 \cdot \eta_o)^{\frac{p^{0{,}75}}{15{,}5}} \qquad (11.1)$$

In the literature, the influence of the pressure-viscosity behavior on the film thickness is often expressed in terms of the factor α in the exponential law

$$\frac{\eta}{\eta_o} = e^{\alpha \cdot p}$$

/114

When applied to Equation (11.1), this leads to the empirical formula

$$\alpha = \frac{\ln(10 \cdot \eta_o)}{15{,}5 \cdot p^{0{,}25}} \qquad (11.2)$$

or with $p = p_o/1.5$

this leads to $$\alpha = \frac{\ln(10 \cdot \eta_o)}{14 \cdot p_o^{0{,}25}} \; . \qquad (11.3)$$

In the measurements which we carried out, α lies in the range between 0.07 to 0.18 mm^2/kp and has only a small influence on the lubricant film thickness with the exponent 0.7 as a review of the results shows. The small deviations at the limiting values of pressure and viscosity are equalized well by this factor.

11.6 Summary of the test results

The investigations therefore lead to the following formula

$$h_o \sim (\cos\vartheta)^{0{,}08} \cdot \alpha^{0{,}7} \cdot \eta_o^{0{,}8} \cdot u^{0{,}72} \cdot p_o^{-0{,}35} \qquad (11.4)$$

where $$\alpha = \frac{\ln(10 \cdot \eta_o)}{14 \cdot p_o^{0{,}25}} \; .$$

The evaluation of all the measurements resulted in a deviation of ± 15% and a proportionality factor of $0.27 \cdot 10^{-3}$. Finally we find the following formula for the lubricant film thickness in mm.

$$h_o = 0{,}27 \cdot 10^{-3} \cdot (\cos\vartheta)^{0{,}08} \cdot \alpha^{0{,}7} \cdot \eta_o^{0{,}8} \cdot u^{0{,}72} \cdot p_o^{-0{,}35} \; . \qquad (11.5)$$

All parameters are to be substituted with the known dimensions. /115
The lubricant film thicknesses therefore lie in the range between 0.3 to 2.5 µm for the indicated ranges.

For the line contact problem, and assuming isothermal and incompressible conditions, several suggestions have been made for representing the various parameters in certain physically reasonable

dimensionless groups, so that a suitable plot could be drawn.

Dowson and Higginson [16] suggested the following four dimensionless parameters

$$\left.\begin{array}{ll} \text{the film thickness parameter} & H = \frac{h_o}{R} \,, \\ \text{the load parameter} & W = \frac{F/l}{E' \cdot R} \,, \\ \text{the velocity parameter} & \bar{U} = \frac{\eta_o' \cdot U'}{E' \cdot R} \\ \text{a parameter} & G = \alpha \cdot E' \,, \end{array}\right\} \tag{11.6}$$

which describe the properties of the material and the lubricant.

Moes [82] uses the following three-dimensionless groups

$$\left.\begin{aligned} N_1 &= \frac{h_o}{R} \cdot \left[\frac{E' \cdot R}{\eta_o' \cdot U'}\right]^{1/2} = H \cdot \bar{U}^{-1/2} \,, \\ N_2 &= \frac{F/l}{E' \cdot R} \cdot \left[\frac{E' \cdot R}{\eta_o' \cdot U'}\right]^{1/2} = W \cdot \bar{U}^{-1/2} \,, \\ N_3 &= \alpha^* \cdot E' \cdot \left[\frac{\eta_o' \cdot U'}{E' \cdot R}\right]^{1/4} = G^* \cdot \bar{U}^{1/4} \,, \end{aligned}\right\} \tag{11.7}$$

where

$$\alpha^* = \left[\int_0^\infty \frac{\eta_o}{\eta} \cdot dp\right]^{-1} \,, \tag{11.8}$$

so that the pressure coefficient is no longer tied to the exponential law, which only applies in a few cases.

Theyse [83] gave an exact mathematical proof that three parameters are sufficient for characterizing the problem for incompressible and isothermal conditions, /116

$$\left.\begin{aligned} \bar{h} &= \frac{h_o}{R} \cdot \frac{F/l}{\eta_o' \cdot U'} = \frac{H \cdot W}{\bar{U}} \,, \\ g_1 &= \frac{\alpha}{R} \cdot \frac{(F/l)^{3/2}}{(\eta_o' \cdot U')^{1/2}} = \frac{G \cdot W^{3/2}}{\bar{U}^{1/2}} \\ \text{and} \quad g_3' &= \frac{(F/l)^2}{E' \cdot R \cdot \eta_o' \cdot U'} = \frac{W \cdot W}{\bar{U}} \,. \end{aligned}\right\} \tag{11.9}$$

Archard [84] accepted the parameters suggested by Moes and proved that they also can be applied for point contact if the load parameter W is replaced by

$$W' = \frac{P}{E' \cdot R^2} \quad ; \tag{11.10}$$

we then obtain

$$H \cdot \bar{U}^{-1/2} \quad G \cdot \bar{U}^{1/4} \quad , \quad \bar{U}^{-1/4} \cdot W'^{1/3} \quad , \quad \frac{R_x}{R_y} \quad . \tag{11.11}$$

Greenwood [85] suggested the following groups, similar to those of Theyse

$$\left.\begin{aligned} \bar{h} &= \frac{h_0}{R} \cdot \frac{F/l}{\eta_0' \cdot U'} = \frac{H \cdot W}{\bar{U}} \quad , \\ g_1 &= \frac{\alpha \cdot (F/l)^{3/2}}{R \cdot (\eta_0' \cdot U')^{1/2}} = \frac{G \cdot W^{3/2}}{\bar{U}^{1/2}} \quad , \\ g_2 &= \alpha \cdot \left[\frac{F/l \cdot E'}{R}\right]^{1/2} = G \cdot W^{1/2} \end{aligned}\right\} \tag{11.12}$$

He showed that the technically possible values of g_2 are contained within a very small band, so that the lubricant film thickness depends primarily on the two groups $\bar{h}$ and g_1.

Finally Johnson [86] attempted to limit the various reagents using elastohydrodynamic limits. He distinguished three variables, which all have the dimension of pressure: /117

$q_r = \frac{(F/l)^{3/2}}{R \cdot (\eta_0' \cdot U')^{1/2}}$ is a measure for the liquid pressure produced by a lubricant when the deformation is ignored,

$\frac{1}{\alpha}$ is a measure for the change of viscosity with pressure

$p_0 = \frac{P}{2 \cdot \pi \cdot R \cdot l \cdot E'}$ is the maximum pressure for dry elastic contact

In this way he defined the following four parameters,

$$\left.\begin{aligned} g_1 &= \alpha \cdot q_f \,, \quad g_2 = \alpha \cdot p_0 \,, \quad g_3 = \frac{1}{\sqrt{2\pi}} \cdot \frac{q_f}{p_0} \,, \\ g_4 &= (2\pi)^{3/4} \cdot (\alpha \cdot p_0) \cdot \left(\frac{q_f}{p_0}\right)^{-1/2} \,, \end{aligned}\right\} \qquad (11.13)$$

and established a diagram for roller lubrication, which included all results known up to that time.

If in the dimensionless groups of Moes given by Equation (11.7) the expression N_1 is expanded by the corresponding contribution of the coefficient $\cos \vartheta$, and if in N_2 the load parameter W' for point contact is introduced according to equation (11.10), we find the following for the elliptical contact case

$$\left.\begin{aligned} N_1' &= \frac{h_0}{R} \cdot \left[\frac{E' \cdot R}{\eta_0' \cdot U'}\right]^{1/2} \cdot (\cos\vartheta)^{-0,08} \,, \\ N_2' &= \frac{1}{3} \cdot (2 \cdot \pi \cdot \xi \cdot \eta)^3 \cdot \left(\frac{p_0}{E'}\right)^3 \cdot \left[\frac{E' \cdot R}{\eta_0' \cdot U'}\right]^{1/2} \,, \\ N_3 &= \alpha \cdot E' \cdot \left[\frac{\eta_0' \cdot U'}{E' \cdot R}\right]^{1/4} \,. \end{aligned}\right\} \qquad (11.14)$$

For this case, Figure 11.1 gives a summary of the investigations carried out. We find the following relationships from the present experimental results between the dimensionless values N_i

$$N_1' = 1,58 \cdot N_2'^{-0,12} \cdot N_3^{0,74} \,. \qquad (11.15)$$

Therefore it becomes possible to characterize any lubrication case within the investigated region and to determine the corresponding film thickness. /119

12. SUMMARY

The investigations extending over many years at the Institute of Machine Elements and Conveyor Technology of the Technical University Braunschweig had been continued by the work described in this paper. Up to the present, the tangential forces which could be transmitted inside the Hertz surfaces were of primary interest in the research activities(Lutz [87], Wernitz [88], Maass [89], and Buschhorn [90]). We made a more detailed investigation of the processes in the separation gap.

It is known that roller pairs such as gear teeth, continuous gears, etc. can only operate with a lubricant. This has the purpose of reducing the number of metallic contact points between the surfaces. It therefore keeps the friction and wear down. According to the elastohydrodynamic lubrication theory, this separation also occurs under high loads. Then there is an equilibrium state between the hydrodynamic pressure and the lubricants and the contact pressure in the elastically deformed rollers.

An extensive review of the known literature shows that this theory has almost exclusively been investigated for line contact between two infinitely long cylinders, and for relatively small loads.

A numerical method has been developed for elliptical Hertz contact areas which makes it possible to calculate the phenomena in the lubrication gap. Considering the pressure dependence of the oil viscosity and oil density, the system of equationswhich describe the problem are solved together. Two different iteration methods provide the desired results for the inlet zone and for the Hertz region proper.

Both contours are mostly parallel when the contact areas are limited on the side, just like four-line contact. Just as the gap size is reduced on the outlet side in their case, we also find that the line of minimum film thickness has the shape of a horseshoe, bent towards the inlet side.

This leads to a steep and arc-shaped peak within the pressure distribution, just like the "pressure tip" for infinitely long surfaces. /120

A test stand and a suitable measurement method have been developed for experimentally determining the lubrication film thickness. Load levels up to the elastic deformation limit can be applied. Other possible parameters will include the circumferential velocity and the geometry of the rollers rolling along each other. Also the characteristics of the oil can be varied. The crack thickness is determined using capacity changes. The measured values are recalculated into distance values, using mathematical formulas. The results can be reproduced very well if the experiments are carried out carefully. There is a complete separation of the surfaces by the lubricant for even small circumferential velocities. The film is not destroyed even under the highest loads. A systematic investigation of the individual parameters has been made. A formula was established which makes it possible to determine the elastohydrodynamic lubrication film thickness for two arbitrary rollers, which roll along each other without slip.

The crack heights vary between 0.3 and 0.25 µm for the range investigated. The agreement with the calculated results is very good. For example, a film thickness of 1.66 µm was measured for the example described in Chapter 7.3. This can be compared with the calculated value of 1.62 µm.

The theoretical and the experimental investigations therefore confirm the existence of an almost parallel lubrication film between the highly loaded roller bodies having elliptical contact surfaces. The shape of the ellipse is of secondary importance.

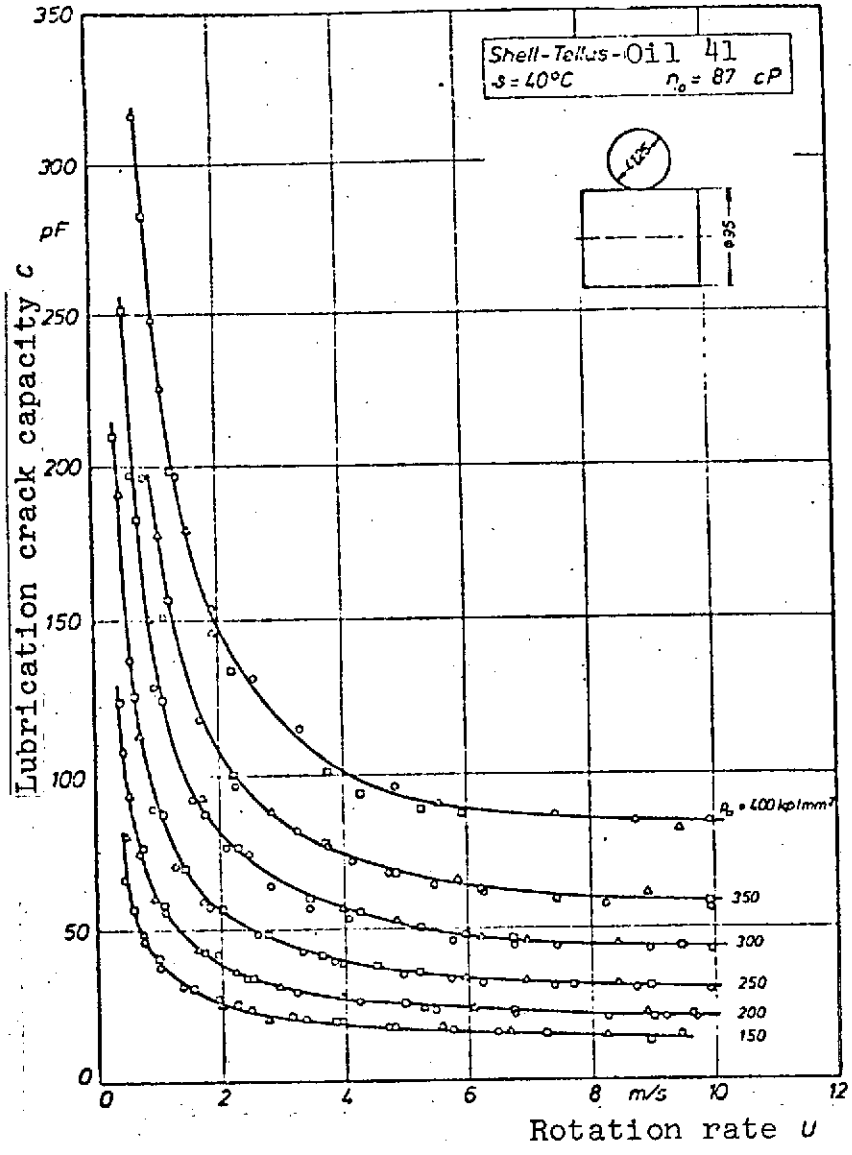

Figure 14.1. Lubrication crack capacity between sphere and cylindrical roller

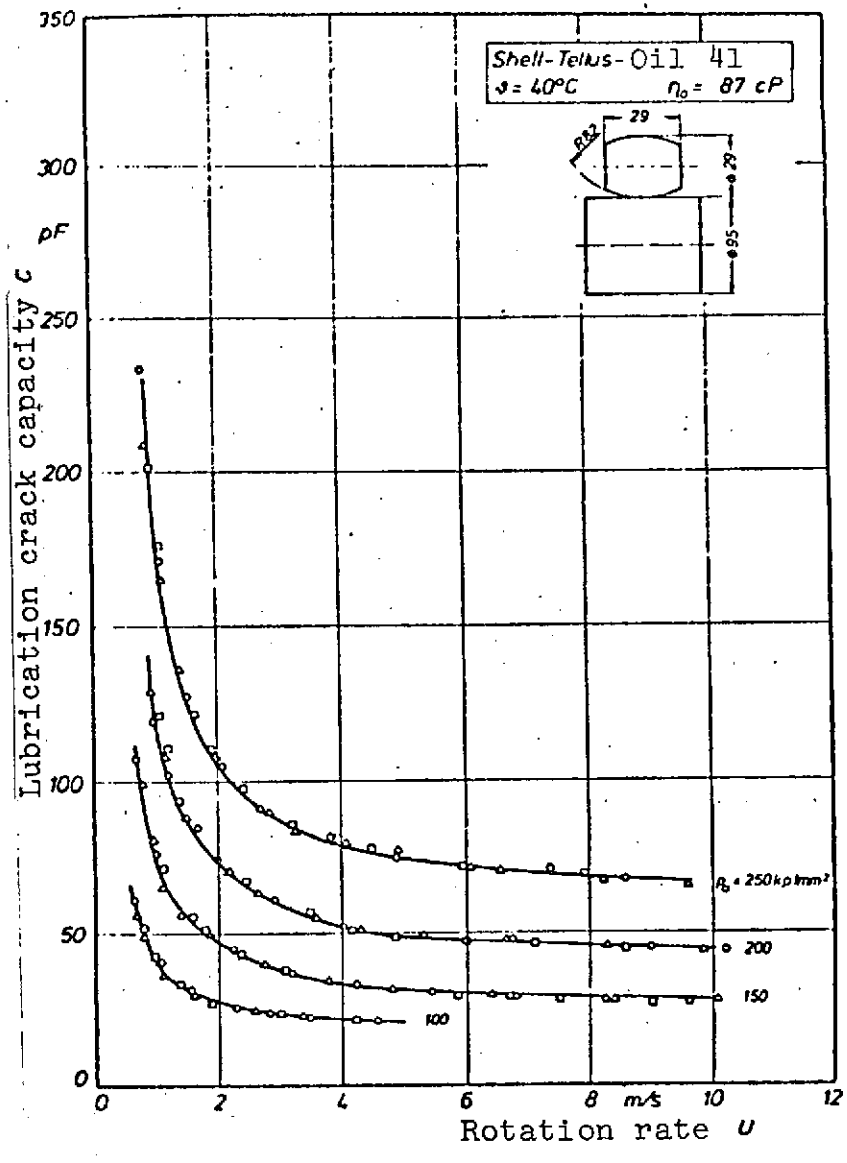

Figure 14.2. Lubrication crack capacity between barrel roller with a large curvature and a cylindrical roller

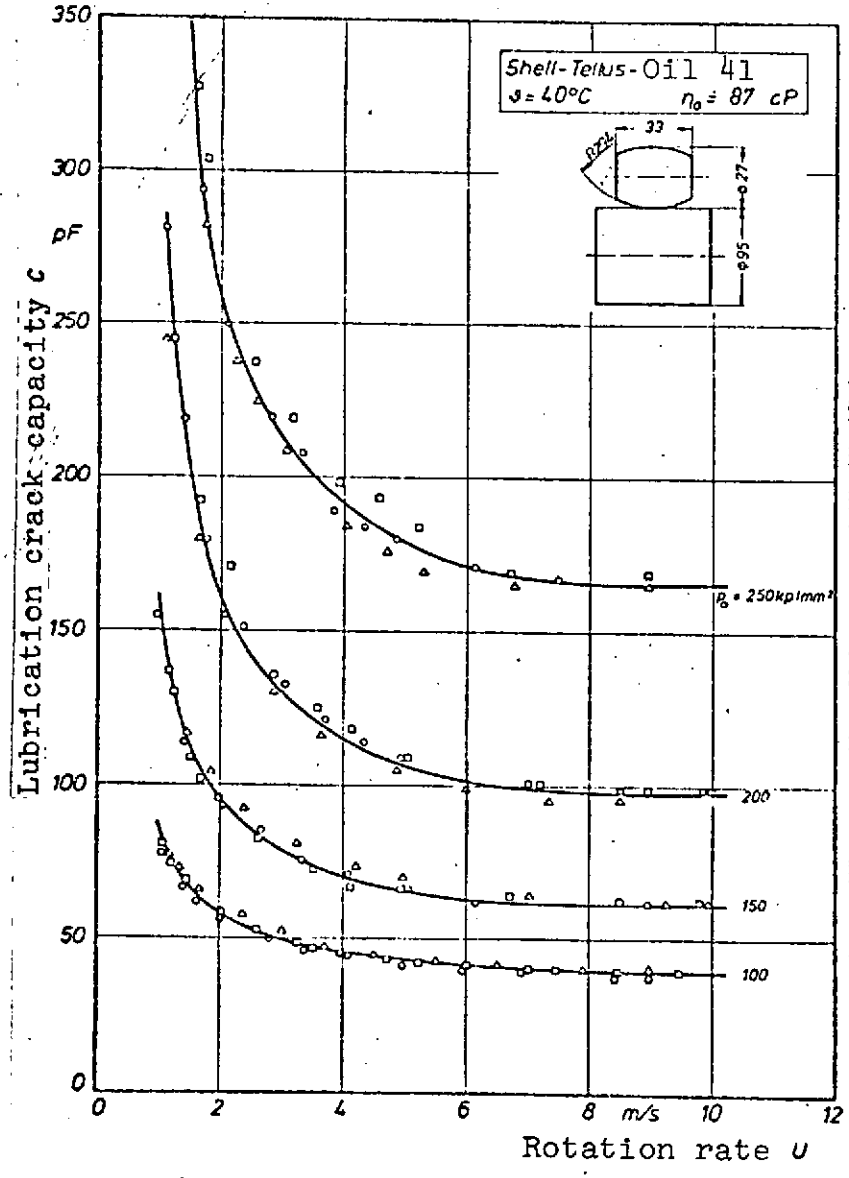

Figure 14.3. Lubrication oil capacity between low curvature barrel roller and cylindrical roller

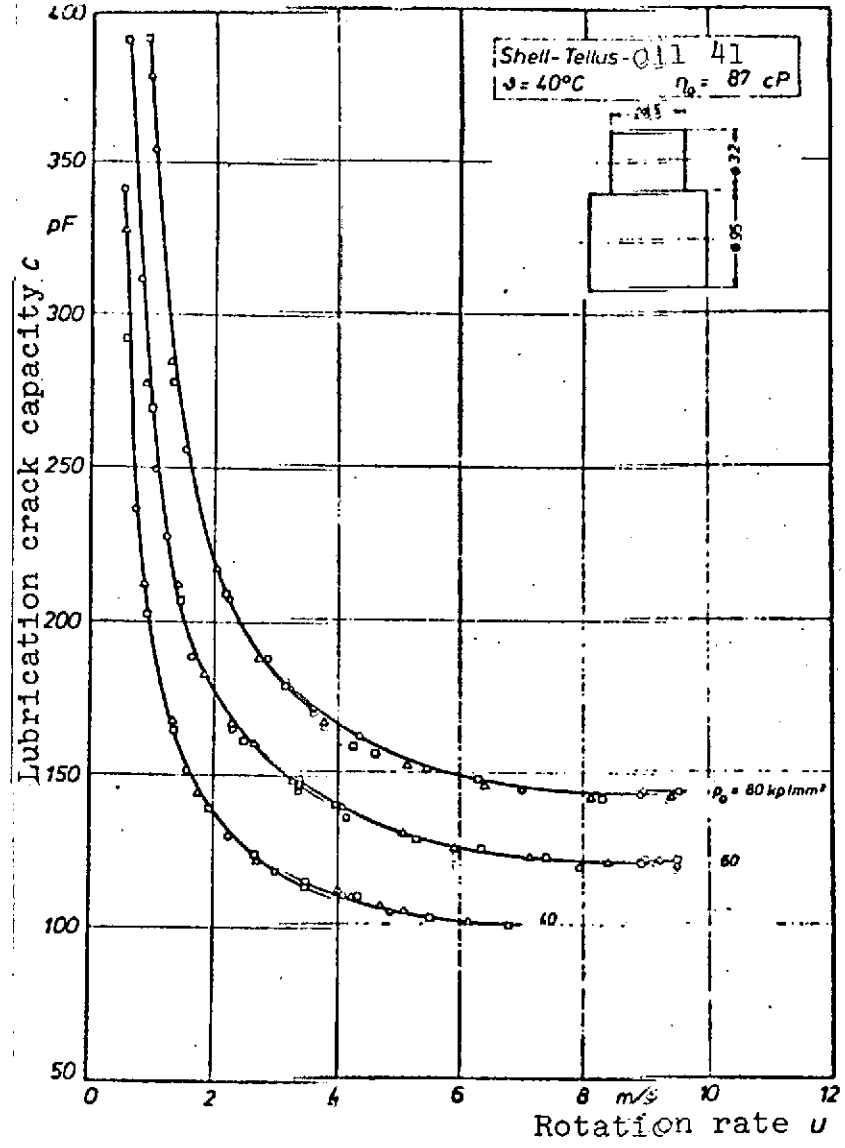

Figure 14.4. Lubrication crack capacity between two cylindrical rollers

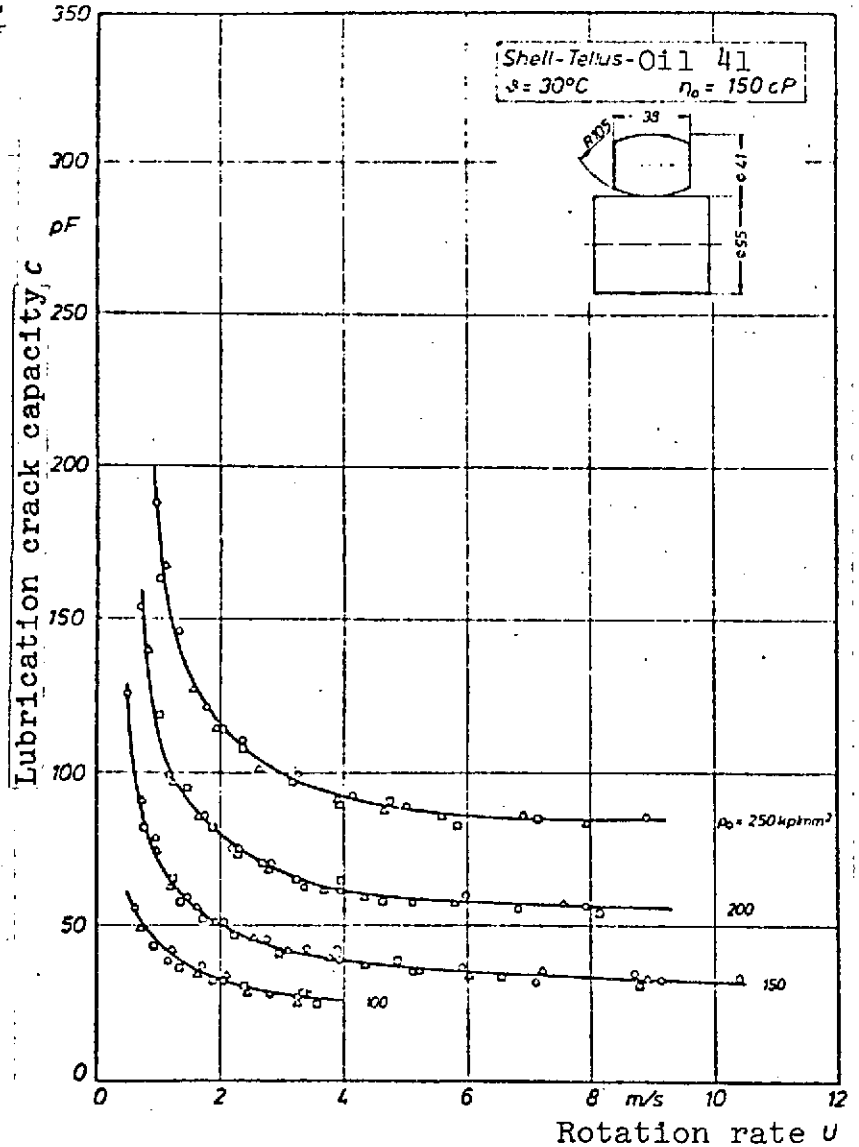

Figure 14.5. Lubrication crack capacity between barrel roller and cylindrical roller at ϑ = 30° C

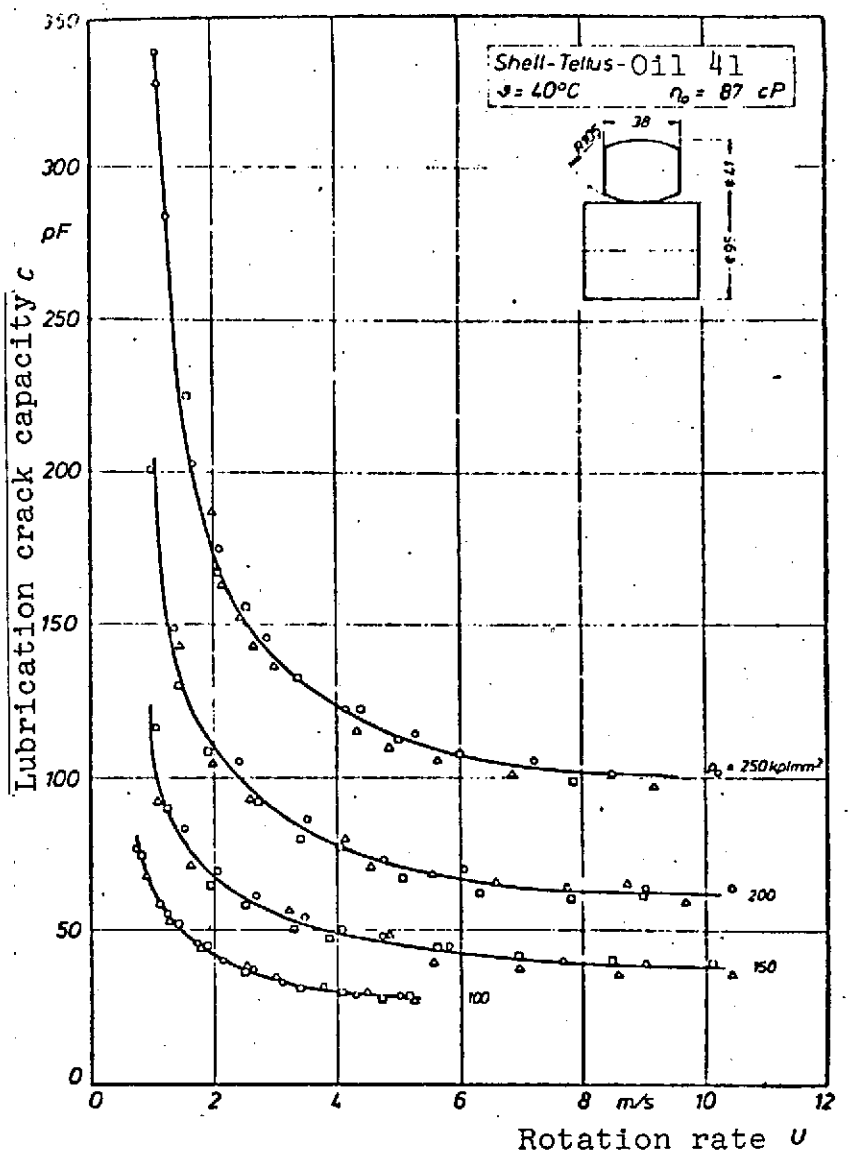

Figure 14.6. Lubrication crack capacity between barrel roller and cylindrical roller at ϑ = 40°C

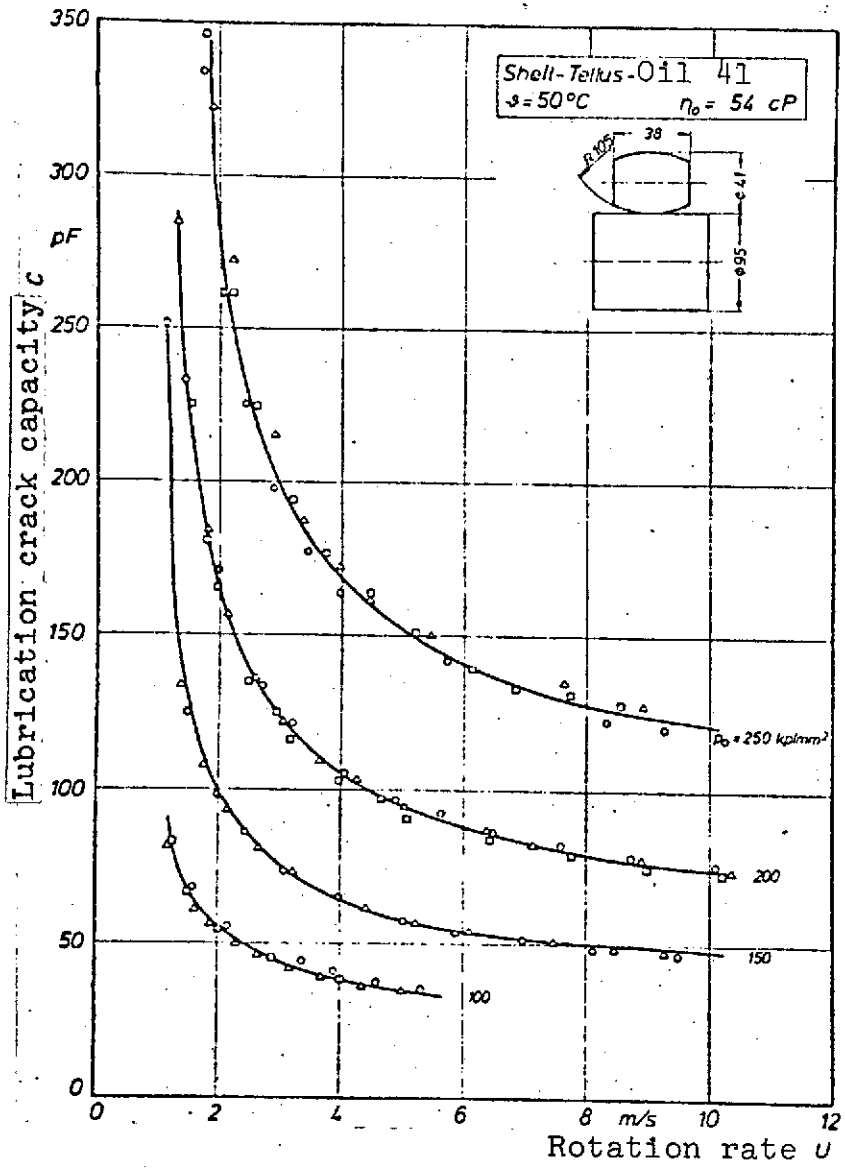

Figure 14.7. Lubrication crack capacity between barrel roller and cylindrical roller at ϑ = 50°C

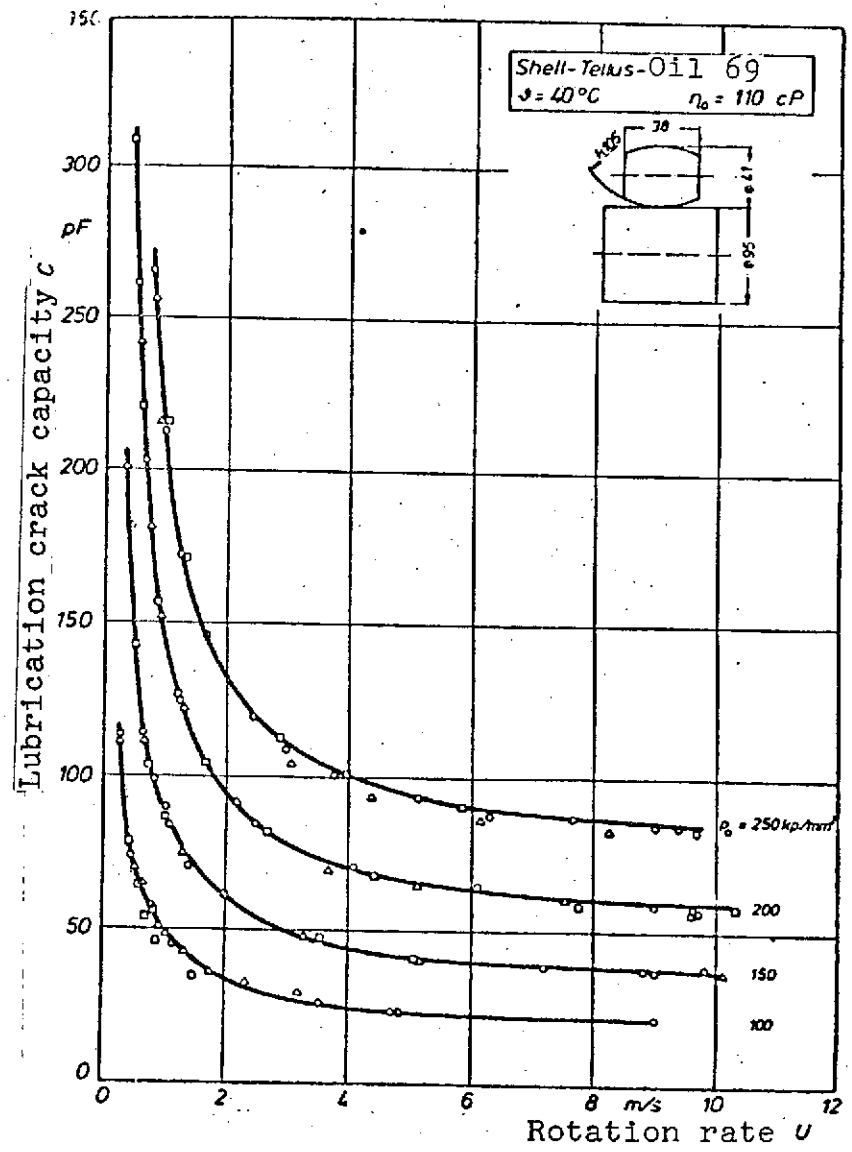

Figure 14.8. Lubrication crack capacity between barrel roller and cylindrical roller at η_0 = 110 cP

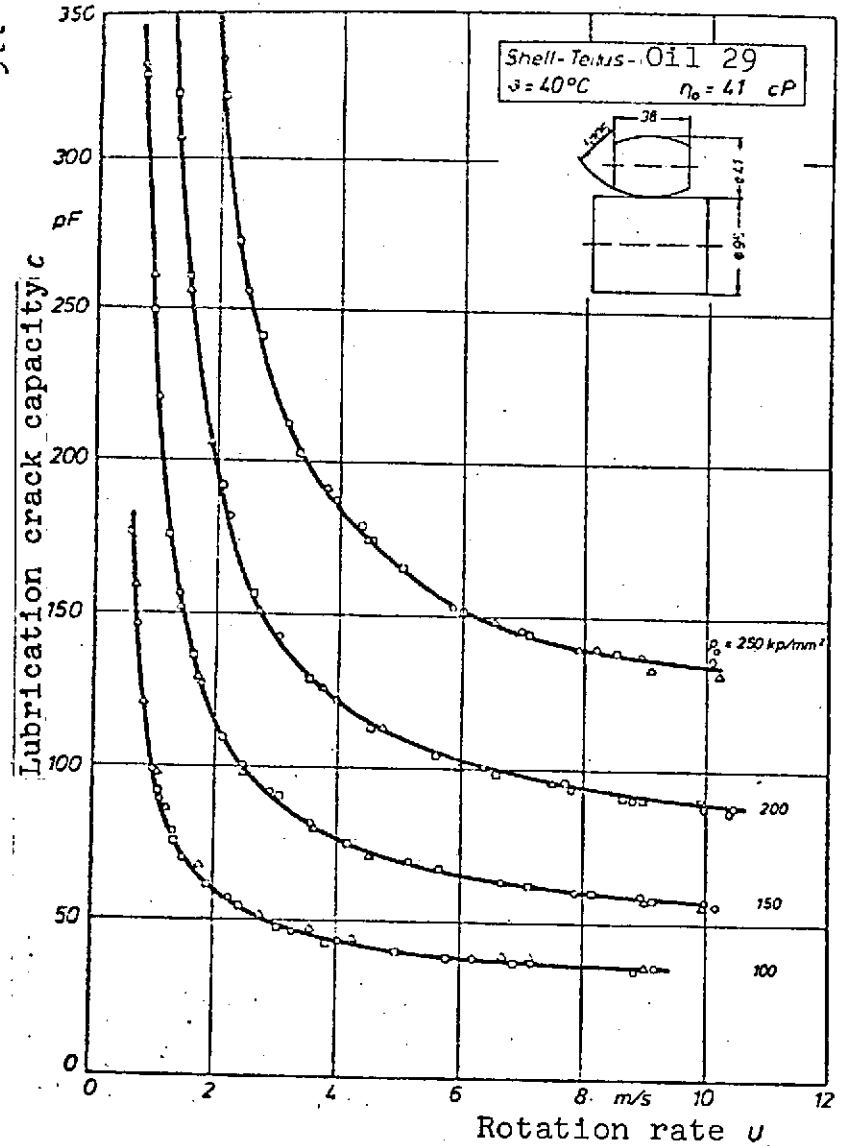

Figure 14.9. Lubrication crack capacity between barrel roller and cylindrical roller η_o = 41 cP

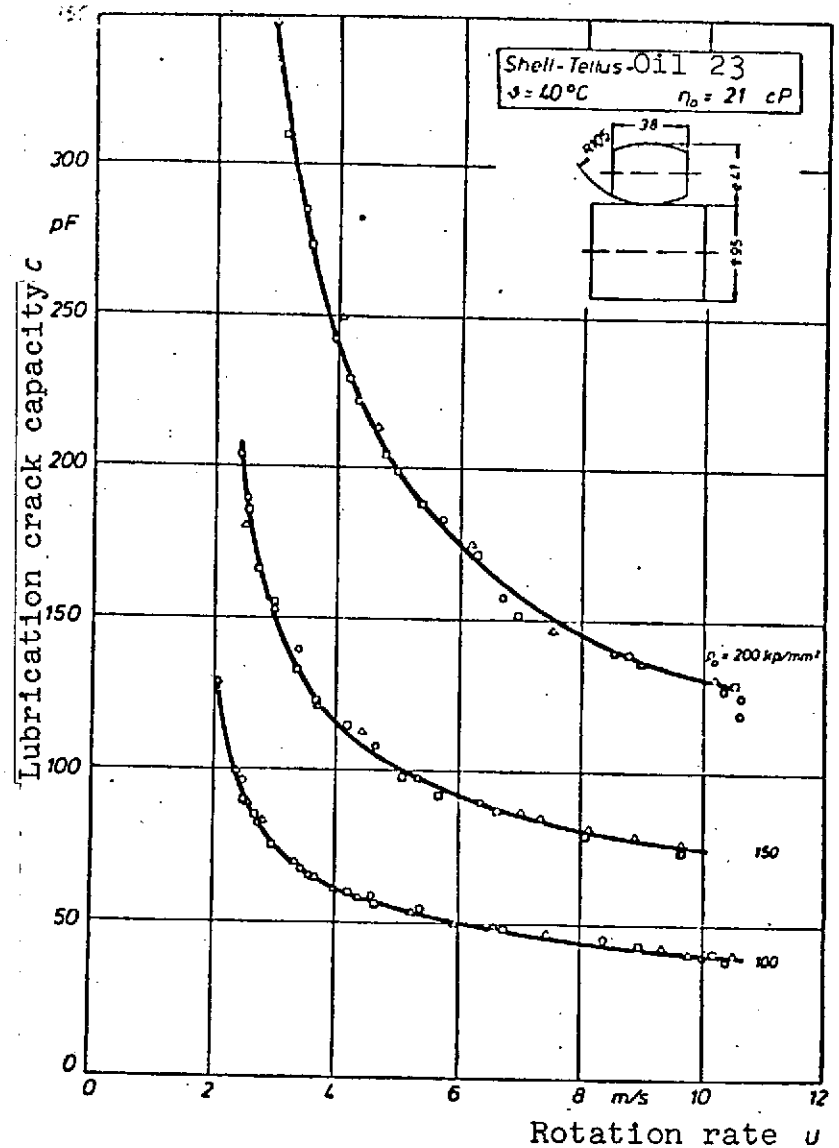

Figure 14.10. Lubrication crack capacity between barrel roller and cylindrical roller η_o = 21 cP

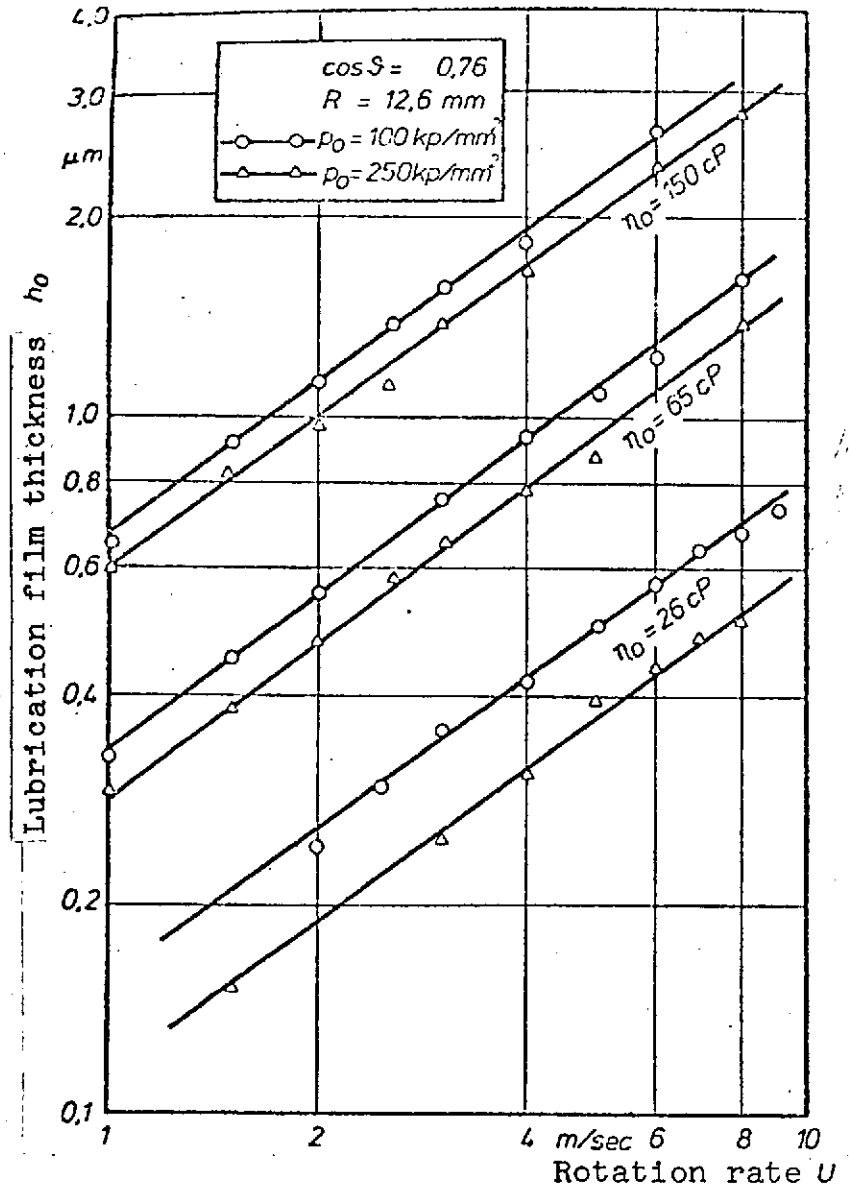

Figure 14.11. Influence of the rotation rate on the lubrication film thickness

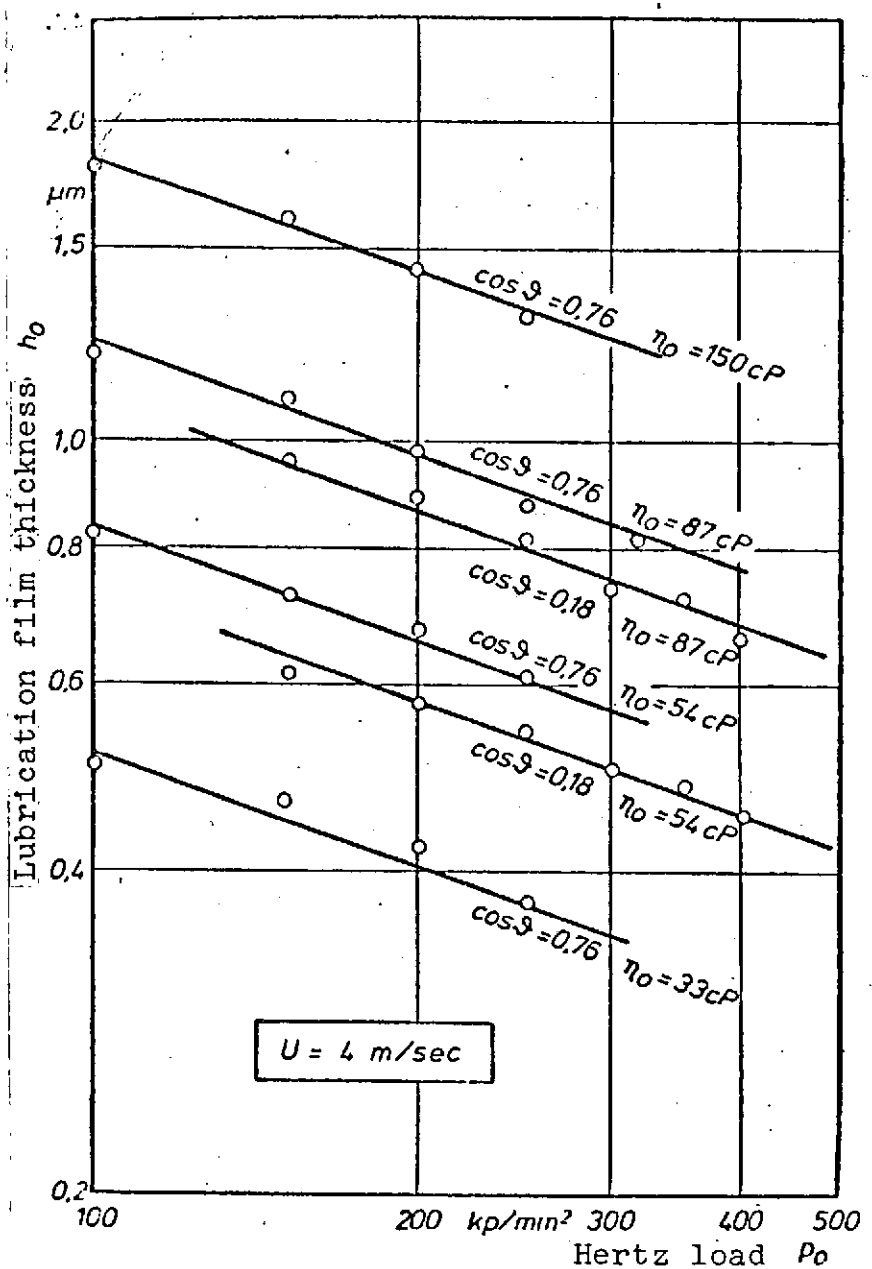

Figure 14.12. Influence of load on the lubrication film thickness

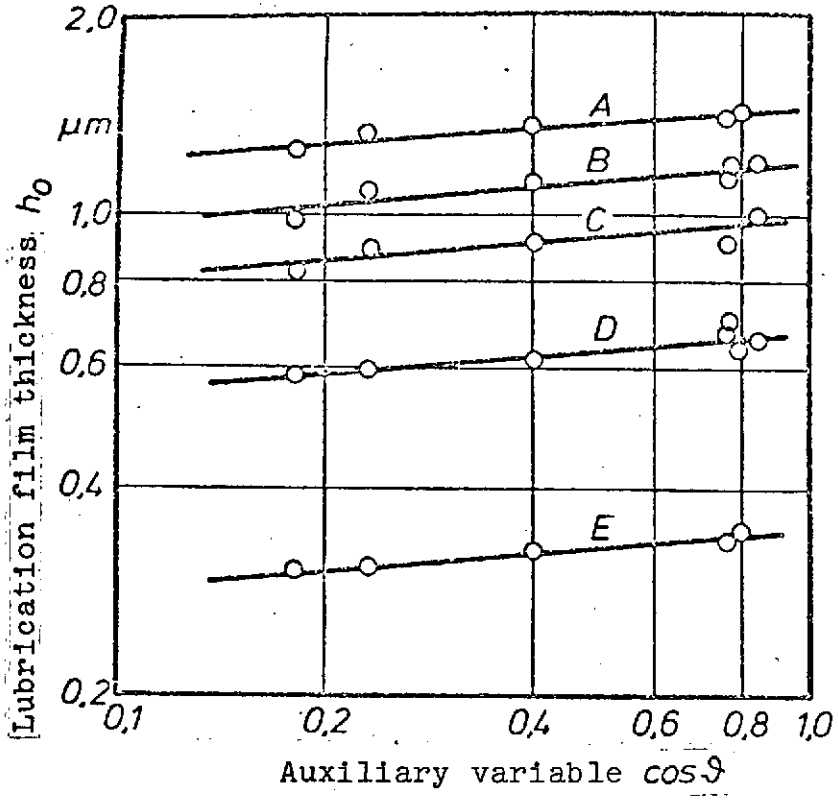

A: U = 8 m/sec, η_o = 87 cP, p_o = 200 kp/mm^2
B: U = 4 m/sec, η_o = 87 cP, p_o = 150 kp/mm^2
C: U = 4 m/sec, η_o = 87 cP, p_o = 250 kp/mm^2
D: U = 4 m/sec, η_o = 54 cP, p_o = 200 kp/mm^2
E: U = 1 m/sec, η_o = 87 cP, p_o = 200 kp/mm^2

Figure 14.13. Influence of the shape of the Hertz contact area on the lubrication film thickness

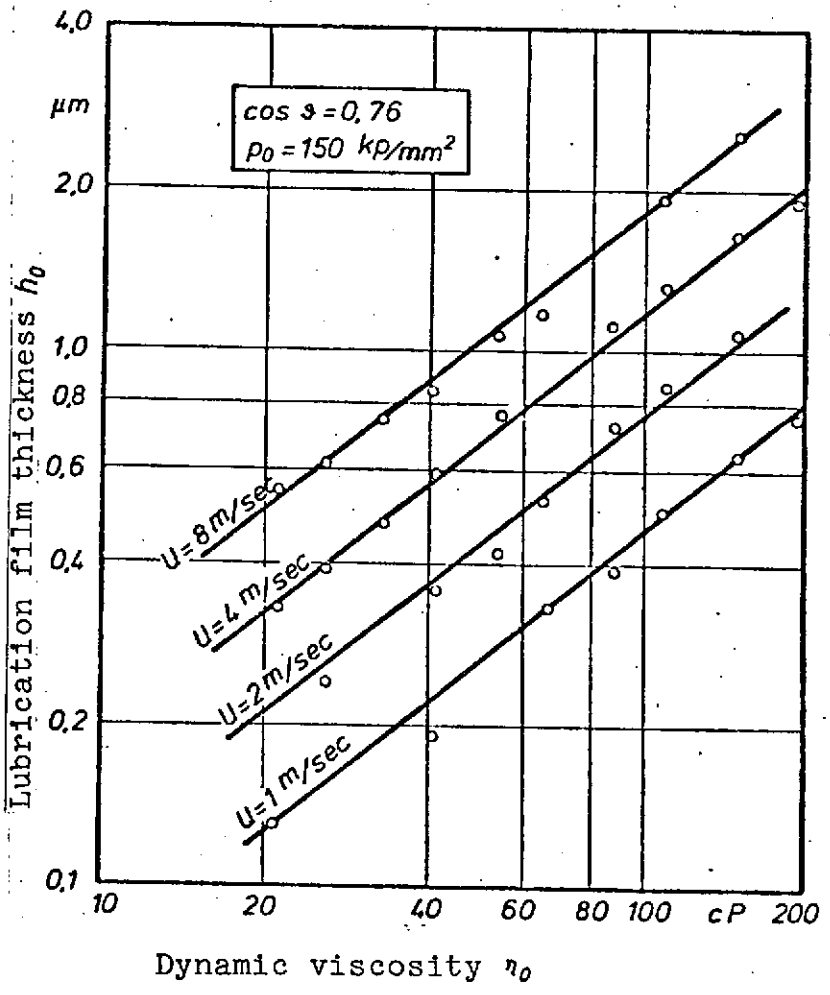

Figure 14.14. Influence of oil viscosity on lubrication film thickness

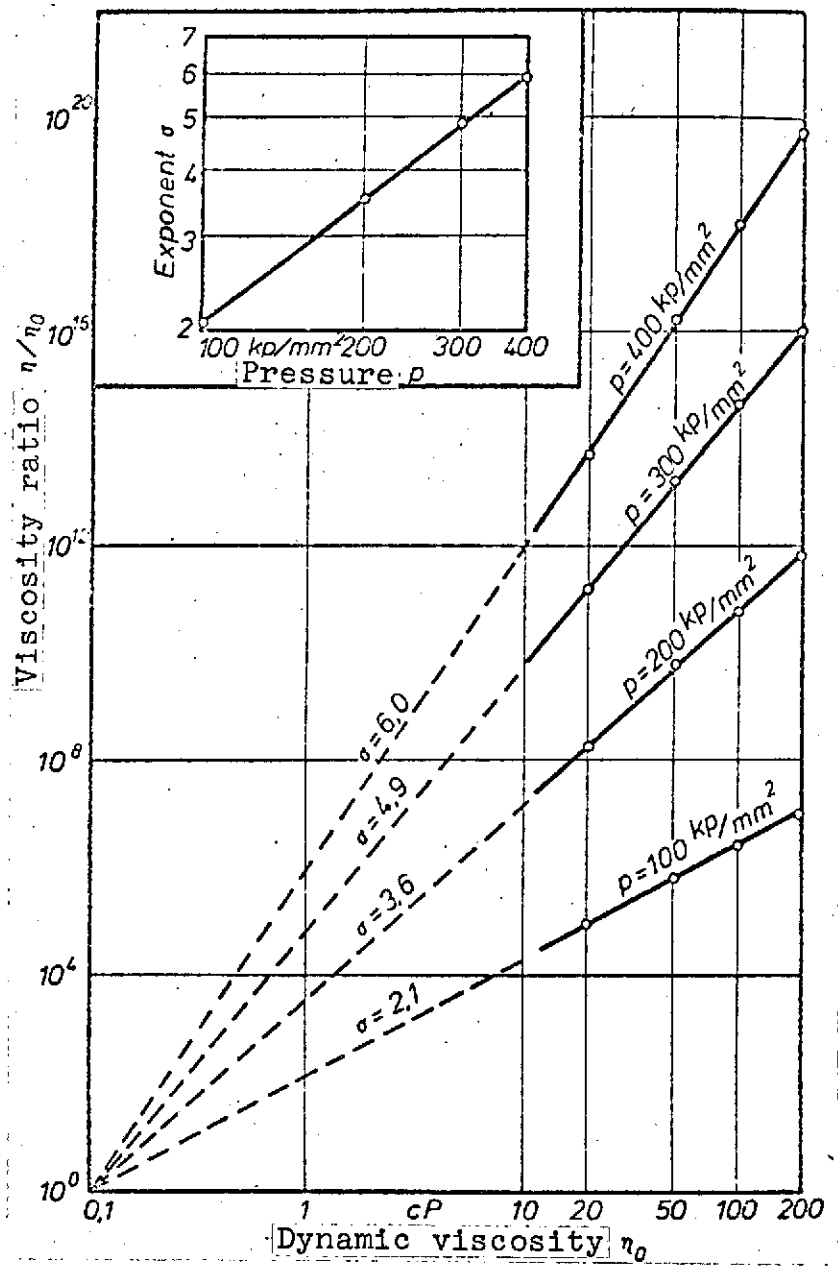

Figure 14.15. Pressure-viscosity variation of lubrication oils.

REFERENCES

1. Münnich, H. Influence of Lubrication on Lifetime Friction and Wear of Rollers. Schmiertechnik und Tribologie, No. 2, 1968, pp. 87-97.

2. Zaretsky, E. V., L. B. Sibley and W. J. Anderson. The Role of Elastohydrodynamic Lubrication in Rolling-Contact Fatigue. Journal of Basic Engineering, Transactions of the ASME 85, No. 3, 1963, pp. 439-450.

3. Zaretsky, E. V. and W. J. Anderson. EHD-Lubrication, Machine Design, Nov., 1968, pp. 167-173.

4. Sibley, L. B. Elastohydrodynamic Lubrication, Machine Design, Oct. 1966, pp. 220-223.

5. Dawson, P. H. Effect of Metallic Contact on the Pitting of Lubricated Rolling Surfaces, Journal Mechanical Engineering Science, Vol. 4, No. 1., 1962, pp. 16-25.

6. Dawson, P. H. The Effect of Metallic Contact and Sliding on the Shape of the S-N Curve for Pitting Fatigue. Proceedings Symposium on Fatigue in Rolling Contact, Paper 4, Institution of Mechanical Engineers, London, 1963, pp. 45-49.

7. Dawson, P. H. Further Experiments on the Effect of Metallic Contact on the Pitting of Lubricated Rolling Surfaces. Proceedings Institution of Mechanical Engineers (London) 180/3B, 1965-1966, pp. 95-100.

8. Tallian, T. E., J. I. McCool and L. B. Sibley. Partial Elastohydrodynamic Lubrication in Rolling Contact. Proceedings Institution of Mechanical Engineers (London) 180/3B, 1965-1966, pp. 169-184.

9. Martin, H. M. The Lubrication of Gear Teeth. Engineering Vol. 102, 1916, pp. 119-121.

10. Peppler, W. Druckübertragung an geschmierten zylindrischen Gleit- und Wälzflächen (Pressure Transfer to Lubricated Cylindrical Sliding and Roller Surfaces). VDI-Forschungsheft 391, 1938, 24 pages.

11. Grubin, A. N. Publication No. 30 of the Central Scientific Research for Technology and Machine Design, Moscow, 1949; see Cameron, A. The Principles of Lubrication, Longmans, London, 1966, pp. 203-208.

12. Crook, A. W. The Lubrication of Rollers II, Transactions of the Royal Society of London A, Vol. 1040, No. 254, 1961, pp. 223-236.

13. Weber, C. and K. Saalfeld. Lubrication Film for Rollers with Deformations. Zeitschr. f. angewandte Mathematik und Mechanik, Vol. 34, No. 1/2, 1954, pp. 54-64.

14. Dowson, D. and G. R. Higginson. A Numerical Solution to the Elastohydrodynamic Problem. Journal Mechanical Engineering Science. Vol. 1, No. 1, 1959, pp. 6-15.

15. Dowson, D. and G. R. Higginson. New Roller-Bearing Lubrication Formula. Engineering, Vol. 192, 1961, pp. 158-159.

16. Dowson, D., G. R. Higginson and A. V. Whitaker. Elastohydrodynamic Lubrication: a Survey of Isothermal Solutions. Journal Mechanical Engineering Science, Vol. 4, No. 2, 1962, pp. 121-126.

17. Archard, G. D., F. C. Gair and W. Hirst. The Elastohydrodynamic Lubrication of Rollers. Proceedings of the Royal Society A, Vol. 262, 1961, pp. 51-72.

18. Stephenson, R. R. and J. F. Osterle. A Direct Solution of the Elastohydrodynamic Lubrication Problem. Transactions of the ASLE, Vol. 5, 1962, pp. 365-374.

19. Cheng, H. S. On Forward and Inverse Iteration of the Elastohydrodynamic Problem. Mechanical Technology Incorporated, New York. MTI-62 TR 37,1962.

20. Cheng, H. S. Preliminary Results on Thermal-Elastohydrodynamics. Mechanical Technology Incorporated, New York, MTI-63 TR 48, 1963.

21. Cheng, H. S. A Numerical Solution to the Thermal Elastohydrodynamic Lubrication of Rolling and Sliding Cylinders. Mechanical Technology Incorporated, New York, MTI-64 TR 7 1964.

22. Wernick, R. J. Some Computer Results in the Direct Iteration Solution of the Elastohydrodynamic Equations. Mechanical Technology Incorporated, New York. MTI-62 TR 38, 1962.

23. Cheng, H. S. and B. Sternlight. A Numerical Solution for the Pressure, Temperature and Film Thickness between Two Infinitely Long, Lubricated Rolling and Sliding Cylinders, under Heavy Loads. Transactions of the ASME, Journal of Basic Engineering, 1965, pp. 695-705.

24. Dowson, D. and A. V. Whitaker. A Numerical Procedure for the Solution of the Elastohydrodynamic Problem of Rolling and Sliding Contacts Lubricated by a Newtonian Fluid. Proceedings Institution of Mechanical Engineers (London) 180/3B, 1965-1966, pp. 57-71.

25. Liesegang, R. Der nichtisotherme hydrodynamische Schmierfilm zwischen hochbelasteten elastischen Walzen (The Non-Isothermal, Hydrodynamic Lubrication Film between Highly Loaded Elastic Rollers). Diss. Karlsruhe, 1967, p. 123.

26. Herrebrugh, K. Solving the Incompressible and Isothermal Problem in Elastohydrodynamic Lubrication through an Integral Equation. Transactions of the ASME, Journal of Lubrication Technology, 1968, pp. 262-270.

27. Howlett, J. Film Lubrication between Spherical Surfaces: with an Application to the Theory of the Four-Ball Lubricant Testing Instrument. Journal of Applied Physics Vol. 17, No. 3, 1946, pp. 137-149.

28. Kapitsa, P. L. Lubrication of Rollers and Spheres (in Russian). Zhurn. Tekh. Fiz. Vol. 25, 1955, pp. 747-762; see Cameron, A.: The Principles of Lubrication, Longmans, London, 1966, pp. 181-183.

29. Lutz, O. A New Form of the Reynolds Equation for Lubrication Hydrodynamics. Ingenieur-Archiv, Vol. 39, No. 5, 1970, pp. 291-301.

30. Archard, J. F. and E. W. Cowking. Elastohydrodynamic Lubrication at Point Contacts. Proceedings Institution of Mechanical Engineers, 180/3B, 1965-1966, pp. 47-56.

31. Cameron, A. and R. Gohar. Theoretical and experimental Studies of the Oil Film in Lubricated Point Contact. Proceedings of the Royal Society, A No. 291, 1966, pp. 520-536.

32. Cheng, H. S. A Numerical Solution of the Elastohydrodynamic Film Thickness in an Elliptical Contact. Transactions of the ASME, Journal of Lubrication Technology, 1970, pp. 155-162.

33. Lane, T. B. and J. R. Hughes. A Study of the Oilfilm Formation in Gears by Electrical Resistance Measurements. British Journal of Applied Physics, Vol. 3, 1952, pp. 315-318.

34. Crook, A. W. Simulated Gear-Tooth Contacts: some Experiments upon their Lubrication and Sub-surface Deformations. Proceedings Institution of Mechanical Engineers, Vol. 171, 1957, pp. 187-214.

35. El-Sisi, S. J. and G. S. A. Shawki. Measurement of Oil-Film Thickness between Discs by Electrical Conductivity. Transactions of the ASME, Journal of Basic Engineering, Vol. 82, 1960, pp. 12-18.

36. Furey, M. J. Metallic Contact and Friction between Sliding Surfaces. Transactions of the American Society of Lubrication Engineers, Vol. 6, 1962, pp. 1-11.

37. Cameron, A. Surface Failure in Gears. Journal of the Institute of Petroleum, Vol. 40, 1954, pp. 191-202.

38. Siripongse, C., P. R. Rogers and A. Cameron. Thin Film Lubrication. Engineering, Vol. 186, 1958, pp. 146-148.

39. Mac Conochie, J. O. and A. Cameron. The Measurement of Oil-Film Thickness in Gear Teeth. Transactions of the ASME, Journal of Basic Engineering, Vol. 82, 1960, pp. 29-34.

40. Crook, A. W. The Lubrication of Rollers. Philosophical Transactions of the Royal Society of London A, Vol. 250, 1958, pp. 387-409.

41. Bell, J. F. Elastohydrodynamic Effects in Lubrication. Dissertation, University of Manschester, 1961.

42. Archard, J. F. and M. T. Kirk. Hydrodynamic Lubrication of Perspex. Nature, Vol. 194, 1962, pp. 965-966.

43. Gohar, R. and A. Cameron. Optical Measurement of Oil Film Thickness under Elastohydrodynamic Lubrication, Nature, Vol. 200, 1963, pp. 458-459.

44. Sibley, L. B. and F. K. Orcutt. Elastohydrodynamic Lubrication of Rolling-Contact Surfaces. Transactions of the American Society of Lubrication Engineers, Vol. 4, 1961, pp. 234-249.

45. Bell, J. C. and J. W. Kannel. Simulation of Ball-Bearing Lubrication with a Rolling-Disc Apparatus. Transactions of ASME, Journal of Lubrication Technology, 1970, pp. 1-15.

46. Lewicki, W. Some Physical Aspects of Lubrication in Rolling Bearings and Gears. The Engineer, 1955, pp. 212-215.

47. Christensen, H. The Lubrication of Rolling Contacts. Measurement of Film Thickness. Acta Polytech. Scand. Mech. Engng., 15 Series, 1963.

48. Christensen, H. The Variation of Film Thickness in Highly Loaded Contacts. Transactions of the American Society of Lubrication Engineers, Vol. 7, 1964, pp. 219-226.

49. Archard, J. F. and M. T. Kirk. Lubrication at Point Contacts. Proceedings of the Royal Society A, Vol. 261, 1961, pp. 532-550.

50. Hashimoto, S. Experimental Studies of the Lubricating Oil Film between Two Rolling Rollers. Bulletin of the Japanese Society of Mechanical Engineers, Vol. 6, No. 22, 1963, pp. 327-335.

51. Dyson, A., H. Naylor and A. R. Wilson. The Measurement of Oil-Film Thickness in Elastohydrodynamic Contacts. Proceedings Institution of Mechanical Engineers 180/3B, 1965-1966, pp. 119-134.

52. Kodnir, D. S. A General Grapho-Analytical and Approximate Method for Solving the Two-Dimensional Problem of the Hydrodynamical Theory of Lubrication and an Approximate Method of Solving the Contact-Hydrodynamical Problem (1960 in Russian), see Dowson, D. and G. R. Higginson, Elastohydrodynamic Lubrication. Pergamon Press, 1966. p. 119.

53. Crook, A. W. Elastohydrodynamic Lubrication of Rollers. Nature, Vol. 190, 1961, pp. 1182-1183.

54. Cheng, H. S. and F. K. Orcutt. A Correlation between the Theoretical and Experimental Results on the Elastohydrodynamic Lubrication of Rolling and Sliding Contacts. Proceedings Institution of Mechanical Engineers 180/3B 1965-1966, pp. 158-168.

55. Tallian, T. E., E. F. Brady, J. I. McCool and L. B. Sibley. Lubricant Film Thickness and Wear in Rolling Point Contact. Transactions of the American Society of Lubrication Engineers, Vol. 8, 1965, pp. 411-424.

56. Hertz, H. The Contact of Rigid Elastic Bodies. Journal für die reine und angewandte Mathematik, Vol. 92, 1882, pp. 156-168.

57. Mundt, R. The Contact of Rigid Elastic Bodies. A Generally Understandable Representation of the Theory of Heinrich Hertz. SKF, 1950, 44 pages.

58. Eschmann, P., L. Hasbargen and K. Weigand. Die Wälzlagerpraxis (Practical Roller Bearing Technology). Oldenbourg-Verlag 1953, pp. 90-100.

59. ASME. Pressure-Viscosity-Report. ASME-Research Committee on Lubrication, New York, 1953.

60. Bradbury, D., M. Mark and R. V. Kleinschmidt. Viscosity and Density of Lubricating Oils from 0 to 150,000 psi and 32 to 425 F. Transactions of the ASME, 73, 1951, pp. 667-676.

61. Hartung, H. A. Density-Temperature-Pressure Relations for Liquid Lubricants. Transactions of the ASME 78, Vol. 2, 1956, pp. 941-947.

62. Wooster, R. C. Discussion Contribution on a Paper of A. E. Bingham: Some Problems for Hydraulic Power Transmission. Proceedings Institution of Mechanical Engineers, Vol. 165, 1951, pp. 254-273.

63. Hersey, M. D. and R. F. Hopkins. Viscosity of Lubricants under Pressure. ASME-Research Committee on Lubrication, New York, 1954.

64. Chu, P. S. Y. and A. Cameron. Pressure-Viscosity Characteristics of Lubricating Oils. Journal of the Institute of Petroleum, Vol. 48, No. 461, 1962, pp. 147-155.

65. Cameron, A. The Principles of Lubrication. Longmans, London, 1966.

66. Orcutt, F. K. Experimental Study of Elastohydrodynamic Lubrication. Transactions of the American Society of Lubrication Engineers, Vol. 8, 1965, pp. 381-396.

67. Dyson, A. Non-Newtonian Behavior in Elastohydrodynamic Lubrication. Meeting of the British Society of Rheology, London 1966, p. 94

68. Dowson, D. and G. R. Higginson. The Fundamentals of Roller Gear Lubrication. Elastohydrodynamic Lubrication. Pergamon Press, 1966.

69. Reynolds, O. On the Theory of Lubrication and its Application to Mr. Beauchamp Tower's Experiments, including an Experimental Determination of the Viscosity of Olive Oil. Philosophical Transactions of the Royal Society of London, Vol. 177, 1886, pp. 157-234.

70. Timoshenko, S. and J. N. Goodier. Theory of Elasticity. Mc Graw-Hill, 1951, pp. 372-382.

71. Stiefel, E. Einführung in die numerische Mathematik (Introduction into Numerical Mathematics). Teubner-Verlag, 1969.

72. Willers, F. A. Methoden der praktischen Analysis (Methods of Practical Analysis). de Gruyter-Verlag, 1971, especially p. 413 ff. .

73. Zurmühl, R. Matrizen (Matrices). Springer-Verlag, 1964, especially p. 58 ff., p. 338 ff. .

74. Herschel, R. Anleitung zum praktischen Gebrauch von Algol 60 (Practical Applications of Algol 60). Oldenbourg-Verlag, 1968.

75. ICL-Handbuch, herausgegeben vom Rechenzentrum der Technischen Universität Braunschweig (ICL Handbook, published by the Computer Center of the Technical University, Braunschweig).

76. Roth, A. Hochspannungstechnik (High Voltage Technology). Springer-Verlag, 1959, pp. 17-28.

77. Coursey, P. R. Electrical Condensers. London, 1927, pp. 125-142.

78. Schwaiger, A. Elektrische Festigkeitslehre (Electrical Strength of Materials). Springer-Verlag, 1925, pp. 72-96 and 116-121.

79. Van Der Pol, B. Radio Technology and the Theory of Numbers. Journal of the Franklin Institute, Vol. 255, No. 6, 1953, pp. 475-495.

80. Clothier, W. K. and H. Bairnsfather. The Guarded Sphere as a Gauging Electrode in Length Metrology. Journal Science Instrum., Vol. 44, 1967, pp. 931-935.

81. Bondi, A. Physical Chemistry of Lubricating Oils. Reinhold Publishing Corp., 1951, pp. 192-196.

82. Moes, A. Discussion Contribution. Proceedings Institution of Mechanical Engineers. 180/3B, 1965-1966, pp. 244-245.

83. Theyse, F. H. Some Aspects of the Influence of Hydrodynamic Film Formation on the Contact between Rolling/Sliding Surfaces. Wear, Vol. 9, No. 1, 1966, pp. 41-59.

84. Archard, J. F. Non-Dimensional Parameters in Isothermal Theories of Elastohydrodynamic Lubrication. Journal Mechanical Engineering Science, Vol. 10, No. 2, 1968, pp. 165-167.

85. Greenwood, J. A. Presentation of Elastohydrodynamic Film-Thickness Results. Journal Mechanical Engineering Science, Vol. 11, No. 2, 1969, pp. 128-132.

86. Johnson, K. L. Regimes of Elastohydrodynamic Lubrication. Journal Mechanical Engineering Science, Vol. 12, No. 1, 1970, pp. 9-16.

87. Lutz, O. Fundamentals on Continuous Roller Gears. Konstruktion, Vol. 7, No. 9, 1955, pp. 330-335; Konstruktion, Vol. 9, No. 5, 1957, pp. 169-171; Konstruktion, Vol. 10, No. 11, 1958, pp. 425-427.

88. Wernitz, W. Beitrag zur Bestimmung der Bohrmomente und der tangentialen Kraftübertragung bei Punktberührung (Contribution for Determining the Bore Torque and the Tangential Force Transfer for Point Contact). Diss. Braunschweig 1957, p. 96.

89. Maass, H. Untersuchungen über die in Hertzschen Flächen Übertragenen Umfangskräfte (Investigation on the Circumferential Forces Transmitted in Hertz Surfaces). Diss. Braunschweig, 1959, p. 87.

90. Buschhorn, H. R. Zur Wälzfestigkeit gehärteter Stahl-Stahl-Paarungen bei Punktberührung und Umfangskraft-übertragung (The Roller Strength of Hardened Steel-Steel Pairs for Point Contact and Circumferential Force Transfer). Diss. Braunschweig, 1966, p. 160.

Translated for National Aeronautics and Space Administration under contract No. NASw 2483, by SCITRAN, P. O. Box 5456, Santa Barbara, California, 93108.